The Role of Natural Nanoparticles and Colloids for Phosphorus Binding in Forested Headwater Catchments

Nina Gottselig

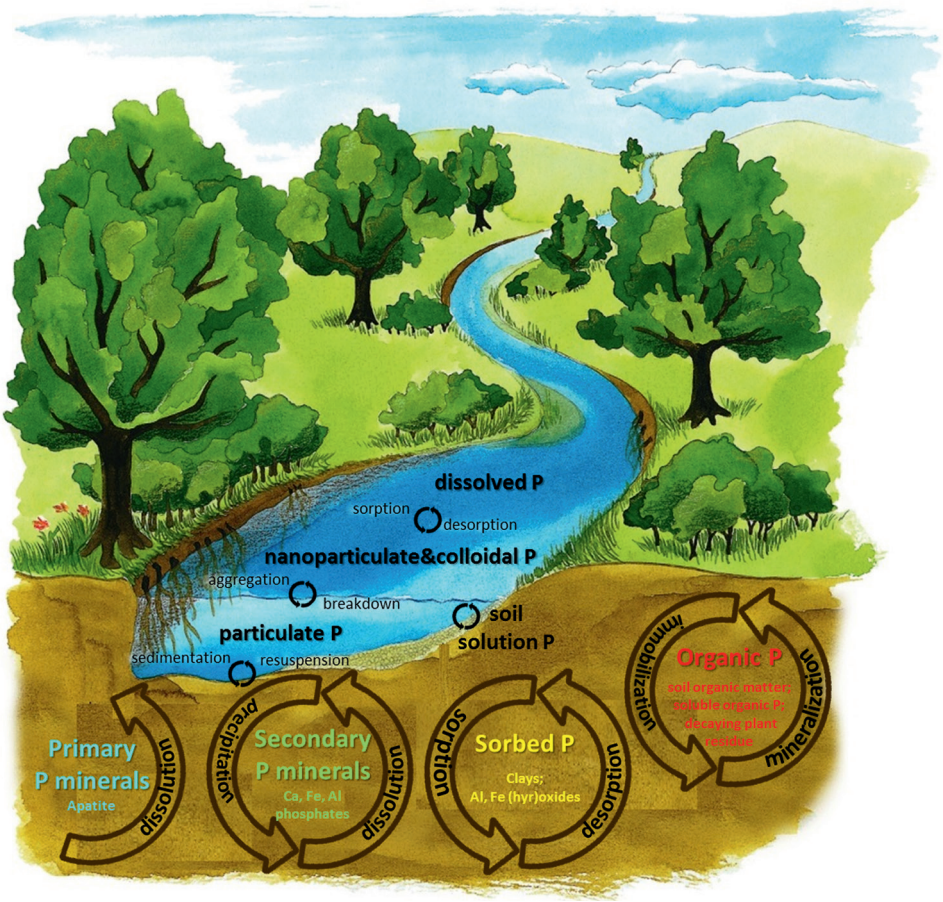

Energie & Umwelt / Energy & Environment
Band / Volume 330
ISBN 978-3-95806-160-6

JÜLICH
FORSCHUNGSZENTRUM

Schriften des Forschungszentrums Jülich
Reihe Energie & Umwelt / Energy & Environment Band / Volume 330

Forschungszentrum Jülich GmbH
Institute of Bio- and Geosciences
Agrosphere (IBG-3)

The Role of Natural Nanoparticles and Colloids for Phosphorus Binding in Forested Headwater Catchments

Nina Gottselig

Schriften des Forschungszentrums Jülich
Reihe Energie & Umwelt / Energy & Environment Band / Volume 330

ISSN 1866-1793 ISBN 978-3-95806-160-6

Bibliographic information published by the Deutsche Nationalbibliothek.
The Deutsche Nationalbibliothek lists this publication in the Deutsche
Nationalbibliografie; detailed bibliographic data are available in the
Internet at http://dnb.d-nb.de.

Publisher and Distributor: Forschungszentrum Jülich GmbH
Zentralbibliothek
52425 Jülich
Tel: +49 2461 61-5368
Fax: +49 2461 61-6103
Email: zb-publikation@fz-juelich.de
www.fz-juelich.de/zb

Cover Design: Grafische Medien, Forschungszentrum Jülich GmbH

Printer: Grafische Medien, Forschungszentrum Jülich GmbH

Schriften des Forschungszentrums Jülich
Reihe Energie & Umwelt / Energy & Environment, Band / Volume 330

D 82 (Diss. RWTH Aachen University, 2016)

ISSN 1866-1793
ISBN 978-3-95806-160-6

The complete volume is freely available on the Internet on the Jülicher Open Access Server (JuSER)
at www.fz-juelich.de/zb/openaccess.

“Don't gain the world and lose your soul, wisdom is better than silver or gold.”

Robert

Abstract

Stream waters reflect the natural load of nutrients and minerals cycled within or released from ecosystems; yet, little is known about natural colloids (1-1000 nm) and especially nanoparticles (NNP, 1-100 nm) as nutrient carriers in the complex biogeochemical system of forested headwater catchments. NNP and colloids are recognized as ubiquitous components in natural aqueous phases and have the potential to encapsulate and bind nutrients, yet are often not included in the analysis of terrestrial nutrient cycling processes. The distribution of elements between the different physicochemical forms in solution is an important precursor to understand the mechanisms of ecosystem nutrition, especially for limiting nutrients like phosphorus (P). The size and composition of NNP and colloids in aqueous phases is therefore relevant for the transport of essential nutrients like P.

Asymmetric Flow Field Flow Fractionation (AF^4) was coupled online to a UV detector for approximation of organic C, a dynamic light scattering device for recording of the hydrodynamic particle diameter, a quadrupole inductively coupled plasma mass spectrometer with collision cell technology (ICP-MS) for elemental size-resolved detection and to an organic carbon detector (OCD) for high sensitive size-resolved organic carbon detection. Method development of hyphenated AF^4 was performed whereas online P detection represented a specific challenge due to the low concentrations in many natural waters. Methodological considerations on the oxidation efficiency of OCD, the capability of ICP-MS to detect organic C and on a setup to be able to determine the bioavailability of NNP and colloid bound P were assessed. Stream waters of forested headwater catchments were sampled as representative medium for mobile components in ecosystems. To assess a more universally valid role of NNP and colloids, an upscaling approach of the catchment based analysis was chosen from regional to national to continental scale.

The aim of the regional sampling study was to characterize NNP and colloidal bound P of distinct hydromorphological areas in stream water of the Wüstebach catchment. The NNP and colloidal P could be fractionated in two size fractions (2-20 nm and >20-300 nm), which constituted up to 100% of the total river P discharge depending on hydromorphology. For the small size fraction, variations in P concentrations followed the Al variations; in addition, a high Fe presence in both fractions was accompanied by high P concentrations. Moreover, organic C was approximated together with P in the presence of Fe and Al, suggesting that Fe and Al are potential carriers of P and associated with organic matter. Tracing the origin of NNP and colloid fractions revealed mixed inputs from soil and vegetation of the catchment. The data enables the inputs and source regions of NNP and colloidal fractions to be traced and conceptually defined for the first time within a small river of a headwater catchment.

For the national sampling campaign it was tested if the majority of P is bound to NNP in forest streams but that their size and composition varies for different forested headwater systems. Five forested sites, which differ in total P content, were sampled for stream water during base flow conditions and analyzed for NNP and colloidal fractions. Through the refined AF^4 method combined with exploratory data analysis, the results showed that the NNP and colloids of all sites could be distinguished into three distinct fractions (approx. 1 nm-20 nm, >20 nm-60 nm, >60 nm-300 nm), yet the elemental concentrations in the fractions were not homogenously distributed. Exploratory data analysis showed that each fraction had unique elemental signatures with different preferential P binding partners. P was preferentially associated to Fe in the smallest size fraction, with increasing contribution of organic C associated P as the hydrodynamic diameter of the fractions increased. The

largest fraction was dominated by aluminosilicate minerals. The relative contribution of the NNP and colloidal fractions for ecosystem nutrient supply can be expected to rise as total P concentrations decline. Moreover, the stream water C to P ratio revealed that NNP and colloids are potentially capable of predicting the nutritional status of an ecosystem. The first flush effect is a potential major loss factor of nutrients bound to NNP and colloids but showed no significant effect on the identified fractions. The factors influencing NNP and colloid inputs to the stream were investigated in a first approach.

On continental scale, a systematic variation with respect to size and composition of NNP and colloids across Europe was found. 96 stream water samples from 26 forested headwater catchments along two transects across Europe were simultaneously collected from base flow. Three fractions (approx. 1 nm-20 nm, >20 nm-60 nm, >60 nm-300 nm) of NNP and colloids were identified. NNP and colloids contributed up to 100% to total element concentrations, indicating a variable but potentially significant contribution of particles for element transport across different geographic regions. Two types of distribution patterns were found: org C, Fe and Al showed linear distribution patterns among particle bound to total concentrations, whereas Si, Mn, P and Ca was independent of total concentrations. Within the fractions, element patterns were able to discriminate sites according to pH value. These analyses suggested a geographical divide of NNP and colloid bound element transport at 45° and 57° latitude in Europe, corresponding to a categorization of streams into pH classes. Hence, NNP and colloids are a relevant component of element cycles across Europe. Site specific ecosystem parameters also showed to have relevant impacts on the composition of NNP and colloid fractions with a clear effect of dominant tree type (coniferous) and mean annual temperature.

NNP and colloids play an important role in forest stream waters for P transport and thus P cycling by binding up to 100% of total P present in the stream. Three fractions of NNP and colloids, each with unique composition patterns and variable P binding, are present throughout European forested headwaters. The fractions follow predictive element specific patterns and compositions on all scales, also allowing a first assessment based on their ecological relevance. This work enhances the understanding of NNP and colloids for P transport and facilitates their inclusion into terrestrial ecosystem cycling processes.

Kurzfassung

Gewässer reflektieren die natürliche Nähr- und Mineralstofffracht, die innerhalb eines Ökosystems zirkuliert oder von ihm freigegeben wird, jedoch ist bisher wenig bekannt über natürliche Kolloide (1-1000 nm) und besonders Nanopartikel (NNP, 1-100 nm) als Nährstoffträger in einem komplexen biogeochemischen System wie das eines bewaldeten Quellgebietes. NNP und Kolloide sind anerkannt als ubiquitäre Komponenten in natürlichen wässrigen Phasen und haben ein hohes Potential Nährstoffe zu binden und einzukapseln, dennoch sind sie oftmals nicht in die Betrachtung terrestrischer Nährstoffkreisläufe eingeschlossen. Die Verteilung eines Elements zwischen den verschiedenen physikochemischen Formen in Lösung ist eine wichtige Vorstufe um Ökosystemernährung zu verstehen, besonders für limitierende Nährstoffe wie Phosphor (P). Die Größe und Zusammensetzung von NNP und Kolloiden in wässrigen Lösungen ist daher relevant für den Transport von essentiellen Nährstoffen wie P.

Asymmetrische Fluss Feld Fluss Fraktionierung (AF^4) wurde an einen UV Detektor zur Abschätzung des organischen C Gehaltes, ein Gerät zur Messung der dynamischen Lichtstreuung zur Bestimmung des hydrodynamischen Durchmessers der Partikel, ein Quadrupol induktiv gekoppeltes Plasma Massenspektrometer mit Kollisionszellentechnologie (ICP-MS) zur Bestimmung von Größen-spezifischen Elementgehalten und an einen organischen Kohlenstoff Detektor (OCD), zur hoch empfindlichen Bestimmung von organischem C, gekoppelt. Methodenentwicklung für gekoppelte AF^4 wurde zunächst durchgeführt, wobei P Detektion eine zentrale Rolle gespielt hat auf Grund der niedrigen Konzentrationen in vielen natürlichen Gewässern. Methodischen Überlegungen wurden angestellt über die Oxidationseffektivität des OCD, die Möglichkeiten organische C Konzentrationen mit ICP-MS zu bestimmen und über einen Aufbau zur Bestimmung der Bioverfügbarkeit von NNP und kolloidal gebundenem P. Bachläufe von bewaldeten Quellgebieten wurden beprobt als repräsentatives Medium für mobile Komponenten in Ökosystemen. Um eine universellere Validität der Ergebnisse zu erzielen wurde eine Hochskalierung in Bezug auf die Standorte durchgeführt von regionaler zu nationaler zu kontinentaler Skala.

Das Ziel der regionalen Kampagne war es NNP und kolloidal gebundenen P von deutlich unterschiedlich ausgeprägten hydromorphologischen Bereichen des Wüstebachs zu charakterisieren. Der NNP und kolloidale P konnte in 2 Fraktionen getrennt werden (2-20 nm und <20-300 nm), welche bis zu 100% der Gesamtkonzentration von P im Bach ausgemacht haben in Abhängigkeit der Hydromorphologie. Für die kleinere Fraktion folgten P Variationen dem Verlauf des Al, zusätzlich bedingte aber auch eine hohe Fe Konzentration hohe P Gehalte. Des Weiteren wurde es angenähert, dass organischer C zusammen mit Fe und Al vorkommt, welches die Vermutung zulässt, dass Fe und Al potentielle Träger von P sind und mit organischem C assoziiert sind. Verschiedene Einflüsse vom umgebenden Boden und der Vegetation wurden festgestellt indem der Ursprung der NNP- und Kolloidfraktionen nachverfolgt wurde. Diese Daten ermöglichen zum ersten Mal, dass die Einflüsse und Quellregionen von NNP und Kolloidfraktionen einen bewaldeten Quellgebietes nachverfolgt und konzeptionell definiert werden können.

Für die nationale Probennahme wurde getestet, ob der Großteil des P in Waldbächen an NNP gebunden ist, aber dass ihre Größe und Zusammensetzung für verschiedenen bewaldetet Quellgebiete variiert. Fünf bewaldete Oberläufe, die sich in ihrem P Gehalt unterscheiden, wurden während Basisabflusskonditionen für Bachwasser beprobt und auf NNP- und Kolloidfraktionen analysiert. Durch die weiterentwickelte AF^4 Methode in Kombination mit explorativer Datenanalyse zeigten die Ergebnisse, dass die NNP und Kolloide aller Standorte in drei Fraktionen unterschieden

werden konnten (ca. 1 nm-20 nm, <20 nm-60 nm, <60 nm-300 nm), jedoch waren die Elementgehalte in den Fraktionen nicht homogen verteilt. Explorative Datenanalyse hat gezeigt, dass jede Fraktion einzigartige Elementsignaturen aufweist mit unterschiedlichen präferentiellen P Bindungspartnern. In der kleinsten Fraktion wurde P präferentiell an Fe assoziiert mit zunehmendem Beitrag von organischen C, wenn der hydrodynamischen Durchmesser der Fraktionen zugenommen hat. aluminosilikate Mineralien haben die größte Fraktion dominiert. Es kann angenommen werden, dass der relative Beitrag der NNP- und Kolloidfraktionen zur Ökosystemernährung zunimmt, wenn Gesamt-P Konzentrationen abnehmen. Zusätzlich hat das Verhältnis von C zu P gezeigt, dass NNP und Kolloide möglicherweise den Nährstoffstatus eines Ökosystems vorhersagen können. Der, first flush effect' als potentieller bedeutender Verlustfaktor für an NNP und Kolloide gebundene Nährstoffe zeigte keinen signifikanten Effekt für die identifizierten Fraktionen. In einem ersten Ansatz wurden zudem die Faktoren untersucht, die den Eintrag von NNP und Kolloiden in das Gewässer beeinflussen.

Auf kontinentaler Skala gab es eine systematische Variation der Größen und Zusammensetzungen von NNP und Kolloiden in Europa. 96 Bachwasserproben von 26 bewaldeten Oberläufen entlang zwei Transekten in Europa wurden zeitgleich während Basisabflusskonditionen beprobt. Drei Fraktionen (ca. 1 nm-20 nm, <20 nm-60 nm, <60 nm-300 nm) von NNP und Kolloiden wurden identifiziert. NNP und Kolloide haben zu bis zu 100% der Gesamtelementgehalte beigetragen, welches einen variablen aber potentiell signifikanten Beitrag der Partikel für den Elementtransport in verschiedenen geographischen Regionen andeutet. Zwei unterschiedliche Verteilungsmuster wurden festgestellt: organischer C, Fe und Al haben einer lineare Abhängigkeit der NNP- und Kolloidkonzentrationen von der Gesamtkonzentration gezeigt, während Si, Mn, P und Ca unabhängig hiervon waren. Standorte konnten anhand ihres pH Wertes unterschiedlichen NNP- und Kolloidzusammensetzungen zugeordnet werden. Diese Analysen schlagen eine geographische Aufteilung in Europa bei 45° und 57°N vor mit Hinblick auf den NNP und kolloidalen Elementtransport. Dies korrespondierte mit der Kategorisierung nach Bachwasser pH. NNP und Kolloide sind daher relevante Komponenten der Nährstoffzyklen in Europa, wobei auch Standort-spezifische Faktoren relevante Einflüsse auf die Zusammensetzung der Fraktionen gezeigt haben, insbesondere die vorherrschende Baumart (Konifere) und die mittlere Jahrestemperatur.

NNP und Kolloide spielen eine zentrale Rolle für P Transport und daher auch für die P Rezyklierung in bewaldeten Quellgebieten bei bis zu 100% Bindung des Gesamt-P. Drei Fraktionen von NNP und Kolloiden sind in europäischen Bachwässern vorhanden, jede mit einer einzigartigen Zusammensetzung und variabler P Bindung. Die Fraktionen folgen vorhersagbaren und Element-spezifischen Mustern und Zusammensetzungen auf allen Skalen, welches auch eine erste Abschätzung ihrer ökologischen Relevanz erlaubt. Diese Arbeit verstärkt das Verständnis von NNP und Kolloiden für P Transport und erleichtert ihre Einbeziehung in terrestrische Nährstoffkreisläufe.

Table of Contents

1

Introduction

1.1 Phosphorus in terrestrial forested ecosystems[1]

Phosphorus (P) is an essential nutrient for all living organisms because its inorganic form orthophosphate (PO_4^{3-}) is a major component of biological molecules and processes. P is a key factor of cellular energy generation, storage and transport (ATP, ADP), of cell regulatory processes (phosphorylation), for the storage of genetic information (nucleotides in DNA and RNA) and as structural component of cell membranes (phospholipids). In turn, P most frequently limits biological productivity in terrestrial and aquatic ecosystems (Fent 2007a; Schindler 1977; Turner et al. 2005; Wild 1988). This impact of P is not an effect of limited presence but substantially an effect of the availability of P to plants and microorganisms. During ecosystem progression, easily available PO_4^{3-} is depleted and in turn P is increasingly incorporated in sorbed or occluded forms.

Next to their critical role with respect to the earth's heat balance, the energy input from the sun and the state of the global climate, forested ecosystems critically link the earth's water and nutrient cycles, making them vital components of the global ecosystem (Perry et al. 2008). Studying pristine forested ecosystems gives insight into the naturally occurring cycling of elements and compounds within a complex biogeochemical system, which is especially crucial to understand for limiting nutrients like P (Bol et al. under review). So far, little is yet known on the rates at which P depletion of forested ecosystems may occur, because hardly anything is known on the P fluxes that result in P losses from a forested ecosystem.

[1] Contains excerpts from:
Bol R, Julich D, Brödlin D, Siemens J, Dippold MA, Spielvogel S, Zilla T, Mewes D, von Blanckenburg F, Puhlmann H, Holzmann S, Kaiser K, Weiler M, Amelung W, Lang F, Kuzyakov Y, Feger KH, **Gottselig N**, Klumpp E, Missong A, Winkelmann C, Uhlig D, Sohrt J, von Wilpert K, Wu B, Hagedorn F. Transport of Dissolved and Colloidal Phosphorus in Temperate Forests – An Almost Blind Spot in Ecosystem Research. Journal of Plant Nutrition and Soil Science, under review.

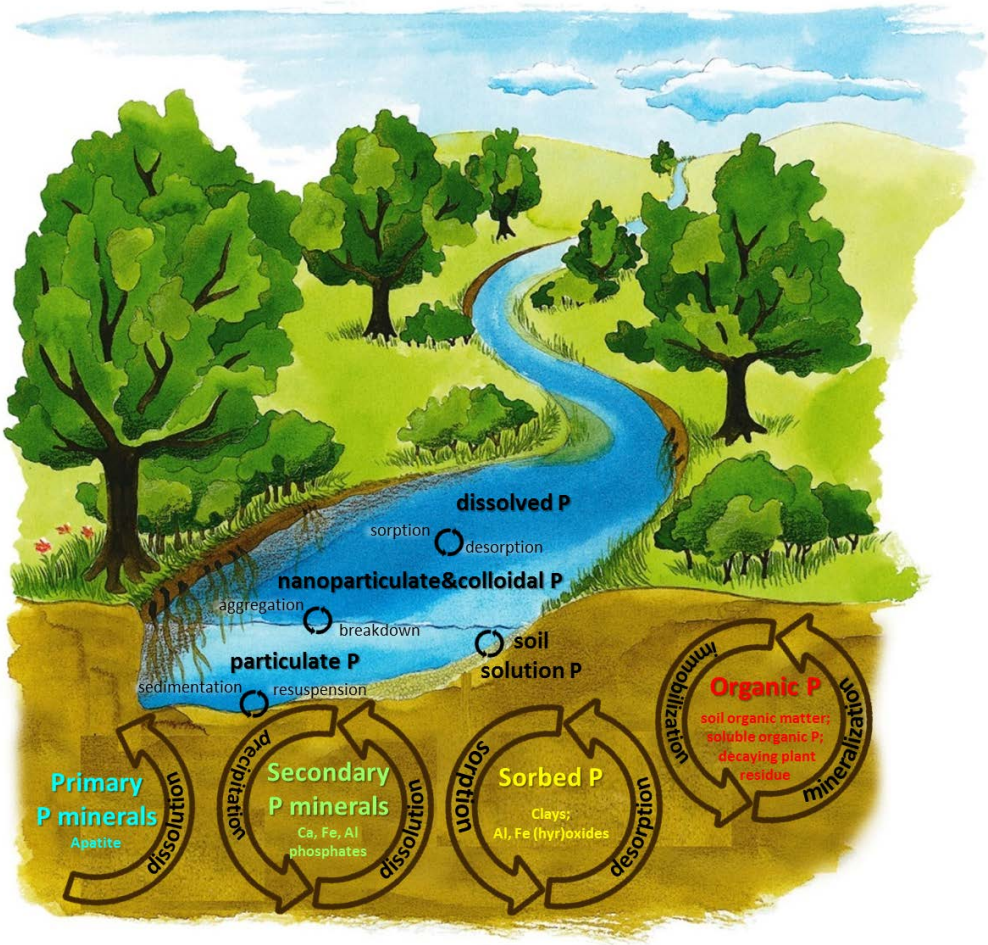

Figure 1.1: *Phosphorus pools in soil and stream water and the processes determining the P addition to and release from the respective pools (adapted according to Dietz and Strock 2016; Wasserwirtschaftsamt Ansbach 2015).*

Forests growing on juvenile substrates rely on P supply from primary minerals, such as apatite released from the parent material (Figure 1.1, Vitousek et al. 2010; Walker and Syers 1976). With progressing ecosystem and soil development, rocks and primary minerals become increasingly depleted as a direct source of P for the biota but at the same time mineral nutrients become increasingly incorporated into biomass. The P within the biomass reenters the cycling process at the end point of senescence, forming a litter layer on top of the soil above the organic layer. Through the organic matter accumulation during soil formation, an increasing portion of nutrients in a terrestrial ecosystem, including P, is organically bound (Darch et al. 2014; Egli et al. 2012; Walker and Syers 1976). In a progressed ecosystem, organophosphorus compounds (PO_4^{3-} bound to organic C through

ester bond) make up a considerable portion of total P in the ecosystem and thus P supply for organisms is largely based on these compounds. Despite this, the ecological role of the different organophosphorus compounds as well as their potential impact on resource partitioning remains largely unknown (Turner 2008). Next to organic P (Figure 1.1), further P species (Spivakov et al. 2009) develop during soil aging (Williams and Walker 1969) and undergo loss factors, limiting the biological productivity of the ecosystem. P can form reactive secondary minerals such as Ca-, Fe- or Al-phosphates (Anderson 1988; Egli et al. 2007) or also be sorbed to aluminosilicate minerals or Al- or Fe-(hydr)oxides (Figure 1.1, Walker and Syers 1976). Soil P pools interact with the soil solution, achieve increased mobility and can therefore also be found in steam waters of the forested catchment.

The network of streams and rivers flowing into the oceans drives the exchange between terrestrial ecosystems and the export of substances from the continents to the oceans (Dynesius and Nilsson 1994). Environmental water samples include many different chemical species (Figure 1.1, Stumm and Morgan 1981), whereas the partitioning between these species controls elemental cycling, transport and loss processes (Stolpe et al. 2010). The composition of headwater stream samples reflects the mobility and availability of nutrients in terrestrial ecosystems. The distribution of the elements between the different binding forms is an important prerequisite for understanding the mechanisms of aquatic and terrestrial ecosystem nutrition (Benedetti et al. 1996; Hasselloev et al. 1999; Tipping and Hurley 1992; Wells and Goldberg 1991), especially for limiting nutrients like phosphorus (Jarvie et al. 2012).

1.2 Natural nanoparticles and colloids

Acquisition and cycling processes in stream waters and terrestrial ecosystems are understood to be driven by the operationally defined 'dissolved fraction' (<0.45 µm) of its constituents (Fent 2007a; Fent 2007b; Lampert and Sommer 1999a; Marschner and Kalbitz 2003 and references therein), yet environmental samples contain a wide variety of chemical species including hydrated ions, molecules, colloidal particles and coarse grains (Stumm and Morgan 1981). It has been widely recognized that colloids (1 nm-1 µm) are ubiquitous components of the 'dissolved fraction' (<0.45 µm) in natural aqueous phases and can comprise up to 100% of the elemental concentrations of metals and for nutrients such as P (Gottselig et al. 2014; Hart et al. 1993; Hill and Aplin 2001; Jarvie et al. 2012; Martin et al. 1995). Aquatic colloids are suspended particles in the aqueous solution which influence the partitioning of chemical species between dissolved and particulate phases.

Settling of the particles does not occur until exceeding the colloidal size range through aggregation processes (Figure 1.1).

The majority of this colloidal material is derived from the weathering of igneous rocks or from plants and animals, which generate organic material and cellular debris (Beckett and Hart 1986). Colloids of stream water samples have the potential to act as predominant carriers of elements in ecosystems (Binkley et al. 2004; Filella et al. 2006; Gottselig et al. 2014; Liu et al. 2011; Qafoku 2010; Stolpe et al. 2010; Wilkinson et al. 1997). As a subset of colloids, natural nanoparticles (NNP) are uniquely specified in the size range of 1 nm to 100 nm due to their larger specific surface area and thus increased reactivity (Hartland et al. 2013; Qafoku 2010) in comparison to larger sized colloids (>100 nm-1000 nm). As demonstrated by Wigginton et al. (2007), the smaller the particle diameter the higher the steps of increasing reactivity become. This effect is especially profound for nanoparticles, where the change in reactivity further accelerates below 10 nm to 1 nm diameter, indicated by the turning point of the nanoparticulate curve (Figure 1.2).

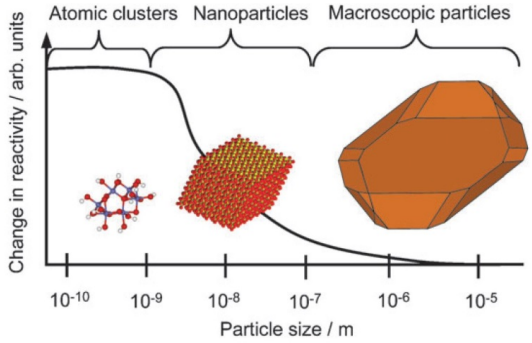

Figure 1.2: *Generalized trend for size-dependent reactivity change of a material as the particle transitions from macroscopic (bulk-like) to atomic. Reactivity can increase or decrease depending on the material and the chemical reaction involved (from Wigginton et al. 2007).*

1.3 Phosphorus bound to natural nanoparticles and colloids

Several studies have already shown that P in stream water is not only present as dissolved P compounds, but also bound in or on colloids in significant amounts (Hill and Aplin 2001; Jarvie et al. 2012; Martin et al. 1995; Mayer and Jarrell 1995; Stolpe et al. 2010). Such fine P-carrying particles may occur both in soil solution (Jiang et al. 2015; Owens and Shipitalo 2006; Regelink et al. 2013) and in surface waters (Gottselig et al. 2014; Hasselloev et al. 1999; Stolpe et al. 2010) where they contain significant concentrations of transferred nutrients and are therefore also important for the availability of P in aqueous phases (Heathwaite and Dils 2000; Montalvo et al. 2015).

In a recent study it was found that P in forest stream waters is predominantly (up to 100%) occurring in NNP and colloidal forms (Gottselig et al. 2014), however with variations in size, composition and relative abundance of the particles. Due to the acidic conditions in forest soils, especially below coniferous forests, and thus stream water, a high adsorption of ions and molecules to particle surfaces is given (Crini and Badot 2010; Franco et al. 2009). Under acidic conditions, surfaces of metal (hydr)oxides are positively charged and thus acting as strong binding partners for negatively charged nutrients like P (Hasselloev and von der Kammer 2008; Richardson 1985) and organic matter (Lyven et al. 2003) and therefore are also relevant for NNP and colloid formation. Aquatic NNP and colloids can be rich in minerals to which P associates or organic matter which contains significant amounts of organically bound P (Darch et al. 2014). All colloidal constituents are present either as these single components (minerals or organic) which can associate P species, or can form organo-mineral complexes (Figure 1.3, Celi et al. 2005; Klitzke and Lang 2007 and references therein; Ognalaga et al. 1994). Additionally, organic matter stabilizes colloids (Ranville and Macalady 1997) so that they are less prone to aggregate to larger size ranges. First studies on the size resolved analysis of NNP and colloids (Andersson et al. 2006; Dahlqvist et al. 2004; Gottselig et al. 2014; Hasselloev et al. 1999; Lyven et al. 2003; Neubauer et al. 2013; Regelink et al. 2014; Regelink et al. 2011; Stolpe et al. 2010; Stolpe et al. 2005) show the importance of colloidal components such as minerals, metal oxides or organic molecules, which can form building block elements or structures (core structures) of these NNP and colloids. These components vary depending on the particle size. It is still disputed whether Fe and Al, both in ionic and oxide forms, are relevant especially for small NNP in the context of associated P transport (Francko and Heath 1982; Hasselloev and von der Kammer 2008; Jiang et al. 2015; Leppard et al. 1988; Richardson 1985; Stolpe et al. 2005) or if organic matter transports P in the smallest size fraction (Lyven et al. 2003; Regelink et al. 2013; Regelink et al. 2011; Shafer et al. 1997). Depending on the pH of the stream water, also Ca can be present in the colloids and associated to P in the form of Ca phosphates. In this case, Ca is enriched in the colloidal phase in comparison to larger suspended matter (Ran et al. 2000) and especially when surface waters drain carbonate-rich soils (Hill and Aplin 2001).

To understand the influence of NNP and colloids on the transport, adsorption and availability of different elements, especially nutrients such as P, differentiating between building block elements or compounds that make up the core of the NNP and colloids versus elements or compounds that are associated with or sorbed to NNP or colloids can be useful (Andersson et al. 2006; Dahlqvist et al. 2004; Hartland et al. 2013; Lyven et al. 2003). Building block elements/compounds can be metal oxides and/or hydroxides of Fe/Al/Mn, aluminosilicates or organic carbon (Hartland et al. 2013; Lyven et al. 2003; Regelink et al. 2011). Also Ca has been assigned as building block element

(Dahlqvist et al. 2004). Transported elements have been reported to be rare earth elements (Andersson et al. 2006), trace elements (Regelink et al. 2014) and nutrients such as P (Gottselig et al. 2014; Regelink et al. 2014; Regelink et al. 2011; Stolpe et al. 2010). Nevertheless, also org C or metals can be associated to and transported by NNP and colloids in contrast to their function as building block elements/compounds.

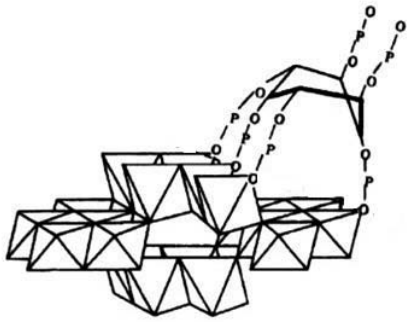

Figure 1.3: *Adsorption of* myo-*inositol hexakisphosphate on a goethite surface at pH 4.5 (from Ognalaga et al. 1994).*

Despite their important role in element binding, NNP and colloids are often not included in the analysis of terrestrial nutrient cycling processes (Fernández-Martínez et al. 2014; Vitousek 1982). The availability of nutrients associated to NNP and colloids may substantially vary in comparison to the availability of hydrated ions or organically bound P. Therefore, examining the significance of NNP and colloids as well as their composition as function of forest stream water pH on a large scale can provide insight into their ecological relevance. Further, developing an approach for estimating the proportion of total elemental concentrations in waters that are associated with NNP and colloids based on widely available data can facilitate the inclusion of NNP and colloids into assessments of nutrients. For essential nutrients like P, knowledge regarding primary adsorption or binding partners in the NNP and colloidal fraction help to estimate their physicochemical form in solution.

1.4 The advantageous technique of Field Flow Fractionation (FFF) for particle analysis

New technical developments aid to better understand the processes determining the availability of the constituents of the 'dissolved fraction' (<0.45 µm) by giving insights into the chemical configuration of nutrients in this fraction. Field Flow Fractionation (FFF; Giddings et al. 1976) is a frequently used method when aiming at the separation and characterization of colloids in aquatic systems (e.g von der Kammer et al. 2011). It is a flexible technique for nearly nondestructive

fractionation of environmental colloids and especially NNP samples (Gimbert et al. 2003) without the need of sample pretreatment, i.e. it is best suited to characterize the size distribution of NNP and colloids in the aqueous environment. FFF combines a large separation range (approx. 1 nm-1 µm) with the possibility of coupling various detection devices online (Giddings et al. 1976). In contrast to FFF, classical techniques to isolate NNP and colloids, such as filtration and centrifugation, include the risk of eliminating particles not specific to the given size due to unknown morphological heterogeneity of the natural particles. Membrane clogging occurs when filtering close to target size ranges of the analytes, which can result in a severe risk of underestimating NNP and colloidal concentrations (Zirkler et al. 2012). In addition, especially the application of flow-based FFF techniques allows a distinction between NNP and colloids and the elements and molecules below 1 nm hydrodynamic diameter (see Chapter 2.1).

Online coupled FFF of environmental aqueous colloids, including soil extracts, with emphasis on NNP and colloidal P are important in understanding the role of different size fractions for nutrient adsorption. Distinct analyses of environmental nanoparticles and colloids via FFF and online coupled detectors have been done for grassland soils (e.g. Henderson et al. 2012), agricultural sites (e.g. Regelink et al. 2014; Regelink et al. 2011), for soils such as podzol (Regelink et al. 2011) or peat (Jirsa et al. 2013) and for wetland runoff (Neubauer et al. 2013). Studies focusing primarily on waterways rather than on soil extracts and soil solution are much less prominent in literature due to the lower concentrations of elements within NNP and colloidal sizes. Streams partially influenced by human activities (Stolpe et al. 2010) as well as important studies on the application of FFF-ICP-MS on urban stream water NNP and colloids (Hasselloev et al. 1999; Lyven et al. 2003; Stolpe et al. 2005) and on forested stream water NNP and colloids (Andersson et al. 2006; Dahlqvist et al. 2004) are published. A common denominator of the stream water studies is a filtration at 0.45 µm prior to FFF fractionation potentially influencing the results (Zirkler et al. 2012). Further, P determination in the fractions alongside relevant carrier elements could previously only be achieved through high resolution ICP-MS. The latter studies show relevant methodological approaches and elemental data, yet the role of P binding to natural nanoparticles and colloids in forest stream waters analyzed through nondestructive FFF fractionation is still rarely investigated.

1.5 Aim and scope of the thesis

The aim of this study was to elucidate the role of natural nanoparticles (NNP) and colloids for phosphorus binding and transport in stream waters as representative medium for mobile components in ecosystems. Despite technical developments which give insights into the chemical composition of the operationally defined 'dissolved' fraction (<0.45 µm), NNP and colloids, overlapping with the 'dissolved' fraction, are still largely neglected as ubiquitous components of this fraction. To allow a correct analysis of the availability of different P forms present in an ecosystem, which is especially relevant for limiting nutrients like P, the chemical composition and structure of the particles included in the operationally defined 'dissolved' fraction first have to be investigated. Further, it is necessary to identify if NNP and colloids are relevant nutrient carriers and if their composition is a variable of ecosystem specific parameters, which then in turn also influence the availability of NNP and colloid bound nutrients. Forested headwater catchments as complex biogeochemical systems nearly lacking anthropogenic influence were analyzed to reflect the naturally occurring nutrient binding of NNP and colloids. To assess a more universally valid role of NNP and colloids an upscaling approach with respect to the sampling site locations was chosen. At first a detailed analysis of a regional catchment was performed, followed by five catchments on a national scale and then by 26 catchments on the continental scale. Prior to catchment based analysis, method development of Asymmetric Flow Field Flow Fractionation (AF^4), a specific type of FFF, coupled online to inductively coupled plasma mass spectrometry (ICP-MS) and to a high sensitive organic carbon detector (OCD) for elemental detection was performed.

Method development (Chapter 4.1): Fractionation of NNP and colloids is dependent on the environmental origin of the sample and needs to be adapted accordingly. A suitable fractionation technique with AF^4 coupled online to a quadrupole ICP-MS with collision cell technology was developed and refined for forested stream water samples. The NNP and colloid size range and composition was intentionally not disturbed through filtration close to target size ranges. The described method is applicable to routine analysis and detects low P concentrations through the use of the collision cell technology for ICP-MS. Further developments were pursued to also include precise organic carbon detection online to AF^4.

Regional scale study (Chapter 4.2): This study aimed at identifying NNP and colloidal bound P of distinct hydromorphological areas in a natural stream of the Wüstebach catchment. Particularly the stream points in the headwaters region are considered a source region of NNP and colloids. It was intended to trace the source regions of the NNP and colloidal fractions recorded at the outlet of the catchment and how their intensities are influenced by tributary into main stream flow. Additionally it

was aimed at evaluating the significance of NNP and colloids for elemental binding with respect to total sample concentrations. The allocation of particles and adhered P was investigated through application of AF^4 online with UV for organic matter estimation and with ICP-MS for quantification of Al, Fe, and P concentrations of NNP and colloidal fractions. After identifying the stream water NNP and colloid fractions, a first approach was tested to trace the origin of these fractions through measurements of Fe isotopic signatures.

National scale study (Chapter 4.3): Evaluating the influence of NNP and colloids for P transport in forested headwater catchments was evaluated across five catchments to assess the validity of NNP and colloids as dominant P binding and transport medium. This project also aimed at going beyond mere raw data to provide new insights on the preferential binding of P, dependent on NNP and colloidal size and elemental composition of the fractions. It was hypothesized that significant amounts of P in stream waters occur in NNP and colloidal forms, however with variations in size, chemistry and proportions in the fractions. Further, a first assessment of the ecological relevance of NNP and colloids was conducted. Base flow events of stream waters and tributaries in five forest catchments of Germany (4 sites) and Norway (1 site) were sampled. The sites differed in total P load and therefore potentially also in the distribution of P among NNP and colloidal size fractions. The samples were analyzed using AF^4 coupled to ICP-MS for Al, Si, P, Mn, Fe and to an online high-sensitive OCD for organic C measurements. Innovative measurements using AF^4 coupled to an OCD were performed for the first time to overcome the uncertainties of UV detection for organic C with special emphasis on the organic carbon content of multiple fractions. This provided detailed online information on the precise potential organic matter contribution within NNP and colloids. With the combined data of ICP-MS and OCD, it was hypothesized that different elements or compounds are responsible for P binding in the varying particle fractions. Hence, it is investigated whether the relevance of NNP and colloids for P fluxes through stream water increases with decreasing easily available P content in headwaters across a gradient of forest ecosystems with different P status. The P flux can potentially be significantly influenced through washout processes of NNP and colloids from the catchment during high precipitation events. In this context, first results on the inferences for stream water NNP and colloids released from surrounding soils, as well as on further input flows to the stream are of interest.

Continental scale study (Chapter 4.4): Following the upscaling approach of this study, a sampling of 26 sites on European scale was conducted to further extrapolate the importance of NNP and colloids as elemental transport medium in the stream waters of forested ecosystems. Fractionation of NNP and colloids as well as their proportion of total elemental sample concentration were assessed throughout Europe. The samples were analyzed using AF^4 coupled to ICP-MS for Al, Si, P, Ca, Mn, Fe

and to an online high-sensitive OCD for organic C measurements. For this study, it is hypothesized that NNP and colloids are ubiquitous carriers for P and other nutrients in European river systems, but that their composition and size distribution changes systematically along continental gradients in Europe. To facilitate the inclusion of NNP and colloids into forest ecosystem nutrient cycling processes, this project aimed at the predictability of the elemental concentrations in the particle fractions through total sample concentrations. The data on pH dependency and the predictability considerations showed a geographical divide in Europe between Southern, Middle and Northern European headwater catchments. By taking these distinctly different geographical regions into account, this work also aimed at identifying the preferential P binding per particle fraction in dependence of the stream water NNP and colloidal characteristics per geographical region.

Further, climatic and overlaying environmental factors like mean annual temperature and precipitation, the site altitude or bedrock composition has profound effects on the site specific soil type, the vegetation and biological processes driving nutrient cycling. The environmental factors and site specific characteristics then influence the stream water chemistry. Thus, most probably also the constituents of the NNP and colloidal fractions are driven by these governing factors and that the elemental concentrations in the fractions varies, especially for P, accordingly in a specific pattern governed by the climatic and environmental determinants. The identification of these patterns can give a first insight to understand which long term effects a significant change in climatic conditions can have on the binding and transport of P through NNP and colloid and how this can potentially affect the availability of this limiting nutrient in forested ecosystems in the future.

II

Theoretical background:

Field Flow Fractionation (FFF)

Field Flow Fractionation (FFF) is a family of fractionation techniques distinguishable through the type of field applied for particle separation. The theory of flow based FFF was developed by Giddings et al. (1976). The separation field can be a thermal gradient between the top and bottom plate of the separation channel (Thermal FFF) for a separation based on molar mass and composition. Further, centrifugal force can also be utilized (Centri FFF) to achieve a separation based on particle density and hydrodynamic size. Whereas Thermal FFF is mostly for polymer applications and particle density always influences separation with Centri FFF, hydrodynamic particle diameter determines separation in Multi Flow FFF. This makes it a universal tool for nanoparticle and colloidal applications. Further less developed FFF techniques exists as well with e.g. electrical or magnetic separation fields (Schimpf et al. 2000). The most common Multi Flow FFF device and also the selected technique for this study is the Asymmetric Flow Field Flow Fractionation (AF^4) where the separation field is a directed outflow of eluent from the channel through a porous frit in the bottom plate of the channel.

2.1 Principle of Asymmetric Flow Field Flow Fractionation (AF^4)

During an AF^4 fractionation process, the sample containing an unsorted mixture of NNP and colloids in matrix solution is loaded into a thin separation channel consisting of an impermeable top cover divided by a spacer from a permeable membrane above a ceramic frit at the bottom. All flow processes in AF^4 are driven by eluent flow which is directed through HPLC (high performance liquid chromatography) precision pumps. The channel is equipped with two inflow ports, the injection flow at the beginning of the channel and the focus flow at the center of the channel, as well as two outflow ports, the cross flow through the membrane and frit in the channel bottom and the detector

flow at the channel end (Figure 2.1). Additionally, a purge flow is installed just above the detector outflow to regulate channel pressure when problems arise. Fractionations are generally conducted at high pressure with up to 15 bar inner channel pressure.

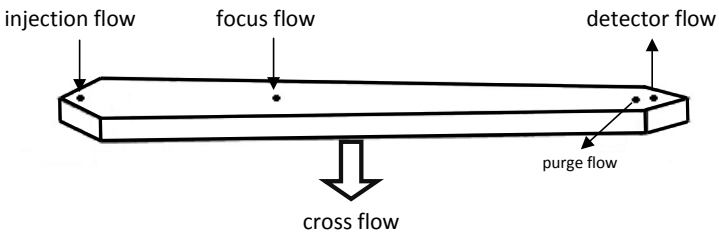

Figure 2.1: *Flow ports and positions on AF[4] channel. The height and length of the separation channel are not shown in correct proportions.*

In an AF[4], particle fractionation is achieved by application of a separation force perpendicular to the channel flow generated by partial withdrawal of eluent and sample matrix through the membrane (referred to as cross flow). Despite the constant Brownian motion of particles in all directions, the cross flow shifts their position closer to the accumulation wall, which is the channel bottom covered by the membrane (Baalousha et al. 2011). After sample injection (orange, Figure 4.1.1a) into the sample loop of the autosampler, the focusing of the particles (red, Figure 4.1.1a) is the first step of the fractionation process and occurs at the same time the sample is still introduced into the channel and also exceeding the time needed for loading the sample into the channel. Through focusing, particles are sorted in an equilibrium cloud near the channel inlet due to the opposing forces of cross flow and particle diffusion rate as well as the strength of the focus flow. In this cloud, smaller particles with larger diffusion coefficients relative to bigger particles are higher relative to the accumulation wall and thus closer to the center of the channel in contrast to larger particles which accumulate closer to the membrane. The absolute thickness of this cloud (l) is defined as the ratio of the particle diffusion coefficient (D) and the induced velocity (U_V). For polydisperse samples, this can only be individually calculated for each population of particles (Baalousha et al. 2011). Flow velocities of cross flow (ν_c), detector flow (ν_d) and injection flow (ν_i) are specifically set to optimize particle fractionation, the focus flow (ν_f) results out of the latter to compensate channel inflow:

$$\nu_f = (\nu_c + \nu_d) - \nu_i$$

Typically ν_c varies between 1.0 and 3.0 mL/min, ν_d between 0.5 and 1.0 mL/min and ν_i between 0.1 and 0.5 mL/min (Dahlqvist et al. 2004; Gottselig et al. 2014; Gottselig et al. submitted; Neubauer et al. 2011; Nischwitz and Goenaga-Infante 2012). Therefore, ν_f is generally between 1.4 and 4.5 mL/min. During focusing, the sample is additionally subdivided into particulates and matrix

components with a molecular weight below membrane pore width, exiting the channel through the cross flow. These components below the nanometer range can potentially be assigned to the 'truly dissolved' phase (e.g. Martin et al. 1995).

Following equilibrium cloud relaxation during transition time (light blue, Figure 4.1.1a), focus flow is turned off and channel flow begins to elute the particles with increasing size regime. To compensate for the reduction in the volumetric flow along the channel and to keep the velocity of the longitudinal flow constant, the AF^4 channel has the shape of a trapezoid, decreasing in width from the channel inlet to the outlet (Baalousha et al. 2011) with the widest point close to channel inlet where focusing occurs. The longitudinal flow profile shows parabolic laminar flow with fastest flow lines at intermediate height of the channel (Figure 2.2). Due to the higher diffusion coefficient of smaller particles relative to the larger ones, smaller particles reach higher and thus faster flow rates, allowing them to elute first (functioning of normal fractionation mode). Therefore, particles eluting from the channel are in increasing size regime. During constant cross flow, the hydrodynamic particle diameter (d_H) can be calculated on account of retention time:

$$d_H = \frac{t_r(2kTV_d)}{\pi\eta w^2 V_c}$$

where t_r=retention time, k=Boltzmann's constant, T=absolute temperature, V_d=volumetric detector flow rate, η=dynamic viscosity of carrier liquid, w=channel thickness, V_c=volumetric cross flow rate (adapted according to Gimbert et al. 2003).

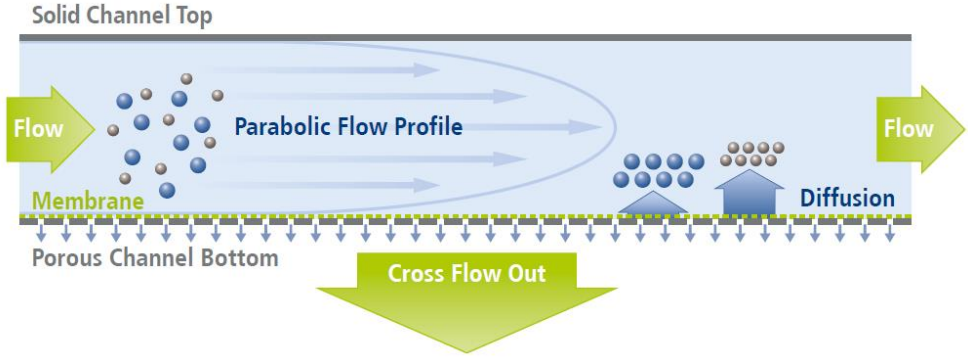

Figure 2.2: *Lateral cross section through the AF^4 channel showing the parameters responsible for natural nanoparticle and colloid elution in increasing size regime (from Postnova Analytics 2015).*

The strength of the separation field is decreased either linearly (dark blue, Figure 4.1.1a) or as a power function after focusing to achieve an elution of the complete size spectrum of particles in the sample. Thus, particle retention increases with decreasing diffusion coefficient and retention ratio (R) can be calculated according to the general AF^4 retention equation:

$$R = \frac{V^0}{V^r} = 6\lambda_r(coth\frac{1}{2\lambda_r} - 2\lambda_r)$$

where V^0=void volume, V^r=retention volume, λ_r=retention parameter (λ=l/w) (Baalousha et al. 2011). Further, the diffusion coefficient (D) can be calculated through the retention parameter (λ_r), the cross flow velocity (v_c), channel thickness (w) and void volume (V^0):

$$D = \frac{\lambda_r v_c w^2}{V^0}$$

To ultimately ensure the elution of all particles after the cross flow has decreased to 0 mL/min, an elution or rinse time at v_c=0 mL/min and set v_i=v_d is generally performed (green, Figure 4.1.1a).

The fractionation process can be optimized through the adjustment of variable AF^4 parameters. Next to the flow rates, these include the molecular weight membrane cut-off, membrane material, spacer thickness and eluent composition.

2.2 AF^4 hyphenation

The fractionation with AF^4 does not yield information about the particles by itself but through the online coupling to detectors (Figure 2.3). Multiple non-destructive detectors can be coupled online and in series to AF^4, whereas information from destructive detectors has to be gained through separate AF^4 fractionation runs (Figure 2.3). Most commonly the UV adsorption at single or multiple wavelengths is recorded directly after the separation channel. Briefly, in UV spectroscopy electromagnetic waves are emitted onto a sample, the valence electrons adsorb the energy and are excited to higher molecular orbitals. The loss of electromagnetic wavelength intensity is recorded after the sample passage and termed as UV absorption. Detectors for size determination can be static or dynamic, e.g. in Dynamic Light Scattering (DLS) in which the diffusive movement of particles under Brownian motion is transferred to the particle size using the Stokes-Einstein relationship:

$$D = \frac{kT}{6\pi\eta r}$$

where D=diffusion constant, k=Boltzmann's constant, T=absolute temperature, η=dynamic viscosity, r=radius. The latter detectors are all equipped with flow-through cells, facilitating an online coupling through the connection of PEEK (polyether ether ketone) tubing between the AF^4 separation channel and the series of detectors.

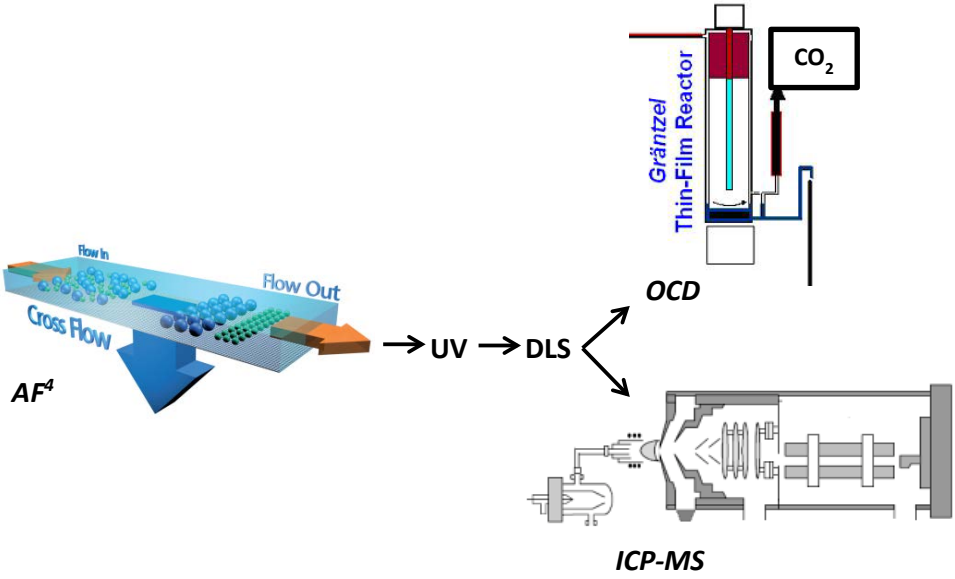

Figure 2.3: *Online hyphenation of AF^4 to non-destructive (UV, DLS) and destructive detectors (ICP-MS, OCD). (ICP-MS from European Virtual Institute for Speciation Analysis 2015; OCD from Huber 2015a; AF^4 from Postnova Analytics 2015).*

2.2.1 ICP-MS for sensitive elemental detection in the fractions

For precise determination of elemental concentrations of the separated particle fractions, inductively coupled plasma mass spectrometry (ICP-MS) has been established as a powerful analytical technique which can be hyphenated to AF^4 (for technical settings see Chapter 3.3). Liquid sample introduction to ICP-MS is performed via a nebulizer and spray chamber for desolvation of the sample solution. The sample aerosol generated by the nebulizer is homogenized in droplet size through the spray chamber and is transported by argon (Ar) as carrier gas to the inductively coupled plasma (ICP) where the analyte is ionized. The ionization potential of Ar (15.75 eV) is typically higher than of the element(s) in question. Initial ionization is created through a high voltage spark which produces free electrons that are accelerated by the applied radio frequency field causing collisions and ionization of the Ar gas. This collision-induced ionization of Ar continues in a chain reaction eventually forming the ICP

discharge. The desolved analyte is further vaporized, atomized and finally ionized through the ICP discharge. The degree of ionization or ionization efficiency (α, Vanhaecke 2012) varies depending on the element in question:

$$\alpha = \frac{n_i}{n_i + n_a} = \frac{\frac{n_i n_e}{n_a}}{n_e + \frac{n_i n_e}{n_a}} = \frac{K_{ion}}{n_e + K_{ion}}$$

where $n_i/n_e/n_a$=density (number of particles per unit volume) of ions/electrons/atoms, K_{ion}=ionization equilibrium constant. The ionization equilibrium constant depends majorly on the ionization potential of the respective element (Saha equation, Vanhaecke 2012):

$$K_{ion} = \frac{n_i n_e}{n_a} = \left(\frac{2\pi m_e k T_{ion}}{h^2}\right)^{\frac{3}{2}} \frac{2Z_i}{Z_a}\, e^{-\frac{IE}{kT_{ion}}}$$

where m_e= electron mass, k=Boltzmann's constant, T_{ion}=ionization temperature in the ICP, h=Planck's constant, Z_i/Z_a= partition functions for ionic/atomic state, IE=ionization potential. The typical ionization temperature of the ICP is 7500 K at an electron density of 10^{-15}cm^{-3} (Montaser et al. 1998). Near complete ionization (α≥0.9) is assured in the ICP up to an ionization energy of 8 eV (Becker 2007). For metalloids α is approx. between 0.3 and 0.8, for nonmetals <0.01 to 0.3 (Vanhaecke 2012).

After ionization, the plasma enters an interface to separate the ion beam from the free electrons. This separation is facilitated through a sampler and a skimmer cone confining stepped vacuum chambers. An average of 0.1% of the sample within the plasma reaches the ion optics in the high vacuum after the skimmer cone. These ion optics guide the ions to the mass analyzer through beam deflection and reject the nonionic species such as neutral species and photons. To further reduce double charged ions, oxides and most importantly polyatomic interferences, a collision or reaction cell allows highly efficient removal through introduction of the collision gas He or the reaction gas H_2. Thereafter, the targeted ions are separated according to their mass to charge ratio (m/z) by e.g. a quadrupole mass filter. A direct current (DC) field is applied on one pair of rods and a radio frequency (RF) field on the opposite pair, therefore ions of a selected m/z are allowed to pass through the rods in stable paths to the detector, while the others are ejected from the quadrupole. The potential of each pair of rods (P) can be calculated according to

$$P = U + V\cos(2\pi f t)$$

where U=DC potential, V=maximum amplitude, f=radio frequency current. The frequency f is fixed, and U and V can be chosen so that only ions having a specific m/z have stable paths through the

quadrupole. When U and V change along time while U/V is constant, P changes so that the targeted mass spectrum is scanned. The selected ions ultimately reach the measurement amplifier (electron multiplier) to divert the amplified signal to the detector.

2.2.2 Organic carbon detector (OCD) for precise organic C detection

To complete the setup of precise elemental concentration measurements, the organic carbon detector (OCD) allows sensitive online monitoring of the organic carbon concentration for liquid flow based separation systems (for technical settings see Chapter 3.3). In general, due to the large volume of the OCD, an offset in the elution time of AF^4 peaks and a peak broadening can be observed compared to e.g. ICP-MS detection.

The OCD setup is based on the Gräntzel thin-film reactor consisting of a cylindrical glass with an inner rotating glass cylinder equipped with short Teflon poles which evenly distribute the liquid sample on the inner wall of the outer cylinder (Figure 2.4). A low-pressure mercury lamp inside the inner cylindrical reactor radiates the UV light of which 82% is at a wavelength of 254 nm and 18% is at a wavelength of 185 nm. The longer wavelength attacks UV active areas in the molecule whereas the shorter wavelength UV irradiation produces OH radicals which react unspecific with organic molecules (Huber and Frimmel 1991). The reactor was continuously modified since its first prototype and is now suitable for the determination of organic carbon in the low µg/L range (Huber and Frimmel 1991). An inflow of acidification solution (2.5 g $K_2S_2O_8$ + 20 mL Suprapur® 85% H_3PO_4 acid in 5 L double distilled water, pH 1.5) constantly ensures a liquid flow in the reactor, acidifies the sample and supports organic carbon oxidation.

In a first step, inorganic carbon is removed from the sample through constant purging with counter current N_2 gas flow in a UV-light shielded section at the top of the reactor. The residence time of the solution in this area is approx. 20 s (Huber and Frimmel 1991). The stripped sample solution then enters the UV area and is exposed to UV radiation promoting an oxidation of organic molecules to CO_2. In this reactor, the principle of wet oxidation is applied. It utilizes the oxygen from the water itself for the oxidation of organic carbon. Through the radiolysis of water at 185 nm, oxygen radicals are formed, which are stronger oxidants than in common wet oxidation systems. The residence time of the solution in the UV exposed area is approx. 60 s (Huber and Frimmel 1991). Two thirds of the N_2 gas entering the reactor is used for stripping inorganic carbon, the remaining one third flows downwards and picks up the CO_2 released from organic carbon. Both gas flows then exit the main reactor and enter customized *Vigreux* condensers for moisture removal before separate CO_2 quantification. The condensers are mounted inside an insulated block which is cooled by Peltier elements to 8±0.1°C to ensure a steady emission spectrum and energy distribution.

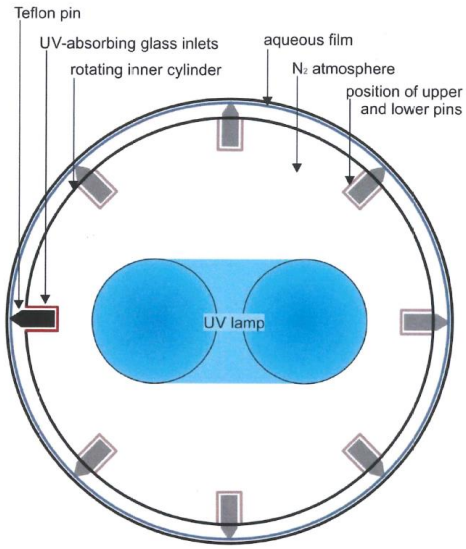

Figure 2.4: *Cross section of the UV exposed area of the OCD (from Huber 2015b). The UV lamp is installed in N_2 atmosphere and surrounded by the rotating inner cylinder. Upper and lower Teflon pins, installed in UV absorbing glass inlets to protect the Teflon from the UV light, are aligned on the inner cylinder which creates an aqueous film on the inner wall of the fixed outer cylinder.*

The gaseous carbon dioxide is quantified by high sensitivity non-dispersive infrared photometry. The detector measures the attenuation of the component specific wavelengths to determine the gas concentration. Intense infrared absorption of CO_2 occurs at λ=2.7 µm, λ=4.3 µm (Langley 1883) and at λ=14.7 µm (Rubens and Aschkinass 1898) (Figure 2.5), but the detector measures absorption only in the λ=2.5-8 µm wavelength range. This is due to the overlapping absorption wavelengths of water vapor and CO_2, which are most specific for CO_2 at 4.3 µm (Figure 2.5).

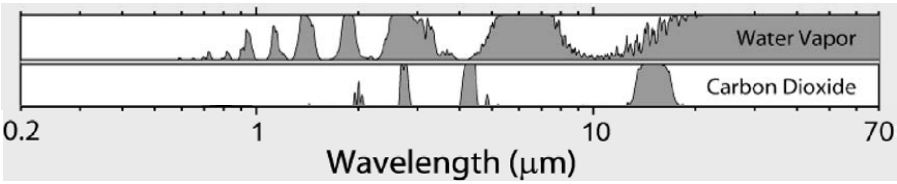

Figure 2.5: *Absorption bands of water vapor and CO_2 in the UV light (0.01-0.4 µm, shown: 0.2-0.4 µm), the visible light (0.4-0.7 µm) and the infrared light (0.7-1000 µm, shown: 0.7-70 µm). Grey areas indicate absorption peaks; y-axis scale in %, maximum y-axis value = 100% (based on data from Gordley et al. 1994; adapted from Rohde 2007).*

III

Materials and methods

3.1 Forested headwater catchments for stream water sampling

The sampling sites were chosen to reflect the upscaling approach of the thesis from the regional (Wüstebach) to national (Germany) to continental (Europe) scale. Furthermore, the Wüstebach catchment was selected as a common denominator of all studies.

3.1.1 Regional scale and common denominator site: Wüstebach[2]

The Wüstebach (W) is a forested headwater catchment at the southernmost outreach of the Rur catchment (Bogena et al. 2014). It is located within the National Park Eifel and is part of the TERENO (Terrestrial Environmental Observatories) Eifel/Lower Rhine Valley Observatory (Figure 3.1, Bogena et al. 2012; Zacharias et al. 2011). TERENO is a large-scale project aiming at monitoring the long-term impacts of environmental change at a regional scale. The site is a small sub-catchment of the River Rur basin and covers an area of ~38.5 ha (Stockinger et al. 2014). The lowest altitude of 595m in the northern part of the catchment increases to 628m in the south with a mean slope of 3.6 % and a maximum slope of 10.4 % (Bogena et al. 2010). The soil texture of the catchment is mainly silty clay

[2] More detailed information on the studies conducted at the experimental test site Wüstebach in the framework of the TERENO project can be found in:
Bogena HR, Bol R, Borchard N, Brüggemann N, Diekkrüger B, Drüe C, Groh J, **Gottselig N**, Huisman JA, Lücke A, Missong A, Neuwirth B, Pütz T, Schmidt M, Stockinger M, Tappe W, Weihermüller L, Wiekenkamp I, Vereecken H (2014) A Terrestrial Observatory Approach to the Integrated Investigation of the Effects of Deforestation on Water, Energy, and Matter Fluxes. Science China Earth Science 58:61-75.

Liu S, Herbst M, Bol R, **Gottselig N**, Pütz T, Weymann D, Wiekenkamp I, Vereecken H, Brüggemann N (2016) The Contribution of Hydroxylamine Content to Spatial Variability of N2O Formation in Soil of a Norway Spruce Forest. Geochimica et cosmochimica acta 178:76-86.

Gottselig N and Wiekenkamp I (mutual first authorship), Amelung W, Bogena HR, Bol R, Brüggemann N, Huisman JA, Klumpp E, Pütz T, Vereecken H. Soil Biogeochemistry in a Forested Headwater Catchment – A Three Dimensional View. Journal of Environmental Quality, in preparation.

loam with up to very high amounts of coarse materials (Decker 2010). The climate of the test site is humid temperate. The mean annual precipitation derived between 1961 and 1990 is 1107 mm and the mean annual temperature 7°C (Zacharias et al. 2011). The predominant vegetation consists of two types of coniferous trees: Norway spruce (*Picea abis*) and Sitka spruce (*Picea sitchensis*) (Etmann 2009). The bedrock are Devonian shales with partial sandstone inclusions which is covered by a 1-3 m thick periglacial solifluction layer in which on the hill slopes mainly Cambisols and Planosols/Cambisols and in the riparian zone Gleysols and Halfbogs have developed (Figure 3.1, Rosenbaum et al. 2012). According to the relation between 'dissolved' organic carbon (DOC) and nitrate content derived through the weekly sampling, the tributaries of the Wüstebach stream can be differentiated between groundwater based and overland flow based systems. The Wüstebach is a slightly acidic stream (pH 6.3±0.3, average±SD for 2015) and has a bed lined with mostly small gravels or stones. Tributaries showing high DOC content and in comparison low nitrate concentrations are influenced through significant overland flow input, tributaries showing low DOC content and in comparison high nitrate concentrations reflect a higher groundwater than overland flow input to the tributary.

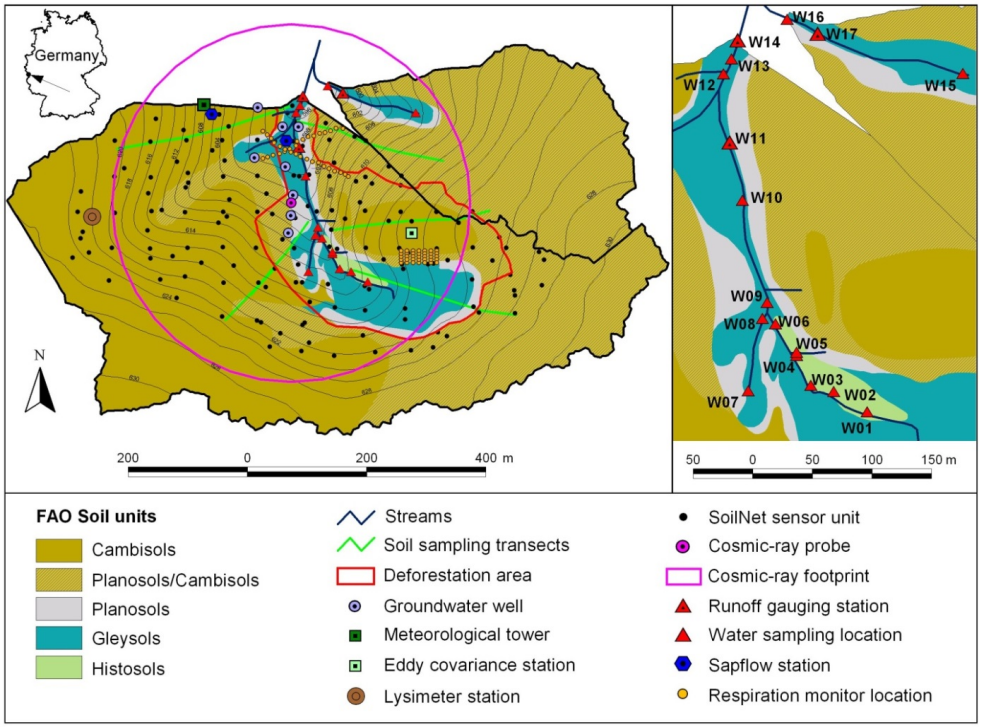

Figure 3.1: *Map showing major soil types and the instrumentation of the Wüstebach experimental catchment and the reference catchment as well as the deforestation area (from Bogena et al. 2014). The depicted stations and sites are all part of the frequent TERENO monitoring and data collection program.*

Currently, the Eifel National Park (authority responsible for managing the Eifel region) aims at a natural regeneration of beech trees from spruce monoculture forest that was originally established for timber production. Within this context, spruce trees were selectively clear felled to investigate the effects of such a disturbance on the functioning of the forest ecosystem in the Wüstebach catchment (Figure 3.1). A connected region of approximately 9ha with spruce vegetation was removed in the Wüstebach site in late August of 2013. This region encompasses the full riparian zone plus an adjacent area of brown earth.

3.1.2 Additional sites on national scale: Conventwald, Mitterfels, Vessertal, Leirelva

Conventwald (CON), Mitterfels (MIT) and Vessertal (VES) are 'Level II' sites (defines specific methods applied to long-term forest observation sites, http://www.forstliche-umweltkontrolle-bb.de) of the Intensive Long Term Monitoring Network of Forest Ecosystems across Europe that are investigated in the framework of the DFG priority program 1685. The forested sites dominated by European beech (*Fagus sylvatica*) are situated in Thuringia (VES), Bavaria (MIT) and Baden-Wuerttemberg (CON), Germany (Figure 3.2). The soil type of all three sites is Cambisol which show acidic soils and thus stream water pH values. Mean annual temperatures are 5.5°C (VES), 4.5°C (MIT) and 6.8°C (CON). The total annual precipitation is 1200 L/m² in VES (1995-2003), 1299 L/m² in MIT (1991-2009) and 1749 L/m² in CON (1997-2005). Bedrock types are paragneis (MIT, CON) and Trachyandesite (VES).

The site Leirelva (LEI) in Sør-Trøndelag is a forested site in Norway (Figure 3.2) dominated by coniferous tree species, which is monitored by the Institutt for vann- og miljøteknikk, NTNU, Trondheim, Norway. In contrast to Germany, Norwegian streams originate mainly from surface water because solid bedrock starts quickly below the thin soil layers. Further, in Scandinavia increased precipitation will lead to high surface runoff and erosion (Kronvang et al. 2007) and thus increased carbon input (Liski et al. 2002). Mean annual temperature is 5.0°C, total annual precipitation averages at 857 L/m² and bedrock type is gneiss.

3.1.3 European sites

The twenty-six sites of the continental scale study were chosen along two transects in Europe between Northern Finland and Portugal and between Scotland and Greece (Figure 3.2). The sites were as follows: Pallas (P) and Lettosuo (L), Finland; Krycklan (K), Norunda (N), Gårdsjön (G) and Aneboda (A), Sweden; Soroe (S), Denmark; Allt a'Mharcaidh (AM) and Cotley Wood (CW), United Kingdom; Wüstebach (W) and Bode (B), Germany; Lägeren (LÄ), Vogelbach (V), Lümpenenbach (LÜ) and Erlenbach (E), Switzerland; Franchesiello (F), Costiglione (C) and Piano Rabelli (PR), Italy; Agia (AG), Greece; Strengbach (SB) and La Peyne (LP), France; Ribera Salada (RS), Muntanyes de Prades

(MP) and Baranco de Porta Coeli (BPC), Spain; Sierra de Cima (SC) and Lourizela (LZ), Portugal. Each site is a forested headwater catchment with low forestry management practices and high tree coverage. Mean annual temperatures range between -1.4°C (Pallas, Finland) and 15.9°C (Franchesiello, Costiglione and Piano Rabelli, Italy) and total annual precipitation between 307.9 L/m² (La Peyne, France) and 2159.0 L/m² (Vogelbach, Switzerland) (Table 3.1). Information on the dominant tree type was available for 22 of the 26 sites. The site BPC has 50% coniferous and 50% deciduous tree species. For RS and MP no information on soil type was available; for AG, CW, MP, RS, S and SB no information on bedrock type was available.

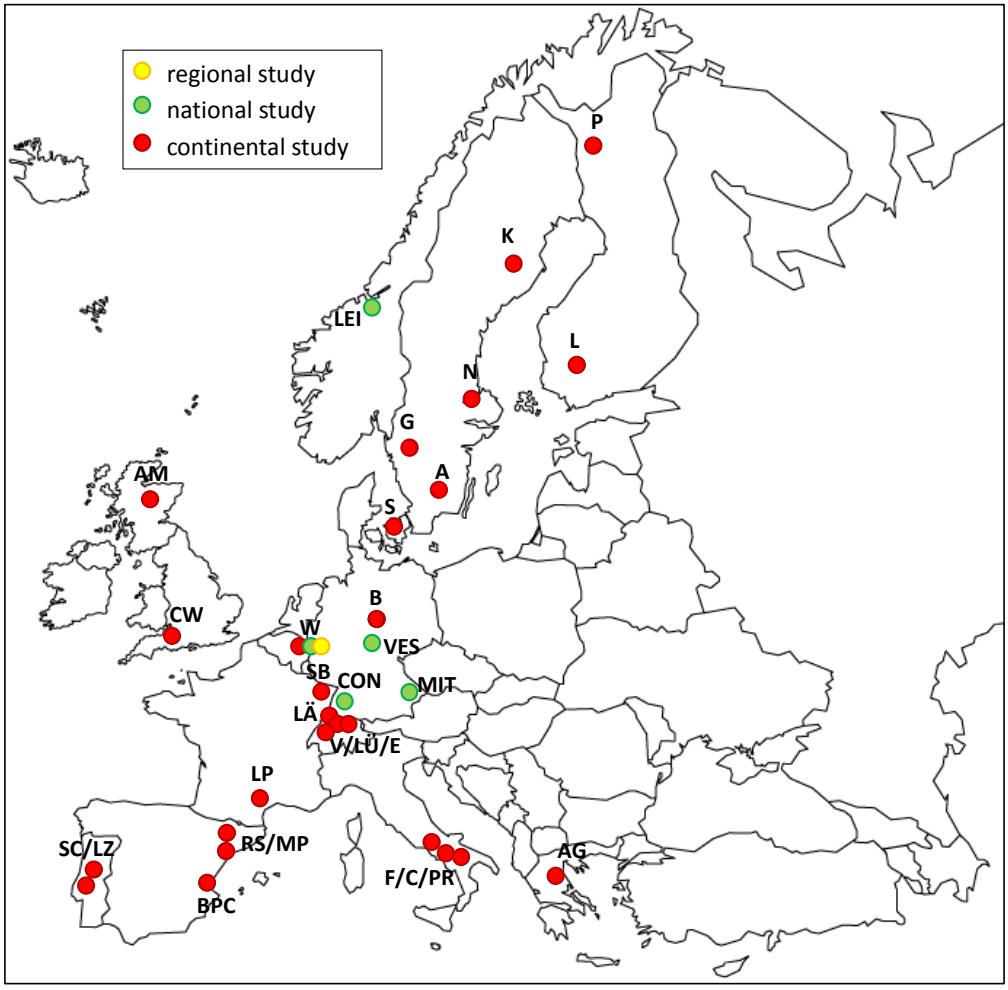

Figure 3.2: *Location of all sampling sites. Color coding according to the three projects conducted in the framework of the upscaling approach: yellow = regional, green = national, red = continental scale sampling. Site names to the abbreviations can be found in Chapter 3.1.1, 3.1.2 and 3.1.3. The continental scale study sites are aligned along two transects in Europe.*

Table 3.1: *Specific characteristics of each European site. Abbr. = site abbreviation, MAT = mean annual temperature, MAP = mean annual precipitation. Climate data, bedrock and soil type and vegetation cover provided by site operators. For site locations see Figure 3.2.*

site	abbr.	MAT	MAP	soil type	vegetation cover	bedrock type
Aneboda	A	5.8	750	Podzol	coniferous	granite
Agia	AG	15.8	690	Cambisol		
Allt a' Mharcaidh	AM	5.8	1110	Podzol	coniferous	granite
Bode	B	7.1	1600	Cambisol	coniferous	shale&greywacke
Barranco de Porta Coeli	BPC	14.5	450	Fluvisol	both	sandstone
Costiglione	C	15.9	1183	Cambisol	deciduous	carbonatic
Cotley Wood	CW	10.1	1044	Cambisol	deciduous	
Erlenbach	E	6.0	2294	Gleysol	coniferous	flysch
Franceschiello	F	15.9	1183	Cambisol	deciduous	carbonatic
Gårdsjön	G	6.7	1000	Podzol	coniferous	granite
Krycklan	K	1.8	614	Podzol	coniferous	graywacke
Lettosuo	L	4.6	627	Histosol	coniferous	gneiss
Lägeren	LÄ	8.4	930	Cambisol	deciduous	limestone
Muntanyes de Prades	MP					
La Peyne	LP	12.0	308	Leptosols	deciduous	schist
Lümpenenbach	LÜ	6.0	2426	Gleysol		flysch
Lourizela	LZ	13.8	1300	Cambisol	coniferous	schist
Norunda	N	5.5	730	Regosol	coniferous	granite
Pallas	P	-1.4	484	Podzol	coniferous	granite
Piano Rabelli	PR	15.9	1183	Cambisol	deciduous	carbonatic
Ribera Salada	RS	15.6	800		deciduous	
Soroe	S	8.5	564	Mollisol	deciduous	
Strengbach	SB	6.0	1400	Podzol	coniferous	
Sierra de Cima	SC	13.8	1300	Cambisol	deciduous	schist
Vogelbach	V	6.0	2159	Gleysol		flysch
Wüstebach	W	7.0	1220	Cambisol	coniferous	shales

3.2 Sampling and preparation

First investigations on the stability of NNP and colloids were conducted prior to the sampling campaigns to elucidate which sampling, storage and transport conditions are favorable to reflect natural conditions at the time of measurement. This resulted in a sampling of non-filtered stream water with Teflon or polypropylene containers; only samples for organic carbon analysis were taken with pre-cleaned and -equilibrated glass vials. For transport and storage the samples were kept at a cool (not frozen) and steady temperature not exceeding the stream water temperature at sampling. Sample analysis was conducted as soon as possible after sampling, especially for organic carbon analysis. For a more detailed discussion on circumstances affecting colloidal stability see Buffle and Leppard (1995).

The sampling was always conducted upstream from catchment outlet to source region with triplicate preconditioning of the containers before taking the actual sample from the center of the flowing stream water without disturbing the sediment. Larger sized parts (e.g. visible fractions of leaves) were not included in the water sample. At each sampling point, stream water pH, temperature and electrical conductivity was recorded in the flowing stream.

For the sampling on regional (Chapter 4.2) and national (Chapter 4.3) scale, pre-cleaned Teflon bottles (manufactured at Forschungszentrum Jülich) were used. For the continental study (Chapter 4.4), pre-cleaned polypropylene and glass container were shipped to the project partners for sampling. All samples were transported or mailed in a steady and cooled environment and stored at 4°C after reaching the laboratory. Directly prior to analysis, samples were homogenized through agitation and filtered through pre-rinsed 5µm cellulose nitrate filters (GE Healthcare, Munich, Germany) to avoid clogging of the micrometer-sized AF[4] tubing.

Regional scale sampling (Chapter 4.2): Samples were obtained in triplicates from points along the course of the Wüstebach stream (Figure 3.3) in beginning of August 2013. The majority of sampling points was selected according to the standard sampling procedure described in Bogena et al. (2014). The weekly standard sampling procedure in the framework of the TERENO project covers several stream points of which three were analyzed in this study: SP1 from the headwaters, the tributary T2, and SP3 at the outflow of the test site. SP2 is originally a tributary sampling point but was sampled as a stream flow point in this study to serve as an intermediate stream flow point. Additional points were added to specifically analyze sources of NNP and colloids from different hydromorphological stream areas. These were in the headwaters region and from regions along the stream with constant inflow through tributaries. The points are from a tributary in close vicinity to SP1 (T1) and two overland flow driven regions in the headwaters (OF1) and in the midst of the stream (OF2). The

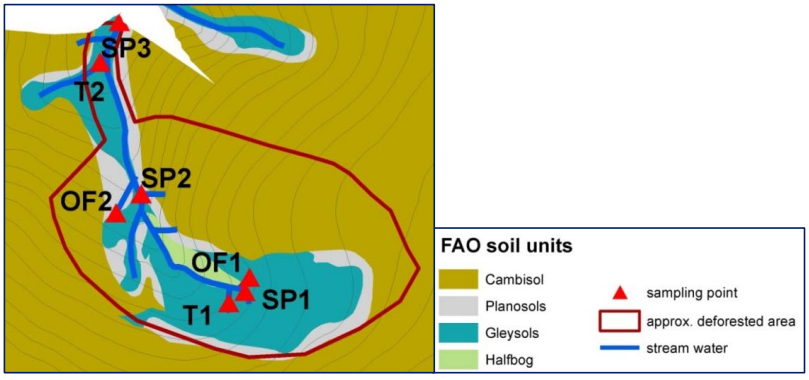

Figure 3.3: *Excerpt from the TERENO experimental test site Wüstebach with soil types, stream area, sampling locations and approximate deforested area. SP = stream point, OF = overland flow, T = tributary.*

tributary shows similar hydromorphology as the main stream bed but with a strong iron-coloring of the water; the overland flow driven regions show high turbidity and are not confined to a specific bed. On sampling day, water chemical parameters were 274.5±1.3 µS/cm electrical conductivity, pH 6.1±0.0, 4.6±1.7 V redox potential, 12.9±0.4 °C water temperature and a turbidity of 2.6±0.4 NTU. For measurements of Fe isotopic signatures, soil and vegetation samples were additionally collected from the catchment, details see 'Annex: Methods of sample digestion, Fe isotope extraction and measurements'.

National scale sampling (Chapter 4.3): Base flow stream water samples were collected during one week in mid-August 2014 from VES, MIT, CON, W and LEI to reflect peak summer conditions. In VES five samples, in MIT eight samples, in CON five samples, in W seven samples and in LEI four samples were collected. The 29 sampling locations were chosen according to findings in Gottselig et al. (2014) to reflect tributary and main stream flow from all sampled streams. At sampling, electrical conductivity at catchment outlet points was 39.9 µS/cm in VES, 21.2 µS/cm in MIT, 36.5 µS/cm in CON, 159.0 µS/cm in W and 119.2 µS/cm in LEI. Stream water pH values ranged between 5.8 (W) and 6.8 (LEI) and stream water temperature between 12.3°C (CON) and 14.9°C (LEI) (Table 3.2).

Table 3.2: *Stream water parameters at catchment outlet points of the national sampling. Abbr. = site abbreviation, T = stream water temperature [°C], cond. = electrical conductivity [µS/cm]. Site names see Chapter 3.1.2.*

abbr.	pH	T	cond.
CON	6.5	12.3	36.5
LEI	6.8	14.9	119.2
MIT	6.6	12.4	21.2
VES	6.4	12.6	39.9
W	5.8	13.6	159.0

For the analysis of the first flush effect, steam water samples from W, MIT and CON were sampled in high frequency intervals during storm events. At CON, additional rainfall, interception water, groundwater and throughflow water samples through three soil depths were collected to analyze further aqueous inputs that reach a stream.

Continental scale sampling (Chapter 4.4): A total of 96 samples with up to six samples per site were taken in the beginning of May 2015 to catch a view across streams in Europe. The majority of sites belong to long term monitoring projects, allowing a high degree of background information on the climatic and environmental factors. These factors include catchment size, average elevation, maximum and minimum elevation, average slope, forest cover, forest management status and mean annual runoff (Annex Table S3). Intense communication was conducted with the site operators before the sampling to specify sampling locations to best reflect main stream flow and tributary flow of each catchment as in Gottselig et al. (2014). During sampling water chemical parameters were

between 12.5 µS/cm (SB, France) and 1775.0 µS/cm (BPC, Spain), between pH 4.2 (G, Sweden) and pH 9.5 (RS, Spain) and between 1.0°C (P, Finland) and 19.9°C (RS, Spain) water temperature (Table 3.3).

Table 3.3: *Stream water parameters at each point of the continental sampling. Abbr. = site abbreviation, T = stream water temperature [°C], cond. = electrical conductivity [µS/cm]. Site names see Chapter 3.1.3.*

abbr.	pH	T	cond.	abbr.	pH	T	cond.
A1	4.7	7.8	47.2	LP1	7.2	14.0	618.0
A2	4.2	7.3	66.3	LP2	7.6	16.5	765.0
A3	4.4	8.2	56.1	LP3	6.7	14.1	369.0
A4	4.7	7.9	49.8	LÜ1	7.5	23.0	130.0
AG1	7.7	13.1	270.0	LÜ2	7.5	23.0	74.0
AG2	8.3	15.3	334.0	LÜ3	7.5	23.0	135.0
AM1	6.3	4.5	17.8	LZ1	6.2	14.0	24.1
AM2	6.3	4.5	17.4	LZ2	5.9	13.2	37.3
AM3	6.4	4.9	19.5	LZ3	6.3	13.7	36.0
AM4	6.4	5.5	28.9	LZ4	6.1	13.8	36.8
AM5	6.4	5.3	21.6	N1	6.7	7.2	94.0
B1	7.8	12.4	190.4	N2	6.5	8.4	86.0
B2	7.3	9.3	80.4	N3	6.8	8.6	87.0
B3	7.9	11.0	94.0	N4	6.9	9.4	89.0
B4	7.9	11.1	162.2	N5	6.8	9.5	148.0
B5	8.0	10.0	126.3	N6	7.1	10.7	85.0
BPC1	8.0	15.9	1712.0	P1	6.6	1.0	
BPC2	8.0	16.4	1775.0	P2	6.5	2.0	
C1	8.7	14.0	213.0	P3	6.6	3.0	
C2	8.2	14.0	338.0	PR1	8.2	14.5	393.0
CW1	7.0	9.7	129.4	RS1	9.5	17.0	411.0
CW2	7.1	9.8	117.1	RS2	8.4	19.9	418.0
CW3	7.0	9.9	125.8	RS3	8.2	15.4	537.0
CW4	6.4	10.4	180.9	RS4	8.2	15.9	404.0
E1	7.5	23.0	141.0	RS5	8.1	16.0	571.0
E2	7.5	23.0	75.0	RS6	8.2	16.1	441.0
E3	7.5	23.0	127.0	S1	7.9	10.4	591.0
F1	7.8	15.4	438.0	S2	7.5	9.7	739.0
F2	8.3	16.9	489.0	S3	7.5	10.9	675.0
F3	8.3	15.4	460.0	S4	7.2	11.3	600.0
G1	4.2	4.1	79.5	SB1	6.4	9.7	24.1
G2	4.3	4.1	84.2	SB2	7.0	13.0	24.7
K1	4.7		24.5	SB3	6.7	15.1	12.5
K2	4.3		21.2	SB4	7.3	12.1	28.4
K3	4.6		17.9	SB5	6.3	7.2	35.4
K4	4.5		23.8	SC1	6.4	13.2	27.2
K5	5.2		18.9	SC2	6.4	13.2	26.7
K6	6.1		21.7	SC3	6.6	13.7	29.3
L1	5.9	6.0	40.0	SC4	5.4	13.6	33.2
L2	4.8	5.0	30.0	V1	7.5	23.0	55.0
L3	4.9	6.0	30.0	V2	7.5	23.0	75.0
L4	5.0	5.0	40.0	V3	7.5	23.0	180.0
L5	4.8	5.0	30.0	V4	7.5	23.0	124.0
LÄ1	7.8	10.3	410.0	W1	5.0	12.7	292.0
LÄ2	8.2	10.6	404.0	W2	7.0	12.3	137.0
LÄ3	7.3	8.7	408.0	W3	6.7	11.9	189.0
LÄ4	7.6	8.8	408.0	W4	5.9	10.9	298.0
MP1	8.2	15.1	118.9	W5	7.1	11.7	190.0

3.3 Analytical approach for the analysis of natural nanoparticles and colloids in forest stream waters

Fractionation of natural nanoparticles and colloids in stream waters was performed with Asymmetric Flow Field Flow Fractionation (AF^4) using a metal-free AF2000 system (Postnova Analytics, Landsberg, Germany) including autosampler and channel oven. AF^4 was coupled online to an inductively coupled plasma mass spectrometer (ICP-MS) and also to an organic carbon detector (OCD). Table 3.4 shows an overview of the AF^4 parameters which were used for the different projects as well as the technical parameters and settings for ICP-MS and OCD. Fractionation conditions were developed prior to the catchment studies and refined as this study progressed. For AF^4 method developments see Chapter 4.1.

ICP-MS calibration was performed through a multi-point linear calibration injected at 0.5 mL/min AF^4 channel flow. Mixed element calibration standards were prepared from commercial single-element stock solutions (NIST certified ICP-MS standards). AF^4 autosampler calibration standards (0 µg/L, 5 µg/L, 10 µg/L and 25 µg/L) were dissolved in the AF^4 eluent and injected via the complete hyphenated system. For a post-column calibration (Nischwitz and Goenaga-Infante 2012) the standard solutions (0 µg/L, 25 µg/L, 100 µg/L, 250 µg/L and 500 µg/L) and the internal standards Rh and Y are dissolved in 0.5 mol/L HCl and injected via a T-piece between the AF^4 and the ICP-MS. The variation of the ICP-MS peak area for triplicate measurements of a representative sample was calculated to be 5.9% for P, 7.6% for Al, 14.0% for Si, 5.3% for Mn and 15.6% for Fe. The limit of detection was 0.1 µg/L for P, 0.01 µg/L for Al, 3.3 µg/L for Si, 0.01 µg/L for Mn and 0.02 µg/L for Fe. Quantitative atomization of the particles in the plasma was assumed based on Schmitt et al. (2002).

While P measurements of stream water NNP and colloids were achieved earlier using high resolution ICP-MS techniques (e.g. Regelink et al. 2013; Stolpe et al. 2005), this study acquired measurements with a quadrupole instrument. The utilized method is applicable to routine analysis and detects low P concentrations through the use of the collision cell technology (Gottselig et al. 2014). It should be noted that through AF^4-ICP-MS coupling, no information on the speciation of P is gained apart from the particle size. Through this analytical approach phosphorus is measured as elemental P, but can be present as any binding form (species) of phosphorus (see also Spivakov et al. 2009).

The OCD system was calibrated using dilutions of Certipur® liquid TOC standard (EN 1484-H3/DIN 38409-H3, Potassium hydrogen phthalate in water, stabilized, 1000 mg/L; Merck Millipore 109017) in double-distilled water at concentrations of 0.05 mg/L, 0.1 mg/L, 0.5 mg/L, 1.0 mg/L, 3.0 mg/L and 5.0 mg/L. The relative standard deviation of the organic carbon concentration for triplicate

measurements of a representative sample was calculated to be 2.2%. The limit of detection for organic C was 0.01 mg/L.

Table 3.4: *Overview of AF^4, ICP-MS and OCD settings and parameters for the analysis of natural nanoparticles and colloids in forest stream waters. KED= Kinetic energy discrimination (bias voltage of the quadrupole mass filter), DLS = dynamic light scattering, RC = regenerated cellulose, PES = polyether sulfone.*

AF^4	*regional project*	*national & continental project*
eluent	10 mM NaCl	25 µM NaCl
membrane	10 kDa RC	1 kDa PES
spacer	500 µm	500 µm
injection volume	ICP-MS: 5 mL	ICP-MS: 5 mL, OCD: 1 mL
injection flow	0.2 mL/min	0.3 mL/min
cross flow	3 mL/min	3 mL/min
channel flow	0.5 mL/min	0.5 mL/min
focus time	ICP-MS: 30 min	ICP-MS: 30 min, OCD: 10 min
UV wavelength	254 nm	254 nm
DLS device	Zetasizer Nano ZS (Malvern Inst., Malvern, UK)	Zetasizer Nano ZS (Malvern Inst., Malvern, UK)
Agilent 7500 settings	*all projects*	
nebulizer	MicroMist	
min. nebulizer flow	0.4 mL/min	
spray chamber type	double pass spray chamber	
gas mode	He collision gas, 4 mL/min	
carrier gas flow	0.86 mL/min	
cone material	nickel	
cooling temperature	4°C	
elements & integration times	Al, Ca, Mn Fe: 0.2 s, Si: 0.4 s, P: 0.8 s	
RF power	1500 W	
KED	2 V	
OCD		*national & continental project*
carrier gas		Nitrogen 5.0; 12 L/h
acidification solution		2.5 g $K_2S_2O_8$ + 20 mL orthophosphoric acid 85% in 5 L double distilled water
CO_2 analyzer		Infrared Photometer AO2020 Uras26 (ABB, Zurich, Switzerland)
measurement range		1-5000 ppb
detection limit		< 5-50 ppb (compound specific)
UV lamp		low pressure mercury lamp
cooling temperature		8°C
rotor speed		350 rpm
liquid volume		2-3 mL
sample residence time		1-3 min
exposed area UV		600 cm^3
exposed area stripping		250 cm^3
thickness of aqueous film		0.1-0.2 mm
wavelengths		254 nm (82%), 185 nm (18%)

3.4 Analysis of fraction specific elemental data

ICP-MS raw data were collected in counts per second (cps) using MassHunter Workstation Software (Agilent Technologies, Japan) and OCD raw data were recorded in volts detector signal (V) with the AF^4 analytical software (Postnova Analytics, Landsberg, Germany). Raw data were exported to Excel® (Microsoft Corporation, Redmond, USA) for baseline correction, peak integration and conversion of peak areas to concentrations through multipoint linear calibration. The 'total concentration' reflects the elemental concentrations of a stream water sample post filtration but prior to fractionation with AF^4. The '(total) particulate concentration' is defined as the sum of the concentrations in all particle fractions per element. Further, the elemental distribution in the NNP and colloids respective to the total elemental concentration, as well as the potential predictability of NNP and colloidal composition was analyzed. The difference between the 'total concentration' and the '(total) particulate concentration' can potentially be assigned to the 'dissolved' concentration. All determined elemental concentrations of the particle fractions were transformed to the unit mol/L prior to data processing and exploratory data analysis to serve for comparison on the basis of potential binding and substance amounts. The results are discussed regarding the relevance of NNP and colloids for P transport and thus cycling in ecosystems at various sampling sites. Predictability of elemental concentrations through total and other particulate concentrations was assessed through $\log_{10}$ transformation of the data. A useful prediction was determined at an $R^2 \geq 0.50$ which reflects a prediction certainty ≥50%.

The disagreement over the preferential binding partners of P in the different size fractions as found in the literature is due to the fact that the statements about P speciation are made on account of the maximum likelihood of P binding in the fractions, yet they need further validation through the application of exploratory data analysis techniques (Chapter 4.3 and 4.4). For exploratory data analysis, cluster analysis is applied to the quantitative element distribution obtained for the separated particle size fractions in order to identify fraction specific preferential binding of phosphorus to NNP and colloidal building block elements. Agglomerative cluster analysis with distance measure based on the Pearson correlation coefficient was performed with STATISTICA for Windows, Version 12.0 (StatSoft Inc., Tulsa, USA). In contrast to statistical significance testing, the cluster analysis uses algorithms which are grouping the parameters with highest similarity based on the available samples at the start of analysis. Onwards, the threshold regarding the decision when to declare two or more objects to be members of the same cluster is lowered. This results in clusters as commonly known in genetic analysis phylogenetic trees, where the distance measures between clusters reveals the genealogy of sequenced species.

Further, discriminant function analysis with canonical correlation as measure of effect size (JMP 12.2.0, SAS Institute Inc., USA) was used to determine the effect of the categorical dependent variable pH classification on the NNP and colloidal composition. Discriminant analysis is a method of predicting a level of a one-way classification based on known values of the responses, therefore the technique is based on how close a set of measurement variables are to the multivariate means of the levels being predicted. This type of analysis is used when specific data groups are set beforehand like in this case the stream water pH classification according to the Soil Survey Division of the Natural Resources Conservation Service, U. S. Department of Agriculture (1993). According to this classification, acidic is defined as pH<6.6, neutral pH between 6.6 and 7.3 and alkaline pH values >7.3. The canonical correlation is similar to the eigenvalue, yet is the square root of the ratio of $SS_{between}$ and SS_{total} (SS=sum of squares). In contrast to the discriminant function analysis, cluster analysis aids to determine the categorical variables.

To relate the elemental concentration per particle fraction of the continental scale project to the environmental parameters potentially driving the presence of the elements in the fractions, initially an assessment of the single effects of the environmental parameters was performed. Spearman rank order correlation was performed with Statistica (Version 13.0, Dell Inc., USA). Correlations were validated through randomization tests in R (Version 3.2.3, R Foundation for Statistical Computing, Vienne, Austria) with 10000 repeats; the random probability of valid correlations was set at below 5% of the maximum coefficient probability. Further, path analysis, a subtype of structural equation modelling (c.f. Grace 2006; Grace and Pugesek 1998; Suhr 2008), was performed with the lavaan package in R (Version 3.2.3, R Foundation for Statistical Computing, Vienne, Austria) to identify the relationships between the explanatory environmental parameters and the elemental concentrations per fraction which eventually influence P binding to NNP and colloids. In path analysis, the dependencies between a set of variables is modelled to describe their predicted influences on each other. The pathways between two variables represent linear relationships after data transformation to Gaussian distributions. No transformation was necessary for MAT (1^{st} and 2^{nd} fraction) and water pH (3^{rd}), square root transformation was performed for MAP (1^{st} and 2^{nd}) and P (1^{st}, 2^{nd}, 3^{rd}) and water temperature (3^{rd}), $\log_{10}$ transformation was performed for org C (1^{st} and 2^{nd}) and Fe (1^{st}, 2^{nd}, 3^{rd}) and catchment size (1^{st}). In a first step, an assumption on the potential influential pathways is conducted. This assumption is tested, whereas a highly neglected assumption yields a highly probable value of the model. An evaluation of the model then reveals which pathways are significant and which are non-significant. Despite the presence of non-significant pathways, a resulting model can only be valid with these pathways.

IV

Results and discussion

4.1 Method development for precise fractionation of natural nanoparticles and colloids and elemental detection in the fractions[3]

4.1.1 Parameter optimization for Asymmetric Flow Field Flow Fractionation

The variability and particle-size range of natural nanoparticles and colloids in environmental stream water samples is high, and thus the AF^4 channel and elution parameters have to be chosen to allow monitoring of a large spectrum of nanoparticles and colloids regarding size, morphology and composition. This chapter aims at briefly presenting the decision process for choosing specific fractionation conditions and the reasoning behind the ultimately applied AF^4 parameters for environmental samples. The precise settings and parameters for AF^4 and online detection can be found in Table 3.4. In depth details regarding the selection of specific parameters and their influence on peak retention times and particle recovery can be found in the Field Flow Fractionation Handbook (Schimpf et al. 2000) and in Chapter 2.1. Detailed information for optimizing elemental detection can be found in Chapter 2.2.

Basic AF^4 parameters include the selection of carrier solution, the membrane and the channel height. For carrier solutions, recent AF^4-ICP-MS studies on aquatic colloids used a phosphate solution (Plathe et al. 2013) or hydrogen carbonate (Regelink et al. 2013) buffer solutions. However, when focusing on the online detection of P and also organic C, a carrier with low blank concentrations of these elements is required. Besides maintaining the size and elemental composition of the NNP and

[3] Excerpts published in a peer-reviewed journal:
Gottselig N, Bol R, Nischwitz V, Vereecken H, Amelung W, Klumpp E (2014) Distribution of Phosphorus-Containing Fine Colloids and Nanoparticles in Stream Water of a Forest Catchment. Vadose Zone Journal 13:1-11. Permission granted by Soil Science Society of America.

colloids of interest, the interaction with the membrane needs to be minimized for high recovery rates, and compatibility with online detection by ICP-MS and OCD needs to be ensured. Sodium chloride, commonly used for AF^4 bovine serum albumin analysis (e.g. Sohmen et al. 2012), was chosen as the best compromise. Membrane type and molecular weight cut-off (MWCO) influence the lower size cut-off of the nanoparticles and the interaction of the sample with the membrane. A 10 kDa regenerated cellulose (RC) membrane showed best sample recovery in previous studies with AF^4 (e.g. Hagendorfer et al. 2011). Baseline stability and avoiding pressure induced baseline drifts are facilitated through the use of a higher MWCO, yet, compared with lower MWCOs (1 kDa or 300 Da), the smallest nanoparticle fraction (<2 nm hydrodynamic diameter, Erickson 2009, equation 2.2) can be lost during the fractionation process. Through optimization of the AF^4 channel pressure during fractionation, baseline stability, clear peaks and good detection limits were achieved also through the application of the 1kDa polyether-sulfone (PES) membrane without losing a part of the smallest fraction (Regelink et al. 2013; Stolpe et al. 2010). Beside the carrier solution, the quality of the particle separation will be determined by the space given for diffusion which is adjusted through the height of the channel (= spacer thickness). Higher channels have to be utilized to allow ideal retention and separation of particles of a broad size range present in environmental samples, especially when wanting to include the low nanometer range. Along with the increased thickness of the equilibrium cloud when fractionating a broad particle size range, the necessity of high cross flows (3 mL/min) for the fractionation of NNP in the low nm range require a high spacer of 500 µm (Loeschner et al. 2013; Schimpf et al. 2000).

The flow regime programmed for the AF^4 is the heart of the NNP and colloid fractionation (Figure 4.1.1a). First approaches for FFF based fractionation of aquatic colloids (Andersson et al. 2006; Dahlqvist et al. 2004; Jarvie et al. 2012; Stolpe et al. 2010) provide a basis for the development of a suitable fractionation regime. Due to the low concentration of particles in the stream water samples, a large sample volume has to be injected into the AF^4 channel. At injection flows of 0.2 to 0.3 mL/min, the focus time has to be adjusted to transport the complete sample volume into the channel, to separate the matrix from the particles and allow sufficient time for equilibrium cloud formation and relaxation. In addition, the cross flow selected during focusing has to ensure a separation of particles with a few nanometers diameter from the (ideally marginal) void peak (Figure 4.1.1b). The void peak typically includes non-fractionizable residuals of the samples which can largely be avoided through appropriate adaption of the focus time. After focusing, NNP and colloid separation is achieved through application of a decreasing cross flow gradient over time. A linear decrease in cross flow over a variable time period is the most universally applicable separation pattern (e.g. Regelink et al. 2014) leading to a non-linear increase in size regime of NNP and colloids.

To ensure complete sample elution, especially for aluminosilicate mineral particles of flat morphology with low degrees of freedom, subsequently a detector flow rate of 0.5 mL/min (v_i=v_d, no cross flow) is necessary at the end of a fractionation. The exact same fractionation parameters have to be utilized for all samples to ensure comparability, yet this poses a difficulty for environmental samples due to their variable nature. A detector flow rate of 0.5 mL/min has been found to be reasonable (Stolpe et al. 2010) to ensure sufficient transit time for the UV-*vis* detector, DLS and to ensure easy coupling to ICP-MS and OCD.

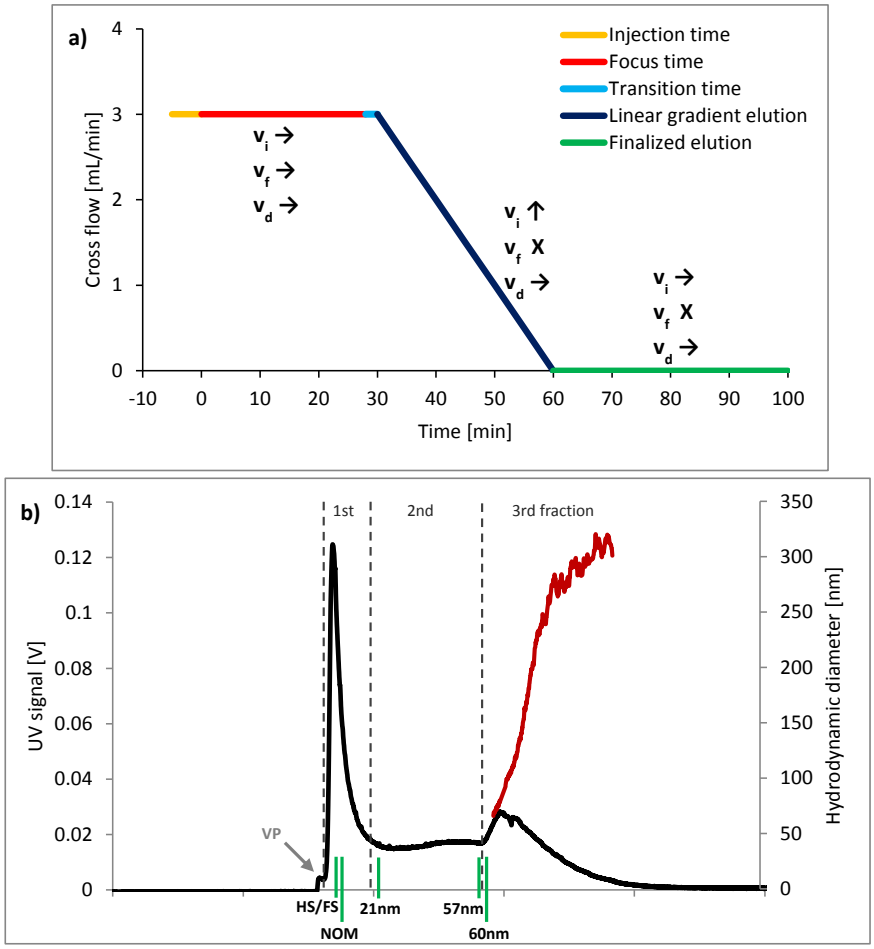

Figure 4.1.1: *a) Flow regime of the developed AF^4 run meeting all requirements for the separation of natural nanoparticles and colloids. Color coding according to different steps defined in the run, for details of the steps see Chapter 2.1. Injection flow (v_i), focus flow (v_f) and detector flow (v_d) are depicted during focus time, linear gradient elution and finalized elution. → = constant, ↑ = increasing flow, X = no flow. During linear gradient elution injection flow compensates decreasing cross flow. b) Exemplary UV (primary y-axis) and DLS signal (secondary y-axis) showing the three fractions, the peak elution times of standard reference material (green lines, HS = Suwanee River Humic Acid II, FS = Suwanee River Fulvic Acid II, 21 nm/57 nm/60 nm = Latex standard in the respective sizes) and the separation of the void peak (VP) and. DLS signal was used to determine the size of the 3rd fraction.*

Reference materials (Suwanee River NOM, Humic Acid Standard II and Fulvic Acid Standard II, International Humic Substances Society, Denver, USA; Sulfate Latex Standards 8% w/v 21 nm-630 nm; Postnova Analytics, Landsberg, Germany) were used with the same AF^4 conditions used for the samples for calibration of the particle diameters included in each size fraction (Figure 4.1.1b). No reference material exists which covers the divers particle morphologies and elemental concentrations of environmental samples. Therefore, the specified hydrodynamic diameters of the particles are equivalent sizes to the elution time of the reference materials. The lower size range of the first fraction was estimated according to the MWCO of the membrane. The technique of dynamic light scattering was applied for online size measurements of especially the largest size fraction (Figure 4.1.1b). Blank runs inserted between sample runs in the measurement sequence showed no significant peaks.

4.1.2 Facilitating online elemental detection of environmental samples

For size resolved detection of NNP and colloidal Al, Si, P, Ca, Mn and Fe a quadrupole ICP-MS with collision cell technology (Agilent 7500, Agilent Technologies, Japan) was coupled online to the AF^4. The ICP-MS became attuned to the specialized low concentration measurements through the usage of a MicroMist nebulizer, He as collision gas and uniquely adjusted integration times per element (Table 3.4). For sensitive P detection, essential settings are a sufficiently high RF power due to the relatively high ionization energy (10.48 eV) of P and an elongated integration time of 0.8 s due to the low concentrations in aqueous samples. To some extent, Si and Ca are also challenging elements especially when operating online with AF^4 due to the high background levels in environmental samples. Sample storage and AF^4 preparation were key variables to ensure especially low background levels of Si.

Two types of calibration approaches, each with unique advantages can be utilized. Calibration standards dissolved in the AF^4 eluent and injected via the AF^4 autosampler through the complete hyphenated system reflect element specific interactions occurring in the AF^4 fractionation channel. For a post-column calibration (Nischwitz and Goenaga-Infante 2012) on the other hand, the standard solutions and internal standards are injected via a T-piece between the AF^4 and the ICP-MS. This calibration technique is more complex in its application, yet allows more precise correction of instrumental drift and calibration to higher concentrations without potentially contaminating the following sample because the standards do not pass through the AF^4 system.

An approximation of the concentration of 'dissolved' organic material (DOM) in the NNP and colloidal fractions can be determined through the respective UV-*vis* signal at 254 nm (Figure 4.2.2, Neubauer et al. 2011). Due to carbon being the major constituent in DOM (Cabaniss et al. 2005), the

technique of Neubauer et al. (2011) can be applied as a proxy for the organic C content of the sample fractions. Neubauer et al. (2011) precisely analyzed the signal of various detectors coupled online to AF^4 and showed that the UV-*vis* signal at 250 nm or 254 nm (more commonly used) represents organic material in the fractions. The technique of the organic carbon detector (DOC Labor, Karlsruhe, Germany) coupled online to the AF^4 is a more promising tool for the precise measurement of organic C which also helped to overcome the compound dependent response for carbon in UV detection, for example failing to detect organic acids (Reszat and Hendry 2005). Further, the common offline TOC detector cannot cope with the low volumes and low concentrations of the particle fractions, thus severely multiplying the effort when several fraction collection steps per samples become a necessity. The OCD system has usually been applied to operationally defined 'dissolved' organic carbon. Huber et al. (2011) confirmed an oxidation rate of almost 100% for sample constituents below 0.45 µm. Due to the high sensitivity of the OCD, for AF^4-OCD coupling approximately one fifth of the sample volume needed for ICP-MS detection is necessary (Table 3.4). Therefore, the AF^4 focus time can be shortened to compile with the lower injected sample volume (Table 3.4). The calibration standards (see Chapter 3.3) were also used for the determination of total organic carbon in the stream water samples. For this, the AF^4 channel was bypassed by connecting the tip inflow tubing to the detector outlet tubing of the channel. The runtime of the AF^4 method for this data acquisition took 20 min at 0.5 mL/min tip flow.

4.1.3 Methodological considerations of organic carbon detection and for assessing the bioavailability of natural nanoparticles and colloids

4.1.3.1 Oxidation efficiency of the organic carbon detector[4]

While the OCD method is established for 'dissolved' organic matter (<0.45 µm), especially as detector of a size-exclusion chromatography (Huber et al. 2011), it remains unclear if the same is true for organic nanoparticles having a size smaller than 450 nm. Potentially a size dependent oxidation of organic matter occurs when aiming at a precise detection of the organic C content of the particle fractions. A recent study utilizing a modified total organic carbon (TOC) analyzer as an online organic C detector for a FFF showed highly reproducible results through the OC detector and the UV (Reszat and Hendry 2005). To similarly test the application of the OCD, the recovery of online carbon detection in polymers and organic nanoparticles was evaluated in a first trial. For this purpose selected standard reference materials were injected into AF^4-UV-OCD without performing fractionation. These standard materials were polystyrene sulfonic acid (PSS) with molecular weights

[4] Contains data from:
Meyn T, **Gottselig N**, Missong A, Klumpp E. Oxidation Efficiency of Online Carbon Detection for Polymers and Nanoparticles, in preparation.

of 3 kDa, 33 kDa, 305 kDa and 976 kDa (Postnova Analytics, Landsberg, Germany), pullulan (PUL) at molecular weights of 6 kDa, 21 kDa, 200 kDa and 708 kDa (Postnova Analytics, Landsberg, Germany), Suwanee River Humic Acid II and Suwanee River Fulvic Acid II (International Humic Substances Society, Denver, USA), sodium alginate (Sigma Aldrich, St. Louis, USA), polymethyl methacrylate (average size 100 nm, Postnova Analytics, Landsberg, Germany) and polystyrene latex beads with average diameters at 21 nm and 100 nm (Postnova Analytics, Landsberg, Germany). A further environmental sample, a soil extract from an organic soil horizon, was also included in the analysis to reflect the oxidation efficiency of the OCD also for naturally occurring particles. All samples were diluted with double distilled water to achieve a concentration of 1 mg/L organic C in 100 mL. Aliquots of these solutions were then analyzed in a commonly used TOC, via online injection on the OCD and via online injection in a UV detector (254 nm). OCD and UV were calibrated with the Certipur® liquid TOC standard (EN 1484-H3/DIN 38409-H3, Potassium hydrogen phthalate in water, stabilized, 1000 mg/L; Merck Millipore 109017) diluted with double-distilled water at concentrations of 0.05 mg/L, 0.1 mg/L, 0.5 mg/L, 1.0 mg/L, 3.0 mg/L and 5.0 mg/L. Both calibrations yielded R^2 values of 0.99. The TOC value was used as the basis of the organic carbon concentration and the recovery of OCD and UV was calculated on account of the TOC value.

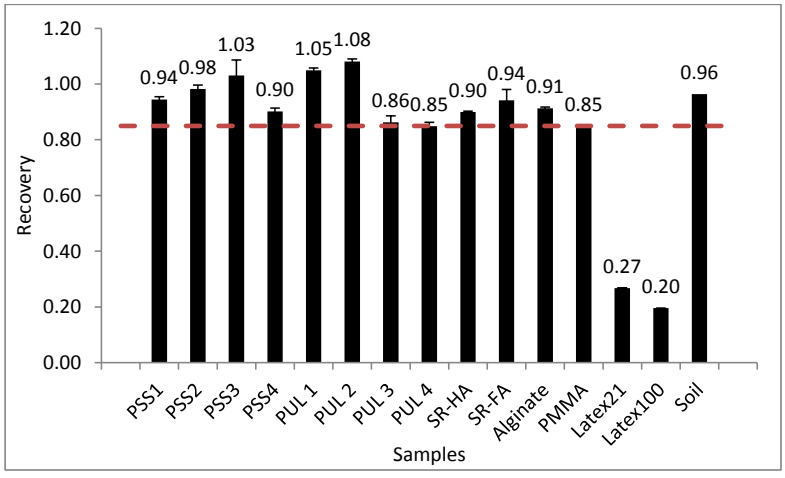

Figure 4.1.2: *OCD recovery from TOC measurements. Displayed is mean recovery ± standard deviation of triplicate measurements of all standards. Red dashed line indicates minimum average recovery of all standards except Latex21 and Latex100. PSS = polystyrene sulfonic acid, PUL = pullulan. PSS1 = 3 kDa, PSS2 = 33 kDa, PSS3 = 305 kDa, PSS4 = 976 kDa, PUL1 = 6 kDa, PUL2 = 21 kDa, PUL3 = 200 kDa, PUL4 = 708 kDa, SR-HA = Suwanee River Humic Acid II, SR-FA = Suwanee River Fulvic Acid II, PMMA = polymethyl methacrylate, soil = soil extract.*

The results showed that with the exception of the polystyrene latex beads, the OCD recovery with respect to the TOC data is 94±0.08% at a minimum recovery of 85% (Figure 4.1.2). Especially the environmental sample yielded excellent recovery of the TOC measurements at 96±0.0%. The data did not reflect a consistent decrease in OCD recovery as PSS or pullulan sizes increased. For the latex 21 nm and 100 nm samples, 27% and 20% OCD recovery, respectively, was found. In contrast to the OCD recovery, the UV recovery of the TOC values for all samples was 0.40±0.68%. For common chromophore compounds such as Suwanee River Humic Acid II and Fulvic Acid II, the UV recovery is 62% and 247%, respectively. Yet, to make precise statements on the UV recovery from TOC data, a further evaluation should be performed.

The trials on the recovery of OCD respective to the TOC data were positive and yielded a good recovery of the OCD around 94% without reflecting a size dependent oxidation of organic C in the OCD. The OCD recovery of the latex particles is not in line with the other standards, yet they do not reflect a relevant environmental component. Therefore, the latex results are not meaningful for the interpretation of stream water or soil extract measurements.

4.1.3.2 Organic carbon detection through ICP-MS[5]

Gaining elemental data from ICP-MS and OCD after particle fractionation is a laborious procedure involving two fractionations of the same sample, one for OCD data and one for ICP-MS data. In theory, the ICP-MS has the potential to monitor carbon in addition to metals and phosphorus and in spite of carbon being one of the key elements in living organisms and environmental processes including climate the potential of ICP-MS for carbon determination has hardly been investigated utilized. Therefore, investigations on the potential of ICP-MS for carbon measurements were conducted, avoiding the effort for isotope dilution, to establish a routine AF^4-ICP-MS method for simultaneous monitoring and quantification of all relevant elements of environmental particles.

The use of ICP-MS for carbon monitoring has been reported by Vogl and Heumann (1998) for chromatographic fractions of humic substances using isotope dilution technique for quantification. This initial study demonstrated species-independent ionization of carbon for three compounds with a molecular weight range from 198 Da to 20000 Da. Luong and Houk (2003) applied a modified dual detector ICP-MS for carbon isotope ratio measurements in aqueous solutions of amino acids, proteins and oligosaccharides. Application of ICP-MS for carbon isotope ratio measurement was reviewed by Santamaria-Fernandez (2010). Smith et al. (2004) investigated the feasibility of using

[5] Contains excerpts from:
Nischwitz V, **Gottselig N**, Missong A, Meyn T, Klumpp E. Field Flow Fractionation Online with ICP-MS as Novel Approach for the Quantification of Particle-Bound Carbon in Stream Water Samples and Soil Extracts. Journal of Analytical Atomic Spectrometry Special Issue on Speciation Analysis, under review.

liquid chromatography online with ICP-MS for detection of low molecular weight organic compounds via the carbon signal. The results indicated that the carbon signal from ICP-MS is proportional to the carbon content of the investigated compounds and thus quantification is possible via external calibration. In spite of the promising results from these initial studies, organic carbon monitoring by ICP-MS has been rarely applied. Recently, ICP-tandem mass spectrometry was employed for carbon determination in plant digests, amino acids and peptides monitoring $^{12}C^{+}$ and $^{12}C^{16}O^{+}$ achieving limits of detection of 0.42 mg/L and 0.17 mg/L, respectively (Amaral et al. 2015). Stolpe at al. (2005) monitored carbon during AF^4-ICP-MS runs of natural water samples but results are given only as intensities without quantification. Despite these efforts, quantitative determination of particulate carbon in natural or engineered nanoparticles and colloids by AF^4-ICP-MS has up to date not been reported. Clear challenges arise when aiming at carbon quantification by ICP-MS: i) Carbon has quite a high ionization potential of 11.26 eV and thus low ionization efficiency leading to rather high limits of detection (LOD) in ICP-MS compared to metals (Luong and Houk 2003). ii) Carbon background levels are high which increase LODs. iii) Substantial amounts of organic compounds (for example using organic solvents in HPLC-ICP-MS) are known to affect plasma characteristics and stability and thus carbon quantification may suffer from matrix effects (Grindlay et al. 2013; Lopez Molinero et al. 1997). iv) Finally, ICP-MS is predominantly applied by inorganic researchers focusing on the metallic elements and using organic mass spectrometry for complementary structural information, therefore only few publications exist. In this study, the performance of quadrupole ICP-MS was first compared for total organic carbon quantification in standard solutions and stream water samples using classical TOC and OCD as reference. Second, AF^4-ICP-MS was applied for particle bound carbon quantification using two independent calibration strategies and results were compared to those obtained by AF^4-OCD for the same samples.

The comparison of four techniques for total organic carbon determination demonstrated the feasibility of using ICP-MS for (organic) carbon monitoring in standard solutions and fresh water samples containing dissolved and particulate organic carbon species (Figure 4.1.3). The results obtained in this study indicate that external calibration provides sufficiently accurate and precise total organic carbon quantification without the need for isotope dilution techniques. Limits of detection for particulate carbon are about 10-fold higher using ICP-MS compared to OCD, thus sufficient for monitoring of organic carbon in real environmental samples above total concentrations of 1 mg/L. The LOD increases to 1.4 mg/L for AF^4-ICP-MS coupling, whereas for AF^4-OCD the LOD can be as low as 0.08 mg/L. Yet, to achieve the low LOD for organic C ICP-MS determination, inorganic carbon in the samples has to be removed by purging with Ar. Purging and maintaining a maximum

removal of inorganic C is a laborious procedure and therefore organic C measurements with ICP-MS are interesting but far from realizable for routine environmental analysis.

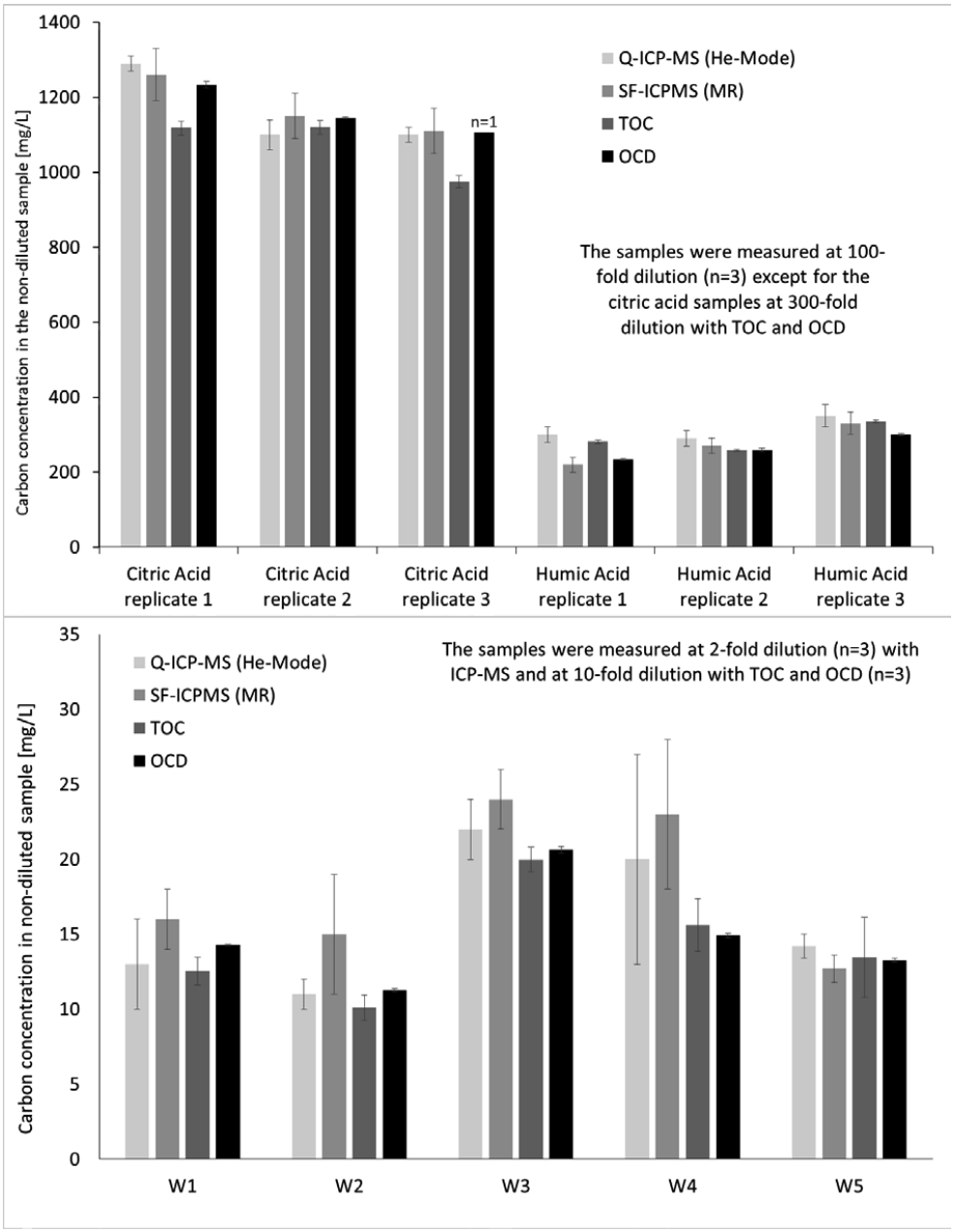

Figure 4.1.3: *Determination of total organic carbon in citric acid and humic acid model solutions (top) and five fresh water samples (W, bottom) by quadrupole ICP-MS (Q-ICP-MS), sector field ICP-MS (SF-ICP-MS), total organic carbon analyzer (TOC) and organic carbon detector (OCD). Displayed are mean values ± standard deviation (from Nischwitz et al. under review).*

4.1.3.3 Potential bioavailability of natural nanoparticle and colloid bound P

Phosphorus has a central role in ecosystem nutrient supply because the many vital compounds have P as a structural component. In ecosystems, many inorganic and organic molecules are known which include P, yet, currently a further structure is being analyzed which is capable of transporting P throughout the hydrological pathways and thus in the aqueous phase of ecosystems. NNP and colloids of soils, soil extracts, drainage waters and in stream water of diverse ecosystems have shown to carry P compounds in different quantities depending on particle composition (e.g. Andersson et al. 2006; Dahlqvist et al. 2004; Gottselig et al. 2014; Gottselig et al. submitted; Regelink et al. 2013; Regelink et al. 2014; Stolpe et al. 2010). Therefore it is questioned if these particles represent a sink for the essential nutrient P in ecosystems or if the P of the compounds forming a NNP or colloid can be enzymatically released as a PO_4^{3-} in its most readily available form and thus remains easily bioavailable for organisms.

A first study has shown that colloidal P is in fact not chemically inert but contributes to the plant available P (Montalvo et al. 2015). Mechanistically the usage of released orthophosphate from P carrying organic or organometallic NNP and colloids is not known, yet it is hypothesized that esterases are not only capable of hydrolyzing the ester bond of organic compounds, but also when these compounds are included in the NNP and colloid fractions. A setup utilizing an equilibrium dialysis machine with 4 mL cells and a 1 kDa MWCO RC membrane was introduced to investigate the activity of esterase enzymes in the presence of NNP and colloids and to identify the percentage of enzymatically released orthophosphate from P carrying NNP and colloids.

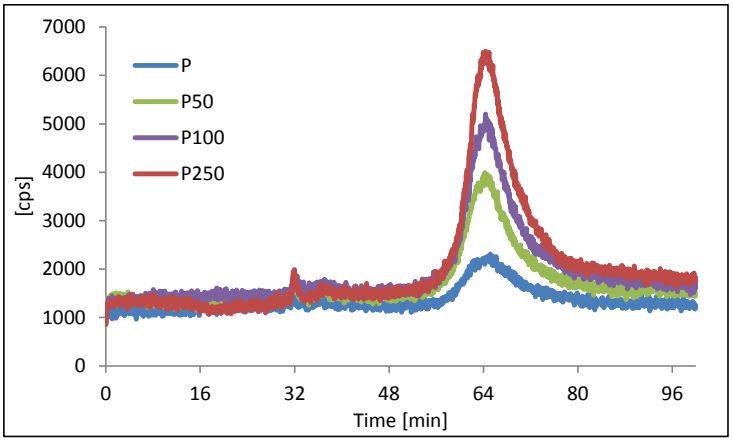

Figure 4.1.4: *Intensity of the ICP-MS P signal in counts per second (cps) as function of the AF⁴ fractionation time in minute (min). The original Wüstebach stream water sample (blue) was spiked through the addition of KH_2PO_4 at concentrations of 50 µg/L (green), 100 µg/L (violet) and 250 µg/L (red).*

Trial experiments with acid phosphatase (wheat germ; Sigma Aldrich, St Louis, USA) and phytase (Ronozyme; Feed enzymes Europe, Ørbæk, Denmark) as well as corresponding model substances glucose-6-phosphate and IHP (inositol hexakisphosphate), respectively, showed that the system was applicable for examining the research question. Maximum activity of acid phosphatase was determined at 44%, of phytase at up to 90%. The developed setup for determining the bioavailability of NNP and colloidal P through enzymatic activity is still pending detailed results with environmental samples. For the examination of natural samples, investigations have to be conducted to be able to estimate the adsorption potential of enzymatically released orthophosphate to positively charged ions additionally incorporated into the structure of NNP and colloids. First data on the spiking of a Wüstebach stream water sample with KH_2PO_4 has revealed an adsorption capacity of orthophosphate to NNP and colloids. This adsorption proved to withstand AF^4 fractionation (Figure 4.1.3).

4.2 Characterization of P-carrying natural nanoparticles and colloids in tributaries and main stream flow within one forest catchment[6]

4.2.1 Natural nanoparticulate and colloidal P, Fe and Al along the stream flow

Coupling of AF^4 to ICP-MS enabled monitoring of the elemental composition of two size-separated particle fractions (Figure 4.2.1). The mean diameter of this first fraction was estimated at about 8 nm, with a range between about 2 and 20 nm and the mean diameter of the second fraction was determined to be about 150 nm, covering a range of about 21 to 300 nm. Fe and Al were detected at high intensity (apart from Sample T2), while P was close to the detection limit in several samples, in particular in the first fraction. It was possible to observe differences in the elemental composition in the nanoparticulate and colloidal distribution of the Wüstebach stream and its contributing flows. An overview of AF^4-ICP-MS fractograms for all sampling points along the stream flow is shown in Figure 4.2.1. There was an increase in particle bound elemental contents from SP1 to SP2, followed by a decrease to SP3. Fractograms recorded for OF1/OF2 and T1/T2 facilitate our understanding of these changes along the stream flow (Figure 4.2.2). The additional first and elevated second fraction recorded at SP2 were due to an additional particle source supplied by T1 (high concentration of the first fraction), a hydromorphological region similar to the main stream, and OF1 (elevated second fraction), a very turbid overland flow supplied point.

[6] Excerpts published in a peer-reviewed journal:
Gottselig N, Bol R, Nischwitz V, Vereecken H, Amelung W, Klumpp E (2014) Distribution of Phosphorus-Containing Fine Colloids and Nanoparticles in Stream Water of a Forest Catchment. Vadose Zone Journal 13:1-11. Permission granted by Soil Science Society of America.

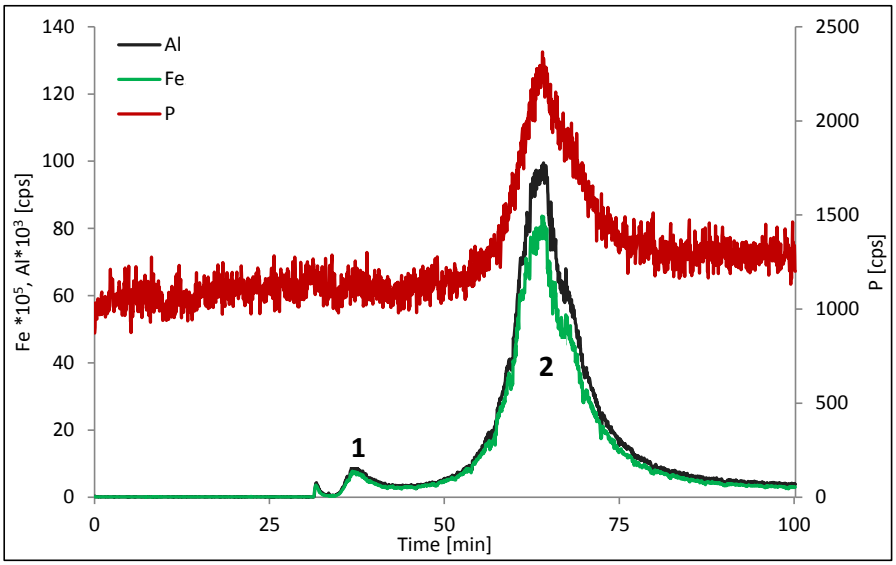

Figure 4.2.1: *ICP-MS data of P, Fe and Al for an AF^4 fractionated water sample of the Wüstebach stream. AF^4 runtime is shown on the x-axis; the y-axes are distinguished according to graphs. 1 = position of first fraction, mean diameter ~8 nm; 2 = position of second fraction, mean diameter ~150 nm.*

The particle-bound elemental concentrations of the fractions shown in Figure 4.2.3 indicate that the headwaters stream point of the Wüstebach (SP1) and the outlet stream point (SP3) have similarly low concentrations of P, Al, and Fe. This can be explained by a dilution effect due to the groundwater inflow tributary T2, occurring between SP2 and SP3. A comparison of the fractograms of SP2 and OF2 reveals a strong influence of overland flow up to this stream area due to the very similar peak forms of the two points, despite different hydromorphological characteristics. Within the course of the stream, the profile of the particle-bound concentrations for P correlated, in particular in the first fraction, with Al rather than with Fe. On the one hand, this result is consistent with the findings from Richardson (1985), who suggested that following washout from adjacent soils, it is mainly Al rather than Fe that controls the P adsorption in freshwater systems. On the other hand it may be possible that the aqueous Al species are mainly attached to (colloidal) organic P. Noteworthy, for both the first and also the second fraction, it was observed that if a highly increased Fe content was present, more P was detected in the nanoparticulate and colloidal fraction. In light of the much lower Al content compared with Fe content (Figure 4.2.3), we suggest that particles in the two peaks did not contain many aluminosilicate minerals but were dominated by oxides or, in fraction 1, by organic compounds binding Al, Fe, and P. However, when looking at the dynamics of the second fraction, no strong correlations of the P contents with the course of Al or Fe concentrations were seen, indicating that the P binding cannot be explained by an interplay of Fe and Al alone. Possibly also other factors like DOM play a role.

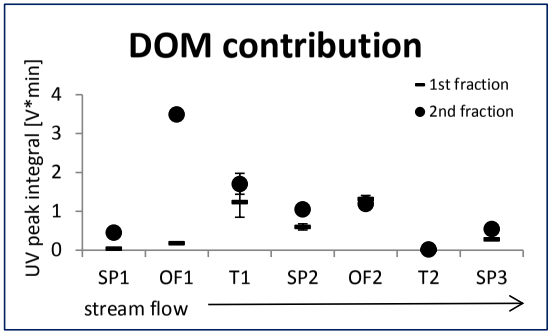

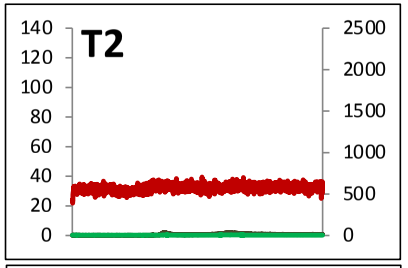

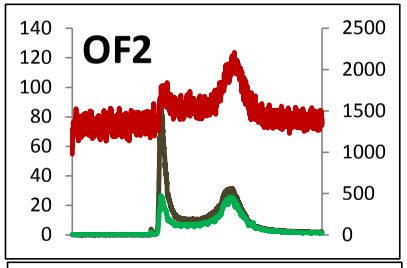

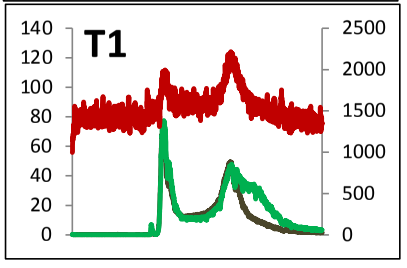

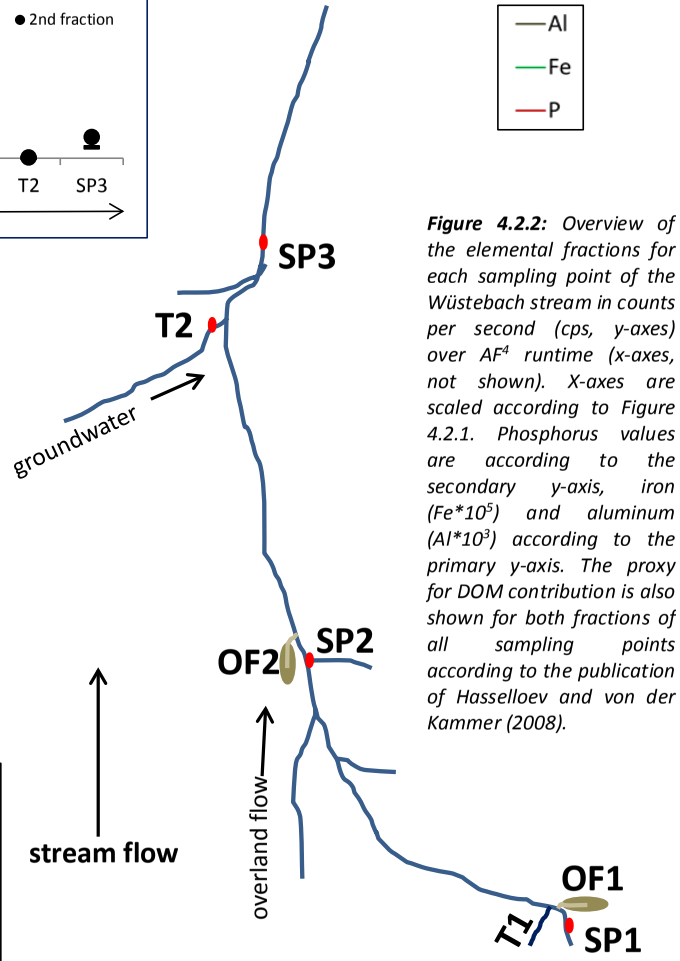

Figure 4.2.2: *Overview of the elemental fractions for each sampling point of the Wüstebach stream in counts per second (cps, y-axes) over AF[4] runtime (x-axes, not shown). X-axes are scaled according to Figure 4.2.1. Phosphorus values are according to the secondary y-axis, iron (Fe*10[5]) and aluminum (Al*10[3]) according to the primary y-axis. The proxy for DOM contribution is also shown for both fractions of all sampling points according to the publication of Hasselloev and von der Kammer (2008).*

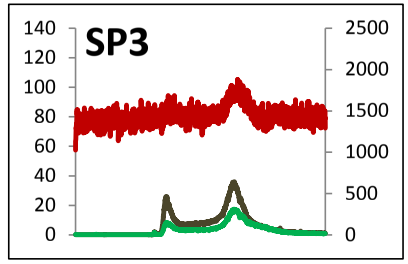

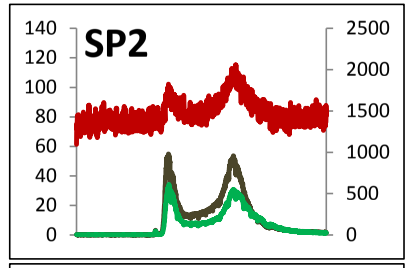

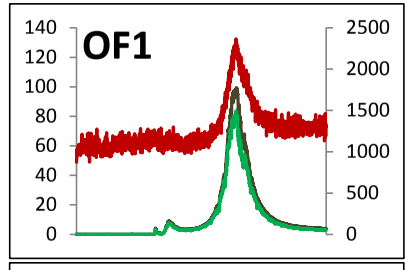

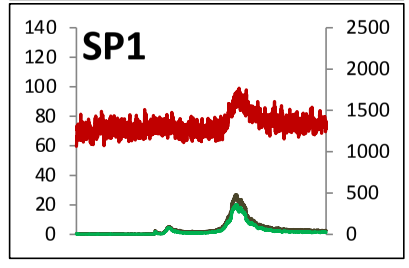

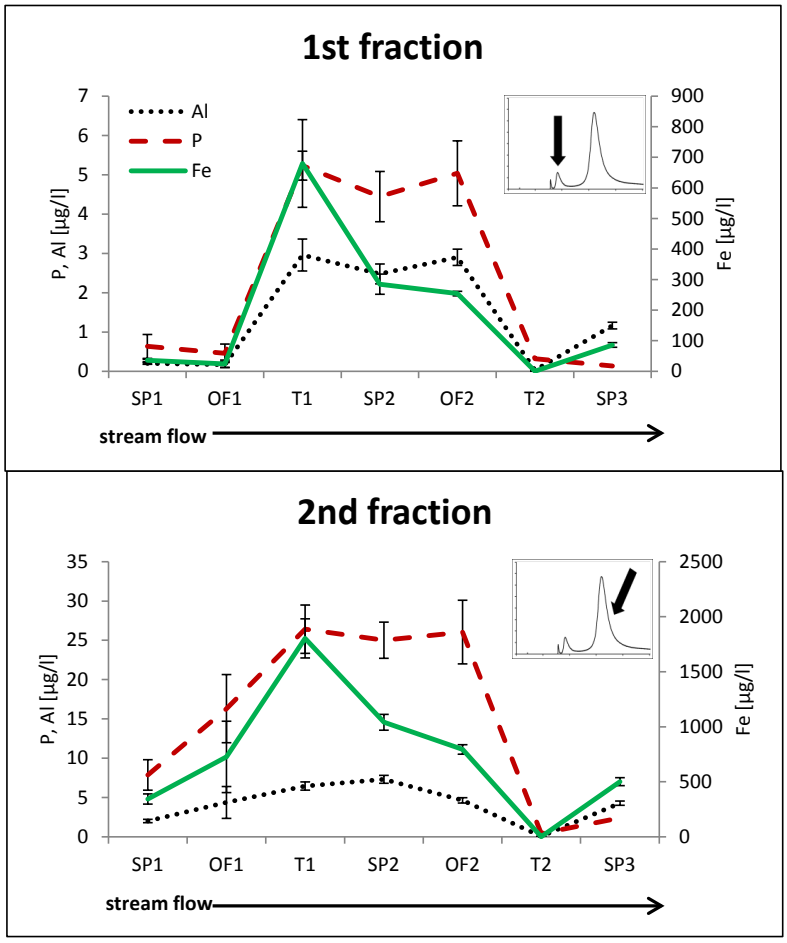

Figure 4.2.3: *Concentrations of P, Fe and Al in the two natural nanoparticulate and colloidal fractions along the Wüstebach stream flow. The small diagrams indicate the respective fractions.*

4.2.2 Proportion of particle-bound relative to total elemental contents

Mean contents of 34.9 ± 11.6% for Fe and 54.1 ± 26.3% for P were bound in the particulate fraction relative to the total elemental concentrations (Figure 4.2.4; Table 4.2.1). Peak percentages for P in colloidal form were recorded at SP2. For Fe, samples from SP2, OF2, and SP3 showed very similar peak values despite differences in the hydromorphology of the sampling sites. The overland flow driven regions are not confined to a specific bed and showed higher turbidity of the containing water than the stream points with the confined bed and baseline turbidity. The Al measured as NNP and colloids was generally low (1.3 ± 0.4%) compared with total sample concentrations. The percentage

of elements in the NNP and colloidal form compared with the total concentrations confirms that elemental transport through them is relevant, especially when comparing with data obtained at the sampling location T2 (a groundwater inflow tributary). The percentages were up to 20 times lower for T2 than for all other sampling points (Figure 4.2.4). Total Al concentration at T2 was similar to the values observed at the other sampling locations, whereas the concentrations of P and Fe at the other locations were three and 10 times lower, respectively. The P concentration at T2 was at a value where, at other sampling points with the same total concentration, a much higher percentage of the total P was present in the NNP and colloidal form. If, therefore, a distinct amount of Al and especially Fe is not present with free binding sites for P, in consequence a lower percentage of P is bound in the NNP and colloidal form. Thus, an essential element such as P needs a carrier such as Fe and Al to be transported in the NNP and colloidal form in aquatic systems.

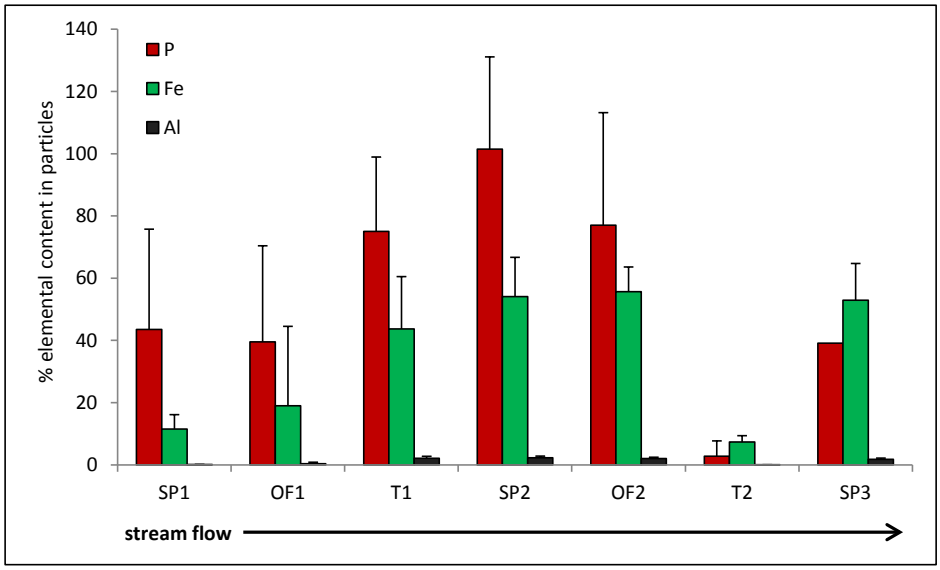

Figure 4.2.4: *Percent elemental concentration in the natural nanoparticle and colloid fraction in comparison to total elemental concentrations of the samples from the sampling points along the Wüstebach stream.*

The work of Liu et al. (2011) shows colloidal P variations across a large scale of a stream (~50 km length) with different geological locations. In contrast, the present study for the first time allows tracing and understanding the inputs and types of the two NNP and colloidal fractions within a small-scale stream flow. Similar studies have varied in the size definition of colloids but well represent the variation in colloidal P due to differences in environmental conditions. In an American river basin, Mayer and Jarrell (1995) detect concentrations of colloidal P (0.05–1 µm) that ranged between detection limit and 0.061 mg/L and which comprised up to 48% of the total P concentrations. For a coastal plain area in Australia (Zhang and Oldham 2001), the observed colloidal P (1 kDa–0.5 mm)

was between 0.009 and 0.207 mg/L. In Swiss lakes (Filella et al. 2006), colloidal molybdate-reactive P (3 kDa–1.2 mm) was as low as 1.2 mg/L. In contrast, this study showed nanoparticulate and colloidal P concentration variations in much lower ranges than Mayer and Jarrell (1995) and Zhang and Oldham (2001). The concentration ranges are similar to those of Filella et al. (2006) but represent distinct nanoparticulate and colloidal size fractions and not all reactive P species. Thus, the measurements of low P concentrations using the proposed AF^4 fractions are a novel achievement. The studies combine surface runoff (Mayer and Jarrell 1995), highly comprised of macromolecular C, with colloidal P by showing a facilitated formation of colloidal P (Zhang and Oldham 2001) through higher surface runoff rates. Moreover, background geology affects the mineral components of colloids and in turn their stability (Filella et al. 2006). These studies underline the complexity and dynamics of nanoparticulate and colloidal P as shown in this study. The description of nanoparticles and colloids in freshwater through AF^4 can now increase our understanding of different fractions within the targeted size range.

Table 4.2.1: *Total elemental sample concentrations from the stream point (SP), overland flow (OF), and tributary (T) sampling points along the Wüstebach stream in contrast to total particulate elemental concentrations ± standard deviations (SD).*

		Al	Al SD	P	P SD	Fe	Fe SD
Total [µg/L]	*SP1*	571.9	9.5	6.5	1.6	1092.9	88.1
	OF1	413.7	92.8	14.2	4.4	1317.9	676.1
	T1	146.5	10.0	14.1	1.7	1893.7	235.6
	SP2	141.1	5.7	9.7	2.0	817.8	54.9
	OF2	123.2	9.3	13.5	1.2	627.7	103.4
	T2	123.4	1.5	2.0	0.1	18.7	1.0
	SP3	98.7	3.8	6.5	1.4	370.3	11.2
Particulate [µg/L]	*SP1*	0.7	0.2	2.9	2.2	122.8	50.2
	OF1	1.6	0.1	5.9	4.6	266.7	21.9
	T1	3.1	0.9	10.6	3.4	827.7	321.2
	SP2	3.3	0.8	9.8	2.9	442.0	104.9
	OF2	2.5	0.6	10.4	4.9	349.4	50.5
	T2	0.1	0.0	0.2		1.4	0.4
	SP3	1.8	0.4	2.6		195.9	43.8

4.2.3 Potential role of organic matter for P-binding

'Dissolved' organic matter (DOM, organic matter <0.45µm) can be present in various forms in natural stream water including humic and fulvic acids and organic coatings attached to inorganic colloids, which are potential binding sites for P. The DOM proxy values of the second fractions of T1, SP2, OF2, as derived from the UV signal, are elevated in comparison with the other sampling points, with the exception of OF1 (Figure 4.2.2). This may indicate the presence of organic compounds in these particles that are potentially involved in the binding of P. Alternative approaches for improved online C detection for AF^4-separated samples are currently being explored for the AF^4 system used in this study but are not yet in a state to offer precise results for the C content. Nonetheless, in connection with the TERENO database (Annex Figure S1), a more precise relationship between 'dissolved' organic C or DOM and NNP and colloidal matter can be drawn for Points SP1, SP3, and T2.

The stream water composition of the Wüstebach main stream results from a mixture of the tributaries and the surface runoff. Through high DOM containing regions with constant inflow into the stream, the influence of the DOM content on the potential NNP and colloidal source regions can be evaluated. Sampling Points T1, SP2, and OF2 show higher DOM contributions of both particle fractions than the other sampling points with the exception of OF1 (second fraction). This correlates with the elevated elemental concentrations (Figure 4.2.3) and the percentage of particles (Figure 4.2.4) detected for these points. The elution time of the first fraction, which corresponds to small-sized particles, matches humic acid standards, and therefore this fraction is likely to contain a significant percentage of organic compounds. This finding is supported by the similar DOM proxy concentrations for T1 and the subsequent sampling points SP2 and OF2.

For the first fraction, the coefficient of determination of the linear regression between the elements P, Fe, Al, and the particulate DOM varies between 0.68 and 0.90 (Table 4.2.2). For the second fraction, a variation between 0.67 and 0.82 was calculated (Table 4.2.2). The determination coefficients of the linear regressions show higher results for the smaller (first) size fraction, indicating a stronger carrier effect. Organic matter can stabilize NNP and colloids in microaggregates by building bridging complexes or being matrix material for potential adhered components (Six et al. 1999). In both fractions, macromolecular C compounds were detected in the presence of P, Fe, and Al. Further investigations are required to determine the exact binding mechanism of P in these NNP and colloidal fractions. This may involve complexes of phosphate with organic matter or complexes of phosphate with Fe and/or Al oxides. Further, an adsorption of organic P compounds to NNP and colloids is possible. The DOM is apparently able to account for a significant portion of the variation in certain metal concentrations (Shafer et al. 1997), which in turn influence P adsorption. The relation

of the variation in P and Al concentrations, as shown above, can also be affected by the DOM components present. Al ions efficiently bind to macromolecular organic compounds (Libecki and Dziejowski 2008) and can, through this connection, also be tightly associated with P through bridging effects.

Table 4.2.2: *Correlation R^2 values between particulate-bound elements and between particulate-bound elements and organic matter (DOM) from the Wüstebach stream samples.*

Correlations 1st fraction

	DOM	Fe	P
Al	0.90	0.70	0.88
P	0.84	0.70	
Fe	0.68		

Correlations 2nd fraction

	DOM	Fe	P
Al	0.67	0.72	0.75
P	0.80	0.72	
Fe	0.82		

4.2.4 Preliminary effect of deforestation

Post-deforestation samples were taken 3 months after the clear-cut in the beginning of December 2013. An alteration in catchment land cover has effects on the overall chemical and physical characteristics of the catchment (Khresat et al. 2008). In the Wüstebach catchment, the alteration in land cover had an effect on the NNP and colloidal load in the stream (data not shown). A concise trend stating the direction of the change in characteristics cannot be seen from the literature (Khresat et al. 2008; and references therein; Lindo and Visser 2003; Neill et al. 2001; Turrion et al. 2000). Possibly, minor differences in climate, vegetation, or soil type make direct comparisons among studies difficult. In the context of NNP and colloidal P in stream waters with additional information on pre- and post-deforestation effects, the literature offers no comparable studies. For the Wüstebach stream, an up to 10-fold decrease in the total elemental concentration of Fe and an up to threefold decrease in P were detected post-deforestation compared with before clear-felling. The Al total elemental concentrations remained similar. For the elemental composition of the NNP and colloidal fraction, a preferential loss of Fe was seen throughout the whole stream. The Al concentration within the colloidal fraction was similar to before deforestation. For P, the decrease caused concentrations to drop to or below the detection limit. A comparison of the stream water level, discharge rate, and turbidity from the TERENO database reveals a ~1 month precipitation event

with high turbidity values at SP3 between deforestation and sampling in December (Annex Figure S2). Possibly, the vast majority of NNP and colloids was washed out during this time. According to Lindo and Visser (2003), the nutrient load of a coniferous forest stand shows highly significant effects from clear-cutting (decrease of the nutrient load of ~20%) in comparison to a deciduous forest. The post-deforestation data outlined here may represent the first immediate effect on the NNP and colloidal bound elements; however, they may additionally or simply reflect seasonal variability. In any case, these data show that the composition of colloidal export within the base flow of the river may be very sensitive to changes in environmental conditions. The sensitivity and methodology of the coupled AF^4 and ICP-MS system will have to be adapted to the decreased concentrations to allow a better assessment of the status of NNP and colloids following deforestation.

4.2.5 Iron isotope signals in different reservoirs of a forested catchment[7]

Iron itself is an important nutrient for organisms, but Fe oxides also have the capacity to adsorb nutrients like P. However, the application of stable Fe isotope ratios as a tool to identify processes and mechanisms in the terrestrial environment is still rare. Through observations of the fractionation of Fe isotopes, in-depth information on the cycling and turnover rates in a forested ecosystem can be gained. This is especially of interest to trace the origin of NNP and colloid fractions. NNP and colloids have already been recognized as ubiquitous components of the operationally defined 'dissolved' phase (Hill and Aplin 2001; Jarvie et al. 2012), largely responsible for nutrient acquisition and cycling, and have been shown to contribute to the plant available P fraction (Montalvo et al. 2015). Further, the cluster analysis (Chapter 4.3.2) has shown that Fe is an important building block element included in all three separated fractions of NNP and colloids, even on European scale (Chapter 4.4.6). Thus, Fe potentially controls the transfer of P-carrying NNP and colloids in forested headwater catchments and can be utilized to trace this nutrient within the ecosystem.

For this analysis, the AF^4 was used for preparative purposes to collect the fractions of NNP and colloids and therefore to allow an offline analysis on the Fe isotopic signature of sufficiently concentrated NNP and colloids from the Wüstebach stream water samples. Samples of further ecosystem compartments of the Wüstebach, from soil horizons and the vegetation, were also collected. For sample digestion, Fe isotope extraction and isotope measurement details see 'Annex: Methods of sample digestion, Fe isotope extraction and measurements'.

[7] Contains excerpts from:
Berns AE, **Gottselig N**, Ockert C, Hezel D, Wombacher F, Bol R, Münker C, Vereecken H, Amelung W, Wu B. Iron isotopes in different reservoirs of a forested catchment, in preparation.

The data already showed clear differences in the Fe isotopic signatures of different ecosystem compartments such as soil horizons, vegetation samples and aqueous samples (Figure 4.2.5). Most interestingly, the Fe isotopic signature of the NNP and colloid fractions (indicated by I and II) is very different of one sampling location (T1 or OF2). For both samples it was seen that the second fraction $d^{56}Fe$ is increasingly negative to the first fraction, whereas the first fractions display a greater difference in isotopic signature than the second fractions. The first fraction of T1 can potentially be highly influenced by iron from the Cambisol top soil layers, whereas the second fraction, showing close similarities in $d^{56}Fe$ value to the top soil Gleysol layers, experienced more input from this differing Fe source. The isotopic signature of spruce needles also fits well to the second fraction Fe of the samples T1 and OF2, most probably due to the significantly higher coverage of spruce than beech tree within the Wüstebach catchment. On the origin and influences of data points such as OF2 II can only be speculated from analysis of the raw data.

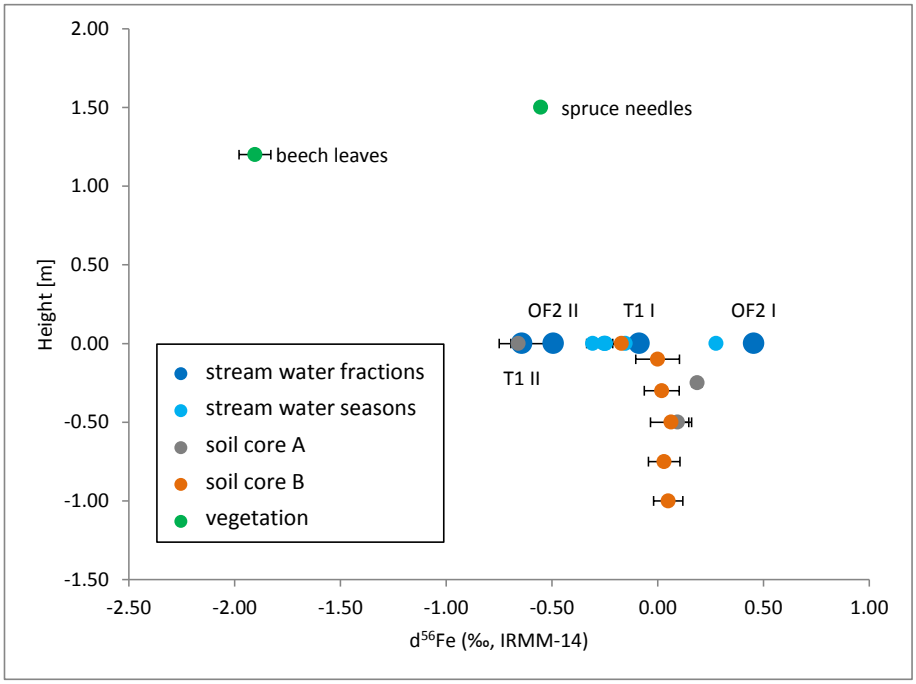

Figure 4.2.5: *$d^{56}Fe$ values in ‰ relative to the $d^{56}Fe$ value of the standard IRMM-14. The height of the sampling location is given with reference to the ground level at the Wüstebach site (0 m). Shown are $d^{56}Fe$ of the NNP and colloid fractions (dark blue with data point labelling), of total stream water samples prior to fractionation (light blue), of soil horizons from a Cambisol soil (orange), of soil horizons from a Gleysol soil (grey) and of vegetation samples (green). Data point labelling indicates the two fractions (I and II) of two Wüstebach stream water samples which were preparatively collected with AF^4 (adapted according to C. Ockert).*

4.3 Identification of P binding patterns to natural nanoparticles and colloids of forested headwater catchments across Germany[8]

4.3.1 Natural nanoparticle and colloid fractions identified with AF^4

The data collection from AF^4-OCD matched well with the respective AF^4-ICP-MS fractograms. Both the coupling of the AF^4-UV to ICP-MS and to the OCD revealed three fractions of NNP and/or colloids in the samples at the same elution times (Figure 4.3.1a, b). Through calibration with reference materials the first fraction was estimated to include NNP between 1 kDa and 20 nm and the second fraction to include NNP >20 nm to 60 nm. Furthermore, the DLS revealed that the third fraction includes NNP >60 nm to colloids up to approximately 300 nm (Chapter 4.1.1b). Broader peaks were obtained using the organic carbon detector compared to ICP-MS due to the large volume of the OCD reactor and thus longer sample passage time. Peak integration times for the three fractions as indicated in Figure 4.3.1a were therefore corrected through prolongation of the integration time by 5 min to comply with this effect.

The first fraction showed narrow high peaks of the detected elements Fe, organic C and P (Figure 4.3.1a) as well as Al and of the UV signal (Figure 4.3.1b). The second fraction peak was not as narrow as the first and differed in elemental peak intensity compared to the first fraction. Here, Fe (Figure 4.3.1a) and Al (Figure 4.3.1b) show clear peaks but also org C and P (Figure 4.3.1a) and a UV signal (Figure 4.3.1b) were present. The third size fraction contained P and all measured elements but in different ratios, with elevated amounts of Al and Si (Figure 4.3.1b) than in the previous fractions. A UV signal was also recorded (Figure 4.3.1b). This trend could be seen across all sampling sites though with variations in fraction yields (Table 4.3.1, Annex Table S1).

On account of multiple elemental peaks within one fraction, first conclusions can be inferred on the chemical speciation of the compounds from reviewing the raw data fractograms (Figure 4.3.1a, b). Besides P, the first NNP fraction was clearly dominated by organic C, Fe and Al, whereas Si was almost lacking. Hence, this fraction did not contain aluminosilicate minerals but rather P associated to Fe-/Al-(hydr)oxides and organic matter, either with P in association to iron/aluminum or to organic C (organophosphorus compounds) and then over the direct binding partner to the other compound. The detected iron is likely to indicate iron (hydr)oxides, known to be carriers for P (Mayer and Jarrell 1995; Stolpe et al. 2010). The presence of Si and Al within the third fraction was indicative of

[8] Contains excerpts from:
Gottselig N, Nischwitz V, Meyn T, Amelung W, Bol R, Halle C, Vereecken H, Siemens J, Klumpp E. Phosphorus Binding to Nanoparticles and Colloids in Forest Stream Waters. Biogeochemistry, submitted.

aluminosilicate minerals. Overall, P carrying nanoparticles and colloids of different hydrodynamic size fractions had a differing elemental composition.

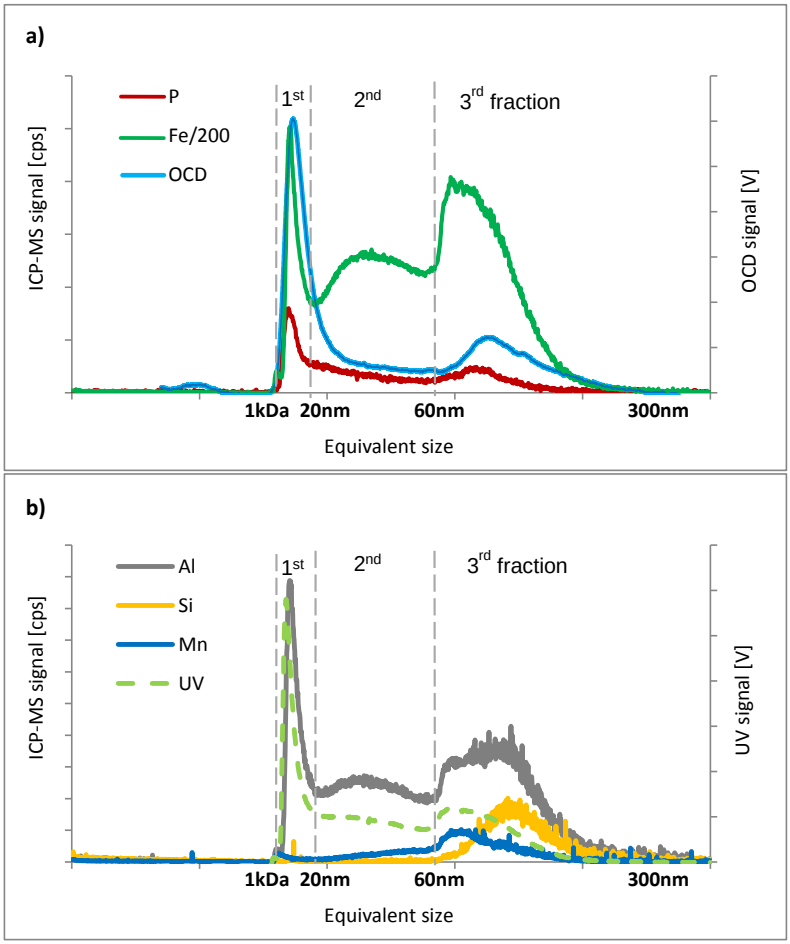

Figure 4.3.1: *Exemplary AF^4 fractograms indicating the three peaks detected for all samples. a) Phosphorus, iron and organic carbon signals. The iron signal was downscaled by a factor of 200 to better visualize the phosphorus signal. b) Aluminum, silicon, manganese and UV signals. The size of the first fraction lies between approx. 1 nm and 20 nm, the second size fraction between >20 nm and 60 nm and the third fraction above 60 nm. Elution time offset for OCD was corrected, peak broadening not. The depicted UV signal was recorded at 254 nm wavelength from the AF^4-ICP-MS run. Fraction borders apply to the ICP-MS signal, for the OCD evaluation these borders were modified.*

Table 4.3.1: *Phosphorus fractionation in stream water samples: The binding percentage of P per natural nanoparticulate and colloid fraction referring to total P concentration as well as their sum over all sampling points per site. Total P = total sample P concentration, particulate P = sum of P concentration over all three fractions. 1st fraction: approx. 1 nm to 20nm, 2nd fraction: >20nm to 60nm, 3rd fraction: above 60nm. Particle fractionation via AF^4 coupled online to ICP-MS and OCD. n = 29.*

	samples	P-binding per fraction [%]				Total P [µg/L]	Particulate P [µg/L]
		1st	2nd	3rd	∑		
Conventwald	1	1.3	1.5	33.9	36.7	40.0	14.7
	2	2.6	2.9	8.0	13.6	28.0	3.8
	3	1.9	1.8	1.3	5.1	14.0	0.7
	4	3.3	3.9	10.1	17.3	13.6	2.3
	5	2.3	9.9	20.2	32.3	10.1	3.3
Mitterfels	6	7.0	11.1	10.4	28.6	23.0	6.6
	7	5.5	8.0	9.4	22.9	27.0	6.2
	8	7.8	10.9	10.1	28.8	57.0	16.4
	9	9.0	17.2	17.3	43.5	15.0	6.5
	10	9.0	16.9	14.6	40.6	20.6	8.4
	11	12.1	21.1	15.9	49.1	14.0	6.9
	12	10.4	17.3	16.6	44.3	13.0	5.8
	13	5.1	9.6	12.9	27.7	19.0	5.3
Vessertal	14	4.2	4.6	13.0	21.8	10.4	2.3
	15	2.2	2.3	3.9	8.4	21.0	1.8
	16	1.4	1.4	2.2	5.0	37.0	1.8
	17	4.4	5.1	10.9	20.5	16.0	3.3
	18	6.7	7.1	11.9	25.8	11.0	2.8
Wüstebach	19	5.1	22.4	44.1	71.7	10.3	7.4
	20	5.4	38.5	37.6	81.4	23.0	18.7
	21	14.8	30.3	36.1	81.2	9.0	7.3
	22	10.0	31.6	45.7	87.3	9.0	7.9
	23	26.4	33.1	33.4	92.9	19.0	17.6
	24	2.8	5.6	16.7	25.1	14.1	3.5
	25	8.1	27.5	48.9	84.5	6.9	5.8
Leirelva	26	18.7	29.2	42.6	90.5	1.5	1.4
	27	20.2	28.4	40.3	88.9	1.3	1.2
	28	19.1	30.2	39.3	88.5	1.2	1.1
	29	15.4	33.5	38.4	87.3	0.9	0.8

4.3.2 Association of P with natural nanoparticles and colloids across 5 forest streams

In order to better understand the associations of P within the NNP and colloidal fractions, agglomerative hierarchical tree cluster analysis with complete linkage and the distance measure '1-Pearson r' was utilized to disentangle the potential associations of organic C, Fe, Al, Mn and Si to P for each size fraction (Figure 4.3.2). According to the results of this analysis, phosphorus clustered with Fe in the fraction 1 kDa to 20 nm with a '1-Pearsons r' distance of 0.16. This clustering supports the relevance of iron (hydr)oxides, possibly in nanocrystalline form (Michel et al. 2007), for P binding in this smallest size fraction (Francko and Heath 1982; Hasselloev and von der Kammer 2008; Jiang et al. 2015; Leppard et al. 1988), but reduces the probability that Al was the major binding partner of P (Richardson 1985) in these nanoparticles. P and organic C did not fall in the same cluster of this very fine NNP fraction. Organic C was clustered more closely to Al and Mn than to Fe, suggesting that organic matter was mainly associated with these elements but questioning that organophosphorus compounds were the main component bound to the Fe oxides (Lyven et al. 2003; Regelink et al. 2013; Regelink et al. 2011; Shafer et al. 1997).

The analysis of the 2nd fraction showed a different clustering. A close relation between P and organic C in the intermediate size fraction, covering particles >20nm to 60nm, was indicated. The further clustering of P and organic C with Fe indicates an association of Fe to one or both of these elements, which would support the assumption that this fraction consisted of organic matter bound to Fe and over Fe to P through ligand exchange (Gerke 1992; Gerke and Hermann 1992) or of organophosphorus compounds associated to iron (hydr)oxides (Gerke 1992; Gerke 2015). The latter is more likely if following the cluster analysis results.

According to the results from cluster analysis, phosphorus is in the 3rd fraction of the analyzed samples strongly associated to Al, Si and Mn rather than to Fe and/or organic C. The distance measure of Si to Al is very small ('1-Pearsons r' = 0.02) reflecting a common compound, such as phyllosilicates, which dominates in this fraction. These phyllosilicates may contain variable amounts of other elements (Grim and Kodama 2014). The clustering of Mn to Si and Al specifically points to the potential presence of 2:1 aluminosilicate minerals. In expansive 2:1 aluminosilicates, which can take up nutrients and water, Al can be replaced by Fe or Mn. Apparently, in this fraction P was sorbed to the edges of aluminosilicate minerals by ligand exchange (Yaghi and Hartikainen 2013). In any case, the analyses clearly show that natural nanoparticles and colloids of forest stream waters did not only differ in hydrodynamic diameter but also in their composition, thus rendering them complex and important carriers for colloidal P and other elements of different binding form and possibly origin.

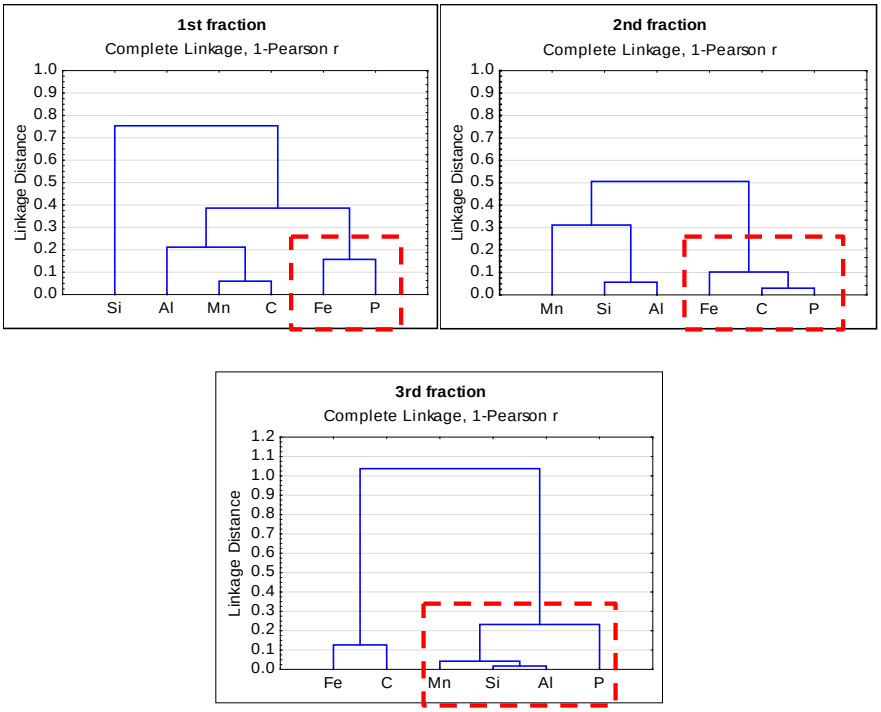

Figure 4.3.2: *Hierarchical tree cluster analysis results with '1-Pearson r' as distance measure and complete linkage rule per fraction across all sampling sites.*

A comparison to other studies reveals that the differentiation of multiple size classes within the NNP and colloids is rarely reported in combination with monitoring of P. Different numbers of particle size fractions separated by the FFF technique seem to be present in different environmental samples (Plathe et al. 2013; Regelink et al. 2013; Regelink et al. 2011; Stolpe et al. 2010). In the latter studies the smaller size range was assigned to organic matter associated to metal oxides and the larger fraction (up to 100 nm) to aluminosilicate or colloidal silica. The present study confirms the associated transport of P and aluminosilicate minerals in the largest size fraction when particles exceed a hydrodynamic diameter of 60 nm.

4.3.3 Potential ecological relevance of natural nanoparticles and colloids for P in forest stream waters

A high relevance of NNP and colloids for nutrient cycling in ecosystems is indicated by the high percentages of essential element binding (especially P, organic C, Mn and Fe) to the NNP and colloidal fractions (Table 4.3.1, Annex Table S1), yet no previous study was found addressing the relation between total and particulate concentration. Up to 100% could be bound to NNP and colloids indicating a high recovery (e.g. Fe, P, org C) in particulate form which lead to the assumption

that no significant amount of particles was lost upon fractionation. For elements which did not reach 100% particulate concentrations, the difference between total sample concentration and particulate concentration could potentially be assigned to the 'dissolved' state (Hill and Aplin 2001; Martin et al. 1995) as hydrated compounds <1 kDa. In case the total concentration as well as the concentration of 'dissolved' elements decreases with simultaneously increasing NNP and colloidal bound proportion of the elements, it can be presumed that nanoparticulate and colloidal bound elements, specifically nutrients, have a high ecological relevance in forest stream waters. It is noted that the interdependency of the NNP and colloidal fractions with the 'dissolved' phase is less known, yet very complex.

The data has shown that the importance of NNP and colloids for P cycling increases with decreasing total P. Through calculation of the correlation coefficient between the total concentration of P per site and the percentage of P binding in the three fractions, the negative relation between the two parameters for P can be seen (Table 4.3.2). A negative coefficient indicates higher NNP and colloidal binding as total concentrations decline. The same trend was observed for the difference between total sample concentration and particulate concentration, potentially representing 'dissolved' P. This is of particular interest because the basic assumption of biological availability depends on the presence of hydrated ions for nutrient uptake. For certain, the higher the total P concentrations, the lower were the portions of P bound to NNP and colloids, or, the other way around, at conditions of low overall P concentrations in the forest stream water systems, higher P binding to NNP and colloids was observed. Therefore the P containing particles will constitute a high relevance for nutrient cycling or similarly represent a major loss factor, which is of high expense to the ecosystem.

Table 4.3.2: *Correlation coefficients of total elemental concentrations to binding percentage of respective element per NNP and colloidal fraction and to sum of all fractions. Coefficients were calculated according to Spearman r correlation. Asterisks (*) denote significant correlations (p<0.05).*

Fraction	*P*	*C*	*Al*	*Si*	*Mn*	*Fe*
Correlation of total elemental concentration to percentage particle bound concentration						
1st	-0.52*	0.58*	0.22	-0.25	-0.66*	-0.05
2nd	-0.54*	0.73*	0.39*	-0.27	-0.52*	0.37*
3rd	-0.66*	-0.36	0.06	-0.31	-0.60*	-0.12
all	-0.56*	0.58*	0.29	-0.25	-0.56*	0.08

Interestingly, there is not only a high relevance of NNP and colloids for phosphorus binding and transport, but also for organic C, Mn and Fe (Annex Table S1). Al and Si were detected in high amounts in the total sample; yet, the percentage of Al bound to NNP and colloids was generally below 5%, for Si even below 2%. Therefore, these low percentages allow a distinct clustering of aluminosilicate minerals to P in the largest size fraction. The percentage of organic C and Mn

associated with NNP and colloids varied between sites from 7% to 50% and 15% to 80%, respectively. These elements did not vary in a comparative way, indicating different factors which influence organic C and Mn concentrations in stream waters and respectively bound in NNP and colloidal structures. Large organic matter inputs can be expected for thick and highly developed organic soil horizons, whereas Mn, as important redox element for multiple biological processes, can indicate microbial activity and turnover (Keiluweit et al. 2015). The percentages of Fe associated to NNP and colloids, which ranged from 26% to 57%, were intermediate and less variable with respect to the observed elements. In contrast, total Fe concentrations varied highly. Hence, Fe binding to NNP and colloids seems to be a favorable and stable process which only declines when Fe is present in very low concentrations.

It was interesting to investigate if such changes are reflected by environmental parameters such as the C to P, Fe to P or other predictive ecosystem response ratios. The relationship between the dissolved P proportion and the NNP and colloid bound P below 450nm is of interest to better understand nutrient cycling and availability. To contextualize phosphorus in freshwater ecosystems, stoichiometry has been used for a long time (e.g. Elser et al. 2000; Hecky et al. 1993; Redfield 1934). For the C:P ratio of freshwaters, Hecky et al. (1993) confirmed a severe phosphorus deficiency of seston above a C:P value of approx. 250 (Hecky et al. 1993). This basic food chain analysis indicates a possible validity of the P deficiency value of 250 for all soluble nutrients of an ecosystem. The boundary value of 250 was recently confirmed for phytoplankton in food webs as well (Elser et al. 2000). Here, the truly dissolved phosphate concentration and the C:P ratio is utilized to represent the proportion of easily available P, in the form of dissolved mineral P from bedrock, in stream water which is increasingly depleted as soil pedogenesis progresses. In order to obtain an estimation of the availability of the P to plants and microorganisms, the C:P ratio was calculated for each stream. In freshwater systems, a value above approximately 250 is usually considered to represent P limitation (Elser et al. 2000; Hecky et al. 1993). This value was exceeded in three of the sites (Figure 4.3.3). When the study sites were sorted according to C:P ratio in the stream water, they can be considered as catchments along a gradient of increasing P depletion: Conventwald ≤ Vessertal << Wüstebach ≤ Mitterfels << Leirelva. Along this trend of increasing C:P ratio values, the concentration of dissolved P declined significantly and intriguingly the percentage of P bound to NNP and colloids increased, significantly for the first fraction (Figure 4.3.3, c.f. Table 4.3.1). Likely, the changes in NNP and colloid bound P reflect the state of weathering. With increasing weathering, P is increasingly stored in organic matrices and occluded in Fe- and Al-(hydr)oxides (Turner et al. 2007; Walker and Syers 1976). Hence, these P forms contribute increasingly to the NNP and colloids as dissolved P is increasingly limited. Finally, almost 90% of total P export occurred with NNP and colloids (Table 4.3.1, Figure

4.3.3). The variations (given as standard deviations) of the mean C:P values in Figure 4.3.3 are mainly due to differences between the individual sampling locations from the same site with contributions from sampling and sample analysis. The C:P values show three distinct groups of sites: low mean values for Conventwald and Vessertal, intermediate values for Wüstebach and Mitterfels and the highest value for Leirelva. Further, the percentage of P binding to the NNP and colloid fractions confirms this trend with the exception of Wüstebach. Thus, despite of elevated standard deviations in a few cases, the observed trends were confirmed and results are consistent with the site characteristics already shown previously through cluster analysis.

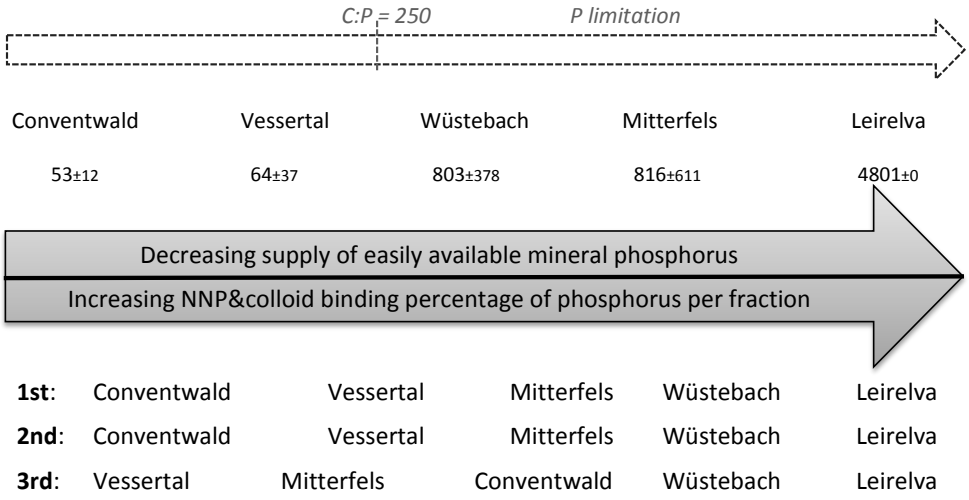

Figure 4.3.3: *Contrasting the availability of mineral phosphorus against the binding percentage of phosphorus in the three natural nanoparticulate and colloidal fractions. The availability of mineral P is also expressed as the C:P ratio of total stream water sample concentrations, the average C:P values ± standard deviation are given below the sites, for binding percentages see Table 4.3.1. A C:P ratio greater than ~250 (Elser et al. 2000; Hecky et al. 1993) indicates P limitation in an ecosystem.*

4.3.4 The first flush effect of stream water natural nanoparticles and colloids

NNP and colloids occur both in soil solution (Missong et al. 2016; Regelink et al. 2013) and surface waters (Andersson et al. 2006; Dahlqvist et al. 2004; Gottselig et al. 2014; Stolpe et al. 2010), whereas P binds and is transported by mineral (iron or aluminosilicates) or organomineral (organic and metal) particles (Gottselig et al. submitted). The aqueous phases of a catchment constantly interact; especially during strong precipitation events a high input from soil solution to stream waters is expected. This high input is termed "first flush effect" and incorporates not only the soil surface runoff water entering the streams but this water also transports mobile soil constituents.

The first flush effect has previously been observed for sediment and dissolved P (<0.45µm) in an agriculturally influenced headwater catchment (Stutter et al. 2008), yet this result could not be significantly seen for mixed land use catchments (Hudak and Banks 2006). Interestingly, the results for first flush effect studies are in general very biased. Many studies in the urban context have evaluated the first flush effect (e.g. Deletic 1998; Hathaway et al. 2012; Soller et al. 2005; Taebi and Droste 2004) for a multitude of parameters. For the majority of studies, solely the total suspended solids (TSS) have shown to exhibit a more or less distinct first flush effect. In highly managed and especially fertilizer influenced catchments, nitrogen or phosphorus can show a first flush effect (Flint and Davis 2007; Lee et al. 2002) as well. Field studies to determine the first flush effect in natural catchments have so far not been conducted.

The first flush effect for nanoparticles and fine colloids is defined as a successive increase in the particulate bound elemental concentrations parallel to the first discharge wave during a high precipitation event (Figure 4.3.4) (de Jonge et al. 2004; El-Farhan et al. 2000; Schelde et al. 2006). In contrast to the expectation that distinct drying and wetting cycles promote the release of colloids from soil (El-Farhan et al. 2000), Kjaergaard et al. (2004a; 2004b) only observed an increased release of colloids from moderately wet soil columns and assumed an accelerated particle bonding and cementation in dried soils. Forested headwater catchments are especially of interest in this context due to the overall low phosphorus concentrations in forest soils in comparison to agricultural or grassland sites (Stutter et al. 2012). The first flush effect has a high loss potential for nutrients from the catchment and can therefore have a significant impact on the mobile and available P pool. Still, a first column study on the first flush effect induced loss of colloidal phosphorus could not confirm this effect (Siemens et al. 2008). Now, through the AF^4 technique coupled online to a multitude of detectors, a more precise and size dependent analysis of the first flush effect of NNP and colloids can be performed.

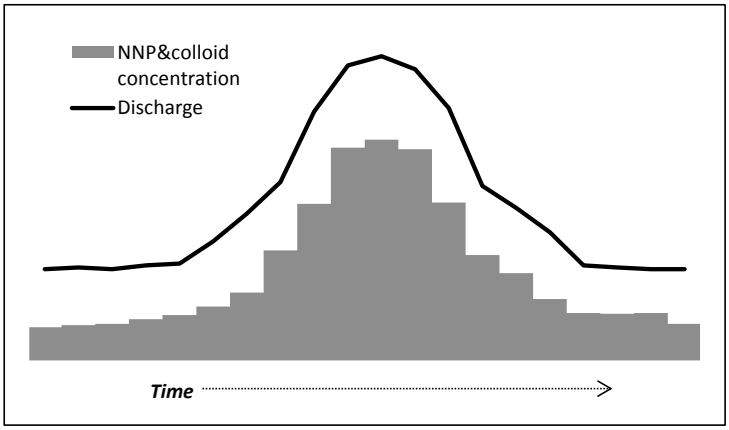

Figure 4.3.4: *Conceptual figure defining the first flush effect of natural nanoparticles and colloids over time. Conceptually it is assumed that the NNP and colloid concentration (grey) at the same time the discharge wave (black) peaks.*

To assess the potential first flush effect of NNP and colloids in forested headwater catchments it was hypothesized that an increased amount of NNP and colloids are washed out of a headwater catchment through the first downstream wave following a high precipitation event. To assess this topic, steam water samples from W, MIT and CON were sampled in high frequency intervals during storm events. The first analysis of this data revealed a profound effect for the organic C increase (up to 13-fold) in the first fraction throughout all three sites. Intriguingly, the NNP and colloidal organic C did not transport other elements, such as phosphorus. Thus also no coupled first flush effect as described for the preferential binding of P to NNP and colloids (Gottselig et al. submitted) could so far be observed. Despite recent findings on the source of dissolved organic matter (DOM, <0.45µm) in a lowland catchment under agricultural impact during storm conditions showing that soil DOM flushing and macropore erosion majorly increase during storm events (Jeanneau et al. 2015), it is unlikely that the flushed organic matter does not co-transport further elements (e.g. Fe) or nutrients (e.g. P).

4.3.5 Inferences for stream water natural nanoparticle and colloid release from surrounding soils

The data from this chapter was compiled with data on NNP and colloids from soil extracts from overlapping sites. These sites were VES, MIT and CON of the national scale project. It was hypothesized that on account of a comparison of elemental concentrations and elemental ratios, it can be elucidated to which extent NNP and colloids from soils are released into the stream waters. Preliminary data analysis already revealed distinct differences in elemental concentrations between soil and stream water, with soils showing significantly higher concentrations of all elements, yet

elemental ratios, between e.g. C and P reflect similar tendencies for the prediction of the nutritional status of a site. Stream water analysis (Figure 4.3.3) revealed a P limitation for MIT, whereas CON and VES did not exhibit this P limitation according to the C:P ratio. These tendencies could be confirmed for the soil extract C:P ratios (data not shown).

4.3.6 A first approach on the natural nanoparticle and colloid composition of aquatic ecosystem samples

The effect of groundwater inflow has previously been found to have a dilution effect on NNP and colloids (Gottselig et al. 2014), yet through rainfall and soil water, further aqueous input reaches a stream. Therefore, in the context of the national scale sampling, monthly stream water samples of the stream source and catchment outlet point, rainfall, interception water, groundwater and throughflow water through three soil depths were collected at the site CON. NNP and colloidal compositions of all aqueous samples were recorded on a monthly basis to define the sample specific signature and their influence on the overall stream sample signature. A first analysis of the data has revealed a sample specific signature which marginally varies over the course of one year, yet is constant in its basis with respect to intensities of the elemental signatures in the predominant fractions present of each sample. For example, as already shown in Chapter 4.2, groundwater from CON exhibits low to no NNP and colloid fractions, whereas the fraction intensities significantly increase from rainfall to interception water, indicating a wash-off of vegetation which could potentially be an interesting input to stream waters.

4.4 Distribution and composition of P carrying nanoparticles and colloids across European stream waters[9]

4.4.1 Fractionation of natural nanoparticles and colloids on European scale

The application of the AF^4 revealed three distinct fractions of NNP and colloids in European stream waters (Figure 4.4.1a, b). NNP were the exclusive constituent of the first two fractions and accounted for approx. 20% of the third fraction. The first and smallest NNP fraction included particles with

[9] Contains excerpts from:
Gottselig N, Amelung W, Kirchner J, Avila Castells A, Båth A, Batalla R, Bol R, Blomkvist P, Estany D, Eugster W, Falgin C, Granger S, Hernandez Crespo C, Herrmann F, Jackson-Blake L, Keizer JJ, Knöller K, Laudon H, Laurila T, Lehner I, Lindroth A, Löfgren S, Ottosson Löfvenius M, Lohila A, MacLeod K, Martín Monerris M, Mölder M, Müller C, Nasta P, Nischwitz V, Paul-Limoges E, Pierret MC, Pilegaard K, Romano N, Stähli M, Sebatià MT, Taberman I, Voltz M, Wendland F, Vereecken H, Siemens J, Klumpp E. Natural Nanoparticles and Colloids in European Forest Stream Waters and their Role for Phosphorus Transport. Global Biogeochemical Cycles, ready for submission.

standard equivalent hydrodynamic diameters between 1 kDa (corresponds to 0.66 nm, equation 2.2, Erickson 2009) and 20 nm, the intermediate NNP fraction above 20 nm to 60 nm and the largest size fraction included NNP above 60 nm up to colloids of approx. 300 nm diameter. Due to the maximum size range, all detected NNP and colloids fall into the operationally defined 'dissolved phase'. Elemental signals were recorded in all three size fractions with varying intensities, with the main focus on the variable P concentrations in the peaks and across Europe (Figure 4.4.1c). These fractions correspond to the fractions detected for multiple stream waters in Germany (Gottselig et al. submitted) and also Stolpe et al. (2010) found three to four fractions of colloids in the Mississippi.

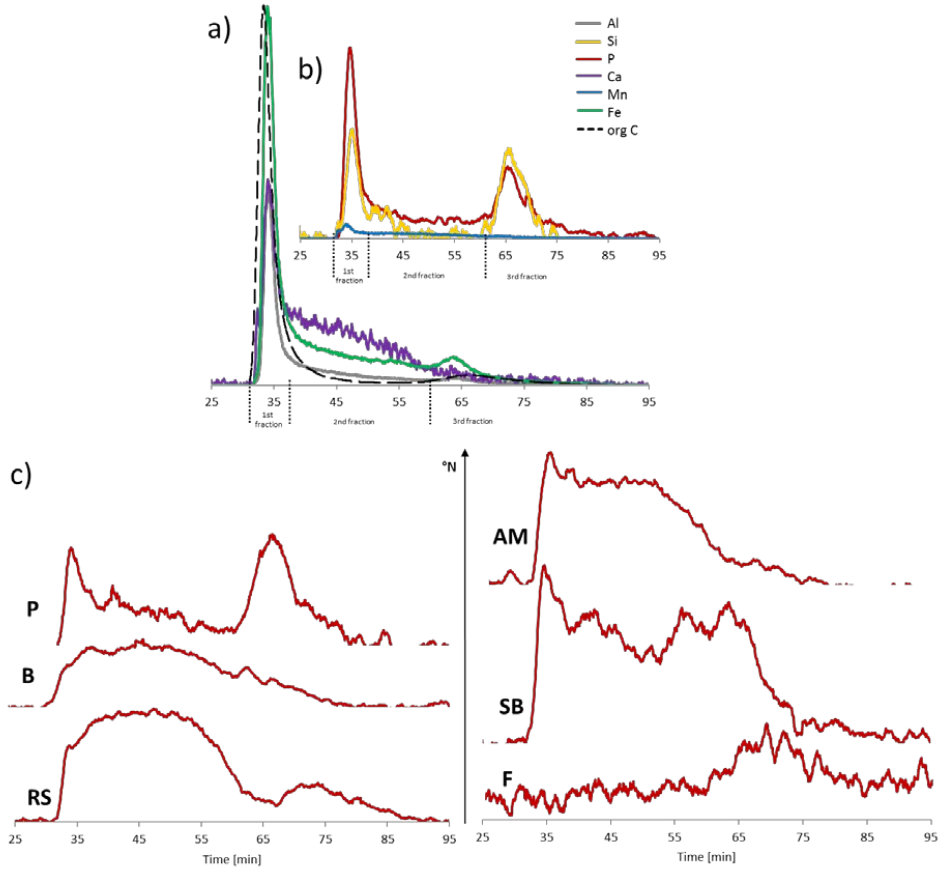

Figure 4.4.1: *AF^4-ICP-MS and AF^4-OCD raw data fractograms. a) Fractogram of Al, Ca, Fe and org C of one sampling point at Krycklan, Sweden (K5); b) Fractogram of P, Si and Mn of one sampling point at Krycklan, Sweden (K5); c) Fractogram of P of three sampling points at different sites, AM = Allt a'Mharcaidh, Scotland, SB = Strengbach, France, F = Franchesiello, Italy, P = Pallas, Finland, B = Bode, Germany, RS = Ribera Salada, Spain. X-axes represent the method time in minutes, focus time was partially cut off, only actual peaks are shown. Y-axes for Al, Si, P, Ca, Mn and Fe represent mass flow in µg/min, for org C it is detector signal in V. Fraction borders apply to the ICP-MS signal, for the OCD evaluation these borders were modified.*

4.4.2 Colloidal significance for element partitioning in water samples

When relating the summed element concentrations in the fractions to the total element concentrations, the minimum proportion of elements that was particle bound were obtained. The proportion is intentionally termed minimal due to the fact that particle loss through AF^4 fractionation is unknown. In any case, the proportions of the different elements under study associated to NNP and colloids ranged from 0.0 (not detected) to 99.5% of total elemental concentration. Thus, the role of NNP and colloids for element transport may be very variable, ringing from insignificant to the complete control of aqueous element cycles.

With respect to the average percentage of elements bound to NNP and colloids (colloidal elemental concentration as percentage of total sample elemental concentration) in the three fractions, the AF^4 results underlined the high relevance of NNP and colloids for the distribution of elements in water samples. Up to 99% of Fe, 96% of P, 96% of Mn, 95% of Al, 92% of org C, 46% of Si and 27% of Ca were associated with NNP and colloids. The average percentage (mean ± standard deviation, n=96) for Fe was 53±21%, for P 50±26%, for Mn 26±29%, for Al 41±24%, for org C 20±20%, for Si 2±5% and for Ca 4±6%. The respective median values were 55% (Fe), 51% (P), 10% (Mn), 37% (Al), 11% (org C), 0.2% (Si) and 1% (Ca). The percentages reflected a significant contribution of the nanoparticulate and colloidal fractions for the operationally defined 'dissolved' elements Fe, P, Al, org C, Mn, Ca and Si (in descending order) which can be up to almost 100% of the total elemental concentration of the sample. Former research on the significance of colloid-bound elements within the operationally defined 'dissolved' fraction indicates a maximum Fe binding in colloidal form between 80 to 100% with averages between 50 and 90% (Hill and Aplin 2001; Jarvie et al. 2012; Martin et al. 1995), for org C between 40 and 80% with averages between 20 and 60% (Jarvie et al. 2012; Martin et al. 1995; Wen et al. 1999) and for Al around 40 to 50% with averages around 45 to 55% (Hill and Aplin 2001; Jarvie et al. 2012). Hill and Aplin (2001) determined up to 50% binding of Mn in colloidal form (average 23%), up to 30% for Ca (average 20%) and low percentages up to a maximum of 10% for Si (average 0%). Dahlqvist et al. (2004) found an average of 16% colloidal Ca in an Arctic and an Amazon river (also assessed with FFF). Jarvie et al. (2012) further found a fraction of up to 90% (averaging at 66%) of organophosphorus compounds associated to colloids. In summary, the data confirmed that particle bound transport is a major pathway of element losses from a given sampling point within the flowing river, yet at variable contributions to overall element fluxes at the sites.

4.4.3 Elemental composition patterns of natural nanoparticles and colloids on the European scale

As indicated, the proportion of elements that was recovered in NNP and colloids was significant, yet with variations across the European sites. Hence, the distribution patterns of the elemental compositions of NNP and colloidal fractions were investigated as a function of the total elemental concentration. The goal was to establish empirical functions for estimating the concentrations and the composition of NNP and colloids in water samples based on the total elemental concentration. Two types of relationships between NNP and colloid concentrations of elements and total concentrations could be observed independent of the fraction in question: rather constant concentrations of elements in the NNP and colloid fraction independent of the total concentration of the respective elements (Si, P, Ca, Mn) and positive linear trends between the concentration of elements in the NNP and colloid fraction and total concentrations (Fe, Al, org C) (Figure 4.4.2). The linear functions with log scaled axes are defined for $x \geq \log_{10}(1)=0$ (Figure 4.4.2). The respective elements exhibited steady percentages of particulates respective to the total amounts, independent of a change in total elemental concentration. Both distribution patterns are consistent on trends for all three fractions but differ in intensity between the fractions (Table in Figure 4.4.2).

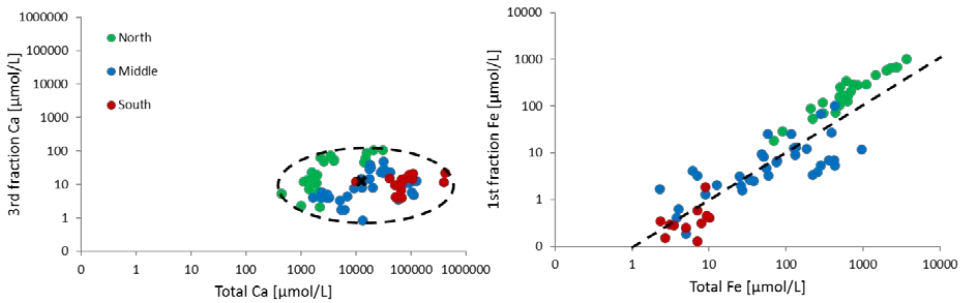

	Si	P	Ca	Mn	Fe		Al		org C	
		median			*m*	*b*	*m*	*b*	*m*	*b*
1st	0.84	1.33	26.7	0.05	1.00	-0.83	0.76	-0.55	1.71	-1.72
2nd	0.43	3.82	52.9	0.16	0.85	-0.47	0.65	-0.57	0.88	-1.55
3rd	2.3	2.41	9.52	0.13	0.72	-0.26	0.5	-0.07	0.56	-1.23

Figure 4.4.2: *Exemplary distribution patterns. Top left: Grouped diagram for 3rd fraction Ca exemplary for Si, P, Ca and Mn across all fractions, black cross indicates cloud center and black dashed line represents extent; top right: Linear distribution with log-scaled axes for 1st fraction Fe exemplary for Fe, Al and org C across all fractions, black dashed line represents mean regression line defined above $\log_{10}(1)=0$; data color coding represents geographical classification as well as predominant pH of the region as in Figure 4.4.4; bottom Table: Classification of distributions per element fraction, Si/P/Ca/Mn: medians represent highest density of data points, Fe/Al/org C: linear regression slope (m) and intercepts (b) of log transformed data. n=96; unit: µmol/L, org C: mmol/L.*

The variable slopes reflect the pH dependent concentrations of Fe, Al and org C which, due to the overlap with the operationally defined 'dissolved' phase, shed new light on the availability of elements below 0.45 µm. Most interestingly the slope of 1st size fraction Fe is 1.0 at an offset to the 1:1 line (=100% of total in NNP and colloids). This implies that a constant proportion of total Fe is present in this very fine nanoparticulate fraction (<20 nm) as average over all European sites independent of pH. This proportion was estimated at 85%.

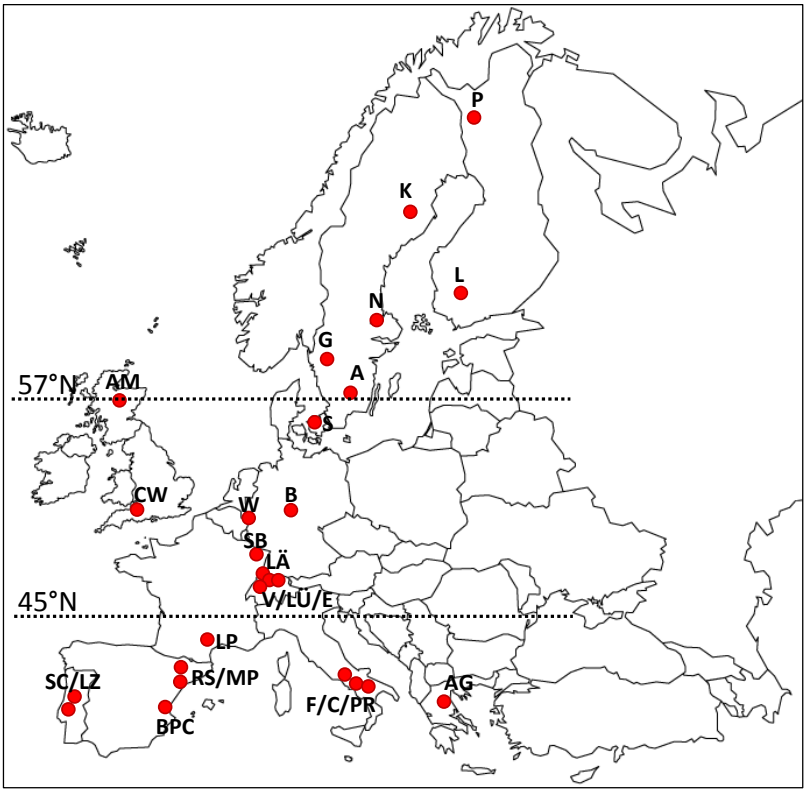

Figure 4.4.3: *Location of the 26 European sites along two transects. Dotted lines indicate geographical separation between northern (north of 57°N), middle (between 45°N and 57°N) and southern (south of 45°N) sites. One site (AM) touches the 57°N border because it partially exhibits tendencies towards the bordering region.*

Furthermore, a geographical effect could be observed for the distribution patterns (Figure 4.4.2) showing variable elemental concentrations across Europe (Figure 4.4.3). The elements exhibiting linear distribution patterns show data point stratification according to geographical region with Southern European sites at the lower end and Northern European sites at the higher end of the data application. This infers that the role of Fe, Al and org C for the binding to if not even formation and/or stabilization of NNP and colloid fractions varies across different geographic regions. Ca, Si, Mn

and P show grouped concentrations in similar particulate ranges at total concentrations which vary between the regions (Figure 4.4.2). In contrast, Ca, Si and Mn, as building block elements, have equal influence on the NNP and colloidal composition across all European sites and P, as transported element, showed steady concentrations within the particulate phase. The presented data clearly showed that it appears possible to predict the proportion of elements bound to particles, as it is either constant (Fe, Al, org C) or independent from total concentration but thus in narrower overall particle bound concentration range. This facilitates the inclusion of NNP and colloidal bound elements into nutrient cycling approaches and in turn refines their statements.

4.4.4 Approach for the pH dependent prediction of particulate elemental concentrations

On account of the pH driven separation between Fe, org C and Ca particles and their demonstrated interdependencies, these elements could potentially be used to estimate the presence of the remaining elements in the NNP and colloidal fraction. The comparison showed that Fe and org C can be utilized to predict the majority of elemental concentrations in the same fraction ≥50% certainty (Table 4.4.1). Al could also predict the same number of elements as Fe, especially interesting was the prediction of 3rd fraction Si at 61% certainty (Table 4.4.1) which underlines the fact that aluminosilicate minerals potentially are the main component of this fraction. The predictability through known Ca concentrations as well as the prediction of Si, Ca and Mn through any of the three dominant elements is not possible with a certainty ≥50% due to the weak linear trend these elements show as a function of total sample concentration.

An accurate estimation of the P concentrations in the fractions across all sites could not be found, but is essential if the straightforward measurement is not implementable. Particulate phosphorus exhibited stable concentrations regardless of pH change (Annex Figure S3) indicating that it can respond flexibly to different stream water pH values by either associating to Fe, org C or Ca. Therefore it was reasonable to differentiate P predictability by pH value. This resulted in a higher degree of certainty for the prediction of P than previously observed when including P data across all stream water pH values. In the acidic pH range P concentrations can be best estimated through Fe (certainty 40%, P=0.03*Fe-0.86) and org C (37%, P=0.35*orgC-0.53). In the basic pH range P can best be estimated through Ca (72%, P=1.11*Ca-1.05). The prediction of NNP and colloidal P in the neutral stream water pH range is primarily determined by the particulate Fe concentration (14%, P=0.20*Fe-0.68).

The shown predictabilities of particulate elemental concentrations give a first good insight into the reciprocal influences between elements in the fractions but they will have to be proven more in detail and potentially on an even larger scale.

Table 4.4.1: *Linear regression equations (m=slope, b=y-intercept) and goodness of fit (R^2) between the log_{10} transformed elemental concentrations per fraction and all particulate concentrations. Only data with a good predictor ($R^2 \geq 0.50$) are shown. Elemental concentrations for Al, Si, Ca and Fe are given in µmol/L, for org C in mmol/L.*

			org C	*Al*	*Ca*	*Fe*
1st fraction	*org C*	m		0.93	1.06	0.74
		b		-0.61	-1.07	-0.68
		R^2		0.74	0.51	0.79
	Al	m	0.8			0.77
		b	0.36			-0.11
		R^2	0.74			0.91
	Ca	m	0.48			
		b	0.52			
		R^2	0.51			
	Fe	m	1.07	1.19		
		b	0.61	0.05		
		R^2	0.79	0.91		
2nd fraction	*Al*	m				0.77
		b				-0.37
		R^2				0.80
	Fe	m		1.03		
		b		0.22		
		R^2		0.80		
3rd fraction	*org C*	m				0.43
		b				-1.47
		R^2				0.50
	Al	m			0.67	0.69
		b			-0.20	-0.21
		R^2			0.61	0.75
	Si	m		0.91		
		b		-0.12		
		R^2		0.61		
	Fe	m	1.17	1.09		
		b	1.33	0.02		
		R^2	0.50	0.75		
all particulate	*org C*	m		0.94		0.79
		b		-1.00		-1.01
		R^2		0.62		0.68
	Al	m	0.66			0.71
		b	0.58			-0.03
		R^2	0.62			0.85
	Fe	m	0.87	1.19		
		b	0.80	-0.01		
		R^2	0.68	0.85		

4.4.5 Forest stream water pH as determining variable for the elemental composition of natural nanoparticles and colloids

The pH value might be a master variable controlling the size and elemental composition of NNP and colloids. Therefore, the concentration and proportion of particle bound elemental contents were correlated with soil pH (Annex Figure S3). First individual relationships were evident, yet colloidal P lacked a relationship to sample pH (slope = 0.01). Hence, it was assumed that relationships are more complex and needed exploratory data analysis techniques.

This analysis yielded an effect of pH on the dominant composition of building block elements/compounds of NNP and colloid fractions, which were only indicative through the individual correlations (see above). The pH changes were now found to be a dividing factor between the sites, dividing them into Ca dominated and org C or Fe dominated NNP and colloidal sites for 1st fraction NNP (Figure 4.4.4). This was indicated by the opposing positions, directions of rays and longer ray length of these elements. P rays of the discriminant analysis did not reflect fundamental composition of the NNP and colloids, yet reflects the potential adsorption partners of P. The biplot of the 1st fraction (Figure 4.4.4a) on the one hand showed the clear distinction between the three pH classes, but also the relation of elements to each other in this fraction. Ca was clearly opposed to org C and Fe, whereas Ca tended towards the neutral to alkaline sites and org C and Fe to acidic sites. Through this, P was assigned a greater adsorption tendency towards Ca, potentially also Si, but opposing to org C. While the role of Si is unclear here, the analysis indicated that organophosphorus was not a main component of these fractions, likely because organophosphorus associates dominate in the larger fractions (Jiang et al. 2015). The tendency of Ca towards alkaline sites was even more prominent in the 2nd fraction (Figure 4.4.4b). Here, org C, Mn and Al were prevalent in the 2nd fraction and Fe could clearly be assigned to neutral sites and showed positive association to P. This possibly indicates changes in Fe-P association with pH. The separation of sites for the 3rd fraction, in contrast, was mainly driven by Al and Si, both common in aluminosilicate minerals. It therefore seemed likely that aluminosilicate minerals were a part of the building units of the larger sized NNP to colloidal fractions, and the opposing sign of the rays would be consistent with changes in variable charges across the given pH range. In the 3rd fraction (Figure 4.4.4c) preferential association of to the aluminosilicate mineral component Si with further association to Mn and Fe was seen. Mn and Fe potentially acted as bridging agents between expansive aluminosilicate minerals and P.

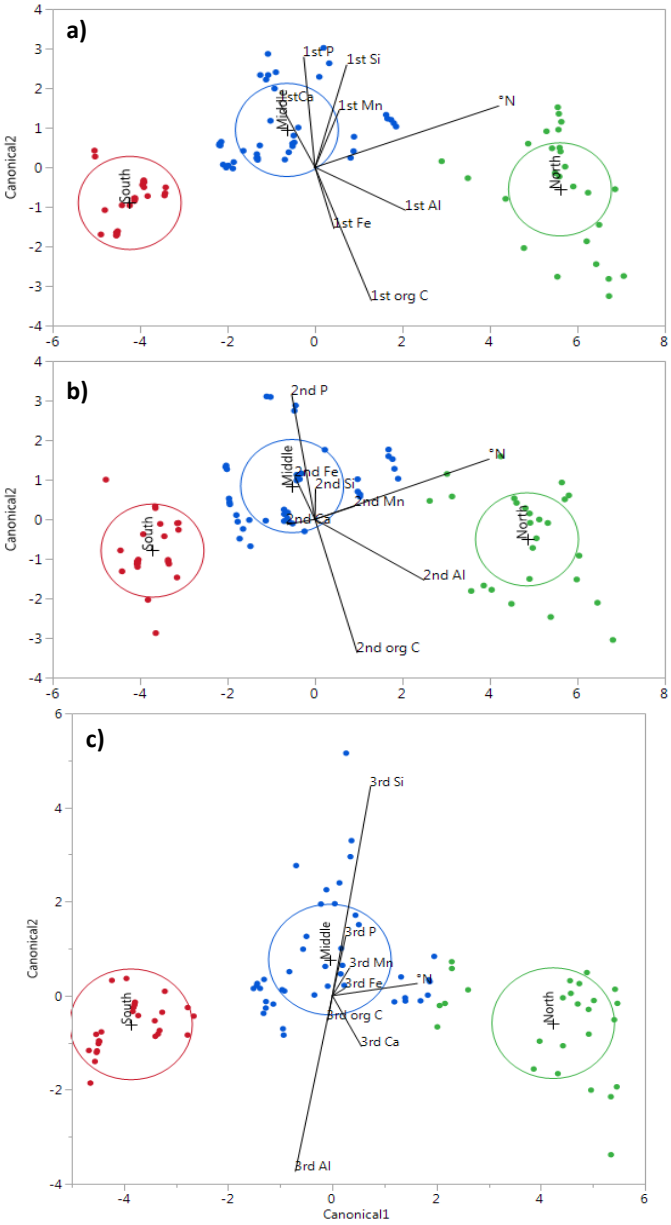

Figure 4.4.4: *Discriminant function analysis biplots for the categorical dependent variable pH classification (green=acidic, <6.6; blue=neutral, 6.6-7.3; red=alkaline, >7.3) to determine the elemental distribution per fraction (mol/L) (a) 1st, b) 2nd, c) 3rd fraction, according to the pH classification. The axes show the measure of effect size as canonical correlation values. Ray length is proportional to measure of effect size, where longer rays indicate a strong effect size and opposing rays indicate contrary tendencies. Small crosses mark the center of the three classes of the categorical dependent variable pH. Circles represent 95% confidence interval of mean pH score. n=96.*

In summary, it can be supported that the stream water pH gradient allowed a separation of three geographical regions in Europe (Figure 4.4.3) because it predetermines the surface charge and thus dominant aggregation behavior of NNP and colloids. According to the stream water pH values at sampling, the borders between the regions could be determined along the latitudes of 45°N between South and Middle and 57°N between Middle and North. The pH differentiation had been identified before for the operationally defined 'dissolved phase' of org C and other elements in water (Brady and Weil 1996; Lampert and Sommer 1999a; Lampert and Sommer 1999b; Lampert and Sommer 1999c) and could now also be confirmed for NNP and colloids (Figure 4.4.4a-c).

The concentration of P bound to NNP and colloids was rather constant across the complete pH range in contrast to the other elements in question (Annex Figure S3), indicating that all above mentioned NNP and colloid types, with particular focus on contrasting Fe and Ca dominating conditions, could act as P-carriers and binding partners, whereas flexible association of P dependent on prominent building block elements of NNP and colloids exists.

4.4.6 Preferential P binding of the different geographic regions in Europe

To identify clear preferential binding of P to another constituent of the distinct size fractions across all European sites and samples, complete linkage cluster analysis with '1-Pearson r' as distance measure was applied. Clear preferential binding partners for P across differing climate parameters could be defined as demonstrated in Chapter 4.3.2, yet at lower Pearson r values. The strongest clustering of P in the 1st fraction is to Fe (Pearson r = 0.30), in the 2nd fraction to organic C (0.07) and in the 3rd aluminosilicate mineral dominated fraction (strong Si and Al cluster, Pearson r = 0.98, Annex Table S2) to Fe (0.48). The results of the cluster analysis contradicted the potential P association to building block elements/compounds identified by the discriminant function analysis. With cluster analysis an actual association of P to building block elements/compounds is identified whereas the discriminant function analysis only reflects major elemental presence on account of the pH classification which determines the canonical variables. In line with the three fractions of NNP and colloids (section 4.4.1), the preferential binding of P to the particles in these fractions across all European sites is also in accordance to the results previously obtained on a national scale (Germany) (Gottselig et al. submitted).

To better understand the element patters within the fractograms, cluster analysis was performed for the elements within the three fractions. It revealed that the 1st fraction was dominated by a close clustering of org C, Al, Ca and Fe, similar to the 2nd fraction, with a slightly higher number of good clustering results for Fe than of the rest, and for the 3rd fraction Si and Al clearly dominate the fraction constituents (Annex Table S2) with further prominent clustering of Fe. The distribution of P

was not a prominent parameter that characterized the composition of the different fractions across all regions, however, in line with the discriminant analysis, clustering of P was closest with Fe for the acidic, Northern Europe, sites, and best with Ca for the alkaline, Southern Europe, streams (Table 4.4.2). Up to date, this is potentially the first time that there is analytical evidence for the relevance of climatic and environmental parameters such as vegetation and soils for the binding of P to the varying NNP and colloids in European stream waters.

Table 4.4.2: *Pearson r values for clustering of phosphorus within all three size fractions per geographic region (c.f. Figure 4.4.3). n=96.*

	North			Middle			South		
	1st	*2nd*	*3rd*	*1st*	*2nd*	*3rd*	*1st*	*2nd*	*3rd*
org C	0.55	0.47	0.2	0.49	0.33	0.48	0.31	0.67	0.17
Al	0.41	0.62	0.33	0.29	0.49	0.20	-0.32	-0.13	-0.04
Si	0.45	0.40	-0.07	-0.22	0.05	0.16	0.27	0.06	0.16
Ca	0.18	0.48	0.71	-0.19	-0.18	-0.04	0.80	0.74	0.86
Mn	0.67	0.74	0.77	-0.22	-0.24	-0.03	-0.39	-0.19	-0.32
Fe	0.81	0.75	0.61	0.40	0.16	0.36	-0.34	-0.14	-0.06

4.4.7 The influence of site specific parameters on element concentrations of natural nanoparticles and colloids

When analyzing stream waters, the surrounding soil and underlying bedrock are the environmental compartments in closest vicinity to the stream and most influential input factors. If no chemical analysis of these compartments is available, like in the present study, these parameters are classified and thus are non-numeric factors. A possibility to estimate the influence of non-numeric data is by grouping the numeric values by the non-numeric classes. In this study, soil, bedrock and dominant tree type were divided into subgroups and cluster analysis was performed with the respective data sets. A resulting difference between the subgroups is regarded as a varying influence and the Pearson r value informs about the intensity of this influence. The grouping of climatic and environmental site specific parameters was applicable for dominant tree species (coniferous vs. deciduous vs. both) and for soil type (dystrophic, eutrophic and semi-terrestrial), whereas a classification of bedrock types was less straightforward and did not serve as comparable basis for classification analysis. Dystrophic soils were Podzol, Cambisol (coniferous), Leptosol and Regosol, eutrophic soils were Cambisol (deciduous) and Mollisol, semi-terrestrial soils were Fluvisol and Gleysol. This comparison yields the effects of soil class and dominant tree type on the elemental composition of the particulate phase. A significant effect (Student's t-test, $p<0.05$) of soil class was found for all particulate Si, P, and Mn (Table 4.4.3). Semi terrestrial soils showed significantly higher

Si inputs to colloids, for Mn this was found to be valid for the eutrophic soils, for P the effect between higher inputs from semi terrestrial to eutrophic soils was found with intermediate dystrophic influence. For the analysis of the effect of dominant tree type the overlapping class 'both' contained equal parts of coniferous and deciduous influences and thus predetermined only two significantly different counterparts. The coniferous class was significantly different of the deciduous class for all particulate org C, Al, Ca and Fe, interestingly not for P (Table 4.4.3). For all elements the washout from coniferous tree stands was significantly higher than the influence from the deciduous stands, in line with the tendency of especially coniferous stands to have acidic soil pH values. This favors the NNP and colloidal formation due to the stronger adsorption partners, especially metals, for negatively charged compounds such as phosphate or organic matter.

Table 4.4.3: *Mean values of molar elemental concentrations per class of site specific parameter and significance level. Significantly different classes per element are marked by a and b, Student's t-test, p<0.05.*

		org C	*Al*	*Si*	*P*	*Ca*	*Mn*	*Fe*
soil class	*dystrophic*	0.41 **a**	1.91 **a**	0.41 **a**	0.31 **a,b**	5.88 **a**	0.03 **a**	3.33 **a**
	eutrophic	0.34 **a**	2.02 **a**	1.56 **a**	0.22 **a**	4.07 **a**	0.05 **b**	5.33 **a**
	semi terrestrial	0.07 **a**	3.43 **a**	4.85 **b**	0.44 **b**	4.05 **a**	0.01 **a**	1.17 **a**
dominant tree type	*coniferous*	0.54 **a**	2.64 **a**	1.03 **a**	0.33 **a**	6.98 **a**	0.03 **a**	5.68 **a**
	both	0.07 **a,b**	0.07 **a,b**	0.04 **a**	0.85 **b**	3.30 **a,b**	0.00 **a**	0.05 **a,b**
	deciduous	0.03 **b**	1.05 **b**	1.30 **a**	0.21 **a**	1.79 **b**	0.03 **a**	0.57 **b**

Different subcategories showed strong clustering of P to another element. Eutrophic soils showed a distinct clustering of P and Fe in the 1st fraction as well as of P and Si in the 3rd fraction. Further, dominant tree type can have explanatory power for P to Ca in the 1st fraction and P to Si in the 3rd fraction again. The 2nd fraction experiences mixing effects of dominant tree type and soil class. For the non-numeric factors in total it was seen that the 1st and 3rd fraction composition is highly influenced by soil, bedrock and dominant tree type.

4.4.8 Central environmental factors driving natural nanoparticle and colloid fraction concentrations

In 48% of the cases, when assuming that each of the seven elements can have a different driving factor per fraction (7 elements per 3 fractions = 21 cases in total), MAT shows highest Spearman rank order correlation coefficients (Table 4.4.4). Besides average slope (19%), average site elevation, annual runoff and water pH only majorly contribute to one (5 times = 5% per case) or two (resource manipulation; 10%) elemental presences in the fractions. MAP, stream water temperature, soil sand

content, catchment size and forest cover do not seem to primarily influence any element in the fractions.

The parameters MAT and MAP are the most decisive parameters for climate descriptions (Peel et al. 2007) and thus potentially also for the elemental presence in the NNP and colloid fractions. In general if a significant effect was observed, an increase in MAT or MAP alone leads to a decrease in elemental concentrations with the exception of MAP on Al and Si in the 3rd fraction (Table 4.4.4). The data has shown that especially MAT significantly ($p<0.05$) influences specific elemental presences in the fractions also as the dominating influence factor (Table 4.4.4). The percentage of MAT as highest parameter influence is 71% for the 1st fraction (5 of 7, cf. Table 4.4.4), 57% for the 2nd fraction and 14% for the 3rd fraction. This result indicates that nanoparticles up to 60 nm (1st and 2nd fraction), which are most probably either organic particles or P associated to metal (hydr)oxides (Gottselig et al. submitted), increasingly occur as MAT decreases. For the organic constituents, this fact seems to be contradictory to the general understanding of stream water organic matter dynamics (e.g. Bol et al. 2015) at first glance, yet these dynamics seems to be equivocal (Kirschbaum 2006) because on the global and local scale the correlation observed for the present study shows validity (Kirschbaum 1995; Post et al. 1982). For NNP a potential increased mobility of 1st fraction organic particles is assumed which are mobilized through the colder MAT (Kalbitz et al. 2000) by more frequent freezing of organic soil horizons, acting as organic NNP sources, thus releasing organic particles from the surrounding soil matrix. With regard to iron (hydr)oxides the negative relationship of Fe and MAT is reasonable when incorporating the temperature dependence into the solubility equation of colloidal versus truly dissolved Fe at a given pH (Lofts et al. 2008). Further, the aluminosilicate mineral dominated fraction >60 nm is increasingly present as MAP values rise, indicating that precipitation plays a key role in soil wash out processes resulting in excess presence of this fraction in the stream waters. Rainfall controls the dissolution of elements into soil solution, thus processes governing aluminosilicate mineral formation are more pronounced under conditions of abundant rainfall (Velde and Meunier 2008). Aluminosilicate minerals can adsorb organophosphorus compounds (Ognalaga et al. 1994) or, in expansive 2:1 confirmation with Fe or Al oxide coatings, sorb P (Yaghi and Hartikainen 2013). Due to the large quantities of large NNP or colloidal aluminosilicate minerals in soil, the relation of MAP to 3rd fraction Al was positive even though the MAP effect is in general negative. The negative effect on org C and Ca presence in the 1st and 2nd fractions and Ca in the 3rd fraction can be related to high precipitations which can exceed a maximum soil capacity. Above this the soil is leached resulting in a decreased presence due to non-sufficient replenishment of the soil (van Ranst et al. 2004). An effect of MAT or MAP on P could only be detected in the 1st and 3rd fractions. This is potentially due to the nature of P binding to NNP and colloid. P is not a primary building block

Table 4.4.4: *Nonparametric Spearman rank order correlation coefficients for all significant correlations (p<0.05) of the elemental concentrations per fraction to all numerical background parameters, bold values are ≤ 0.5 or ≥ 0.5, red = highest correlations per element and fraction. n = 96.*

		MAT	MAP	average elev	catchment size	average slope	forest cover	forest management	annual runoff	water pH	water T
1st fraction	org C	***-0.81***	-0.32	-0.45		***-0.65***	-0.35			***-0.52***	***-0.5***
	Al	***-0.79***		-0.42		***-0.47***	-0.38		-0.37	***-0.5***	***-0.53***
	Si	-0.48		-0.33						-0.26	
	P	-0.34				-0.39					
	Ca	***-0.54***	-0.41	-0.32			-0.29				
	Mn	-0.41		-0.32				0.35	-0.39	-0.42	-0.33
	Fe	***-0.79***		-0.41		***-0.53***		0.33		-0.49	-0.43
2nd fraction	org C	***-0.64***	-0.37	-0.38		***-0.53***	-0.33			-0.45	-0.38
	Al	***-0.77***		-0.33	0.34	-0.44	-0.3		-0.42	-0.44	-0.49
	Si										
	P			0.39		-0.33		-0.33	0.36		
	Ca	-0.38	-0.35								
	Mn	-0.27						0.39			
	Fe	***-0.73***		-0.41		***-0.61***				-0.41	-0.41
3rd fraction	org C	***-0.63***				***-0.64***				-0.27	
	Al	-0.46	0.31			-0.44					
	Si	-0.29	0.28			-0.41			0.49		
	P	-0.37				***-0.49***					
	Ca	-0.35	-0.26								
	Mn							0.41			
	Fe	***-0.57***		-0.31		***-0.59***		0.32		-0.3	
parameter influences [%]	highest	48	0	5	0	19	0	10	5	5	0
	all	20	7	12	1	15	5	6	5	11	7

structure of NNP and colloid but adheres to organic and/or metallic particles, thus it depends on the presence of these building block structures for P to be present in/on NNP and colloids.

4.4.9 Indirect effects of environmental factors on natural nanoparticle and colloid fraction concentrations

Environmental factors do not only influence the elemental presence in the NNP and colloid fractions directly but also indirectly act through their influence on other factors which then directly affect the particles. The assumption was tested if an indirect effect of MAT and MAP, as central environmental factors determining the climatic classification of a site, through site specific variables, which form under the influence of the central environmental factors, such as vegetation cover, annual runoff, stream water pH and stream water temperature can be detected. These site specific variables then in turn influence the building block structure and composition of NNP and colloids which further influences the P concentrations on the particle fractions via the previously identified preferential association partners of P. For parameter data of the European sites, see Annex Table S3. The results neglected this long chain of indirect effects on the P binding to NNP and colloid fractions. Instead, the data revealed a more direct effect on building block elements and structures which influenced P binding. Additionally, site specific parameters such as water pH did show to influence P binding, but through a more indirect pathway than by transmitting the MAT and/or MAP influence (Figure 4.4.5). A strongly valid model for the 1st fraction (p-value = 0.932, Chi square test) shows the negative influence of MAP on organic C, the strong link between organic C and Fe and eventually the significantly positive path from Fe to P (Figure 4.4.5, left), in line with results from Chapter 4.3.2. Further, catchment size has a slight negative influence on stream water NNP Fe. MAT and MAP also have significant inputs in the pathways of the 2nd fraction (p-value = 0.123, Chi square test), yet with the only significant influencing factor to P being MAP. Due to the fact that all other assessed environmental parameters did not yield a valid influence on P, a factor such as microbial activity can potentially link MAP and P. In contrast, in the 3rd fraction (p-value = 0.387, Chi square test) the recorded environmental parameters do not significantly affect P binding to the aluminosilicate minerals of the 3rd fraction but solely the presence of aluminosilicate minerals determines P adsorption in this fraction. The model of the 1st fraction was close to the highest p-value (1) and therefore reflected excellent validity. The 2nd and 3rd fraction results should be validated through larger dataset to see if changing pathways between the parameters arise. Interestingly, the linkage of aluminosilicate minerals to P over a metal component (Gottselig et al. submitted) was confirmed through the path analysis at specifically high agreements (R^2=0.98) between Al and Fe.

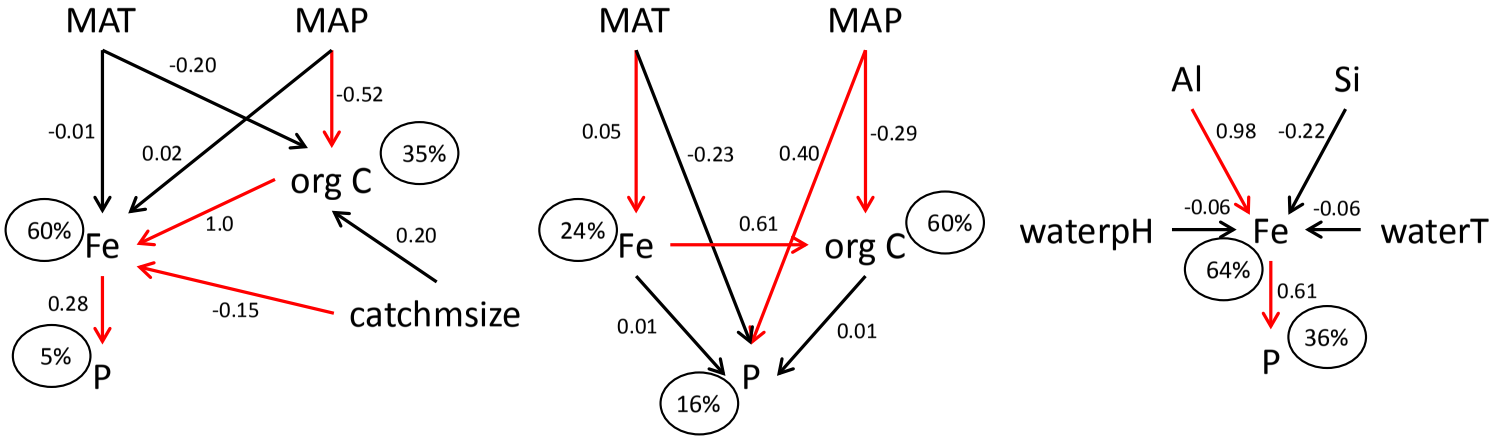

Figure 4.4.5: *Path analysis results for the particle fractions. Left: 1st fraction, p-value (Chi square test) = 0.932; center: 2nd fraction, p-value (Chi square test) = 0.123; right: 3rd fraction, p-value (Chi square test) = 0.387; red arrows indicate significant paths, small numbers on arrows indicate standardized path coefficients (range 0-1), percentages indicate the explained variance (R^2) per parameter. MAT = mean annual temperature, MAP = mean annual precipitation, catchmsize = catchment size, waterpH = stream water pH at sampling, waterT = water temperature at sampling.*

V

Summary, conclusions and outlook

Through this study, the complexity and dynamics of natural nanoparticulate (NNP) and colloidal P fractions in the stream water of forested headwater catchments was shown, enabling novel conceptual definitions of NNP and colloid fractions within the aqueous phases of an ecosystem. The acquired data extends the fundamental knowledge on natural nanoparticles and colloids as nutrient carriers and enhances the need for reviewing nutrient transport, cycling and acquisition processes in ecosystems, particularly for P.

Method development: A method for the fractionation of stream water NNP and colloids was developed with Asymmetric Flow Field Flow Fractionation (AF^4). The advantages of the individual adaptions to the AF^4 parameters are described and their applicability to environmental samples is shown. For the online analysis of the fractions, a UV detector, a dynamic light scattering device (DLS), a quadrupole inductively coupled plasma mass spectrometer (ICP-MS) with collision cell technology and an organic carbon detector (OCD) were successfully used. ICP-MS was especially adapted to P concentrations down to 0.1 µg/L. To further asses the applied methodologies, the oxidation efficiency of the OCD was investigated and showed a minimum recovery of 85% of the TOC measurements, the possibilities of organic C analysis with ICP-MS were investigated and proved to be feasible at organic C concentrations markedly above 1 mg/L and a methodological approach to in future assess the bioavailability of NNP and colloid bound P of environmental samples were performed.

Regional scale study: Next to sampling points in the main stream flow, additional sites with differences in hydromorphology were essential to trace main stream flow variations through tributary inflows. The AF^4 method with an online coupled ICP-MS allowed successful measurements of P, Fe, and Al, showing that up to 100% of P in the stream water is bound in the NNP and colloidal

fraction. This fundamental fact alone underlines the significance for NNP and colloids in aqueous samples and creates a necessity to further investigate NNP and colloids. The fractionation of the stream water samples achieved two distinct fractions. A small-size fraction, eluting first, contained NNP with a mean diameter of 8 nm. For this fraction, variations in P concentrations seemingly followed the course of Al variations. The NNP and colloids of the second fraction, had a mean diameter of 150 nm. In both fractions, high P concentrations were present at high Fe concentrations. Coelution of P, Fe, Al, and organic C compounds was observed for both particle fractions in most samples. For the first fraction, it is supposed that org C is the carrier of metals and nutrients. In the second fraction, org C acted as a matrix material, stabilizing microaggregates with metal (hydr)oxides and organically bound nutrients. The particle-bound P contents changed from before to after deforestation, possibly due to a high wash-out effect of NNP and colloids leading to a level where bound P was below the detection limit of the AF^4-ICP-MS system. In a further analysis, the collected fractions of the stream water samples were analyzed for their $d^{56}Fe$ value due to the fact that Fe is a major component of all NNP and colloid fractions. This showed different NNP and colloidal $d^{56}Fe$ values than from vegetation and soil samples, allowing a first distinction of potential source regions of NNP and colloids. In future, through the application of data analysis techniques such as e.g. end-member mixing analysis (EMMA, e.g. Hagedorn et al. 2000), these problems can be overcome and the numeric linkage of these pools can be conducted.

National scale study: This study showed that P binding to the NNP and colloidal fractions of stream waters is not restricted to a single particle type, but rather that there is a size-dependent binding of P to different chemical or mineral constituents or both. The successful coupling of AF^4 to OCD and ICP-MS revealed three main fractions of these NNP and colloids due to AF^4 method advancement. The OCD proved to overcome the compound dependent response of the UV signal and allowed a precise measurement of the organic C in the NNP and colloid fractions. The first and smallest NNP fraction was between approx. 1 nm and 20 nm, the second and NNP fraction included sizes above 20 nm hydrodynamic diameter to 60 nm and the third fraction covered larger NNP above 60 nm to small colloids of approx. 300 nm. Through exploratory data analysis techniques, cluster analysis with distance measure '1 – Pearson r' was utilized to disentangle the potential associations of organic C, Fe, Al, Mn and Si to P for each size fraction. This revealed the potential primary associations of P were to small nano-sized Fe oxides, while in the nanoparticulate medium sized fraction, P binding was increasingly affected also by the presence of organic matter. Finally, aluminosilicate minerals dominated P association in larger NNP to colloids. A high relevance of NNP and colloids for P binding and transport, but also for organic C, Mn and Fe was seen. Moreover, an increasing percentage of transported P is associated with NNP and colloids, especially as the total P concentration declines. To

contextualize P in freshwater ecosystems, the C:P ratio of NNP and colloid bound concentrations reflected three distinct groups of sites: low C:P values for Conventwald and Vessertal, intermediate values for Wüstebach and Mitterfels and the highest value for Leirelva, whereas a C:P above 250 is regarded as limiting according to literature. The percentage of P binding to the NNP and colloid fractions generally confirmed this trend. Thus, the results demonstrate that NNP and colloids play a relevant role for nutrient transport in and export from forest ecosystems and can be a potential predictor of the nutritional status of an ecosystem. It was assumed that the P flux in ecosystems can be significantly influenced through washout processes of NNP and colloids from the catchment during high precipitation events, yet no first flush effect of the identified NNP and colloid fractions could be observed. In this context, inferences for stream water NNP and colloids released from surrounding soils showed comparable elemental ratios at highly different concentration levels between soils and stream waters. Stream waters are also influenced by other input flows such as rain and interception water. The first characterization of these inputs showed distinctly different NNP and colloid patterns with low monthly variabilities. Further data analysis still has to be conducted to fully infer the numerical release factors for stream water colloids from surrounding soils.

Continental scale study: Stream water sampling across Europe allows a large scale analysis of NNP and colloids, which could be distinguished into three fractions, comparable to the fractions identified for the national scale project. The significant contribution of NNP and colloids could be shown on a continental scale for Fe, P, Al, Mn and org C binding, because up to 95-100% of these elements occurred in NNP and colloidal form. A geographical divide became apparent in Europe on account of the stream water pH and the elemental composition of NNP and colloids. While concentrations of Si, Mn, P and Ca are rather constant across Europe irrespective of stream water pH and geography, concentrations of org C, Fe and Al associated with NNP and colloids increase with increasing total concentration of these elements from the South to the North of Europe with decreasing pH. The sites can be divided into sites that are characterized by the presence of Ca-containing NNP and colloids and sites with an increasing predominance of NNP and colloids that are composed of Fe and/or org C as major NNP and colloid constituent. Integrated over all sites and irregardless of the geographical regions, P preferentially binds to the same elements and compounds per fraction as identified for the national scale project, yet at lower intensities. This revealed a preferential P binding which is specific to geographical region with Ca influence dominating in South Europe, Al and org C in Middle Europe and Fe in North Europe. Site specific parameters such as vegetation and soil type are interlinked with the pH value and thus also predetermine the elemental concentrations present in the NNP and colloid fractions. This analysis has specifically revealed that washout from coniferous tree stands was significantly higher than the influence from the deciduous stands on the NNP and colloids. The

current method does not yield the element specific concentration as function of particle frequency, thus for future research this data should be gained across the continental gradient. The identified geographical divide in Europe is in line with a climatic shift between the sites. The climate variable which reflected the highest direct influence on NNP and colloid composition was mean annual temperature, underlining that a latitudinal shift or changing elevation has profound impacts on NNP and colloids. This was also confirmed for the path analysis of the indirect impact of climatic factors on the NNP and colloids with exception of the third fraction which is apparently determined through the sole presence of aluminosilicates.

Overall, this work has succeeded in underlining the significant relevance of NNP and colloids for elemental binding and transport with up to 100% elemental presence in the NNP and colloid fractions. Depending on the fractionation method, up to three different fractions with unique characteristics could be determined in aqueous samples of forested headwater catchments. The fractions reflected different preferential binding of the essential nutrient P but also showed ecosystem specific composition patterns. In line with the work on iron isotope signals and in combination with the data from this thesis, it seems reasonable to in future aim at tracing the origin of NNP and colloids in forested headwater catchments and their physicochemical abilities to transport nutrients such as P. This work will be conducted in the context of the Nutrient Spiraling Concept (c.f. Marti and Sabater 1996; Peterson et al. 2001; Simon et al. 2005). It is envisaged to work on this topic in the framework of a post-doctoral project.

References

Amaral CDB, Amais RS, Fialho LL, Schiavo D, Nogueira ARA, Nóbrega JA (2015) Determination of Carbon in Digested Samples and Amino Acids by Inductively Coupled Plasma Tandem Mass Spectrometry. Microchemical Journal 122:29-32.

Anderson D (1988) The Effect of Parent Material and Soil Development on Nutrient Cycling in Temperate Ecosystems. Biogeochemistry 5:71-97.

Andersson K, Dahlqvist R, Turner D, Stolpe B, Larsson T, Ingri J, Andersson P (2006) Colloidal Rare Earth Elements in a Boreal River: Changing Sources and Distributions During the Spring Flood. Geochimica et Cosmochimica Acta 70:3261-3274.

Baalousha M, Stolpe B, Lead JR (2011) Flow Field-Flow Fractionation for the Analysis and Characterization of Natural Colloids and Manufactured Nanoparticles in Environmental Systems: A Critical Review. Journal of Chromatography A 1218:4078-4103.

Becker JS (2007) Ion Sources. In: Inorganic Mass Spectrometry: Principles and Applications. Wiley, Weinheim, p 31.

Beckett R, Hart B (1986) The Role of Particulate Matter in the Transport and Fate of Pollutants. Water Studies Centre, Chisholm Institute of Technology (now Monash University), Melbourne:113.

Benedetti MF, Van Riemsdijk WH, Koopal LK, Kinniburgh DG, Gooddy DC, Milne CJ (1996) Metal Ion Binding by Natural Organic Matter: From the Model to the Field. Geochimica et Cosmochimica Acta 60:2503-2513.

Binkley D, Ice GG, Kaye J, Williams CA (2004) Nitrogen and Phosphorus Concentrations in Forest Streams of the United States. Journal of the American Water Resources Association 40:1277-1291.

Bogena HR, Bol R, Borchard N, Brüggemann N, Diekkrüger B, Drüe C, Groh J, Gottselig N, Huisman JA, Lücke A, Missong A, Neuwirth B, Pütz T, Schmidt M, Stockinger M, Tappe W, Weihermüller L, Wiekenkamp I, Vereecken H (2014) A Terrestrial Observatory Approach to the Integrated Investigation of the Effects of Deforestation on Water, Energy, and Matter Fluxes. Science China Earth Science 58:61-75.

Bogena HR, Herbst M, Huisman JA, Rosenbaum U, Weuthen A, Vereecken H (2010) Potential of Wireless Sensor Networks for Measuring Soil Water Content Variability. Vadose Zone Journal 9:1002-1013.

Bogena HR, Kunkel R, Puetz T, Vereecken H, Krueger E, Zacharias S, Dietrich P, Wollschlaeger U, Kunstmann H, Papen H, Schmid HP, Munch JC, Priesack E, Schwank M, Bens O, Brauer A, Borg E, Hajnsek I (2012) Tereno - Long-Term Monitoring Network for Terrestrial Environmental Research. Hydrologie und Wasserbewirtschaftung 56:138-143.

Bol R, Julich D, Brödlin D, Siemens J, Dippold MA, Spielvogel S, Zilla T, Mewes D, Blanckenburg Fv, Puhlmann H, Holzmann S, Kaiser K, Weiler M, Amelung W, Lang F, Kuzyakov Y, Feger K-H, Gottselig N, Klumpp E, Missong A, Winkelmann C, Uhlig D, Sohrt J, Wilpert Kv, Wu B, Hagedorn F (under review). Journal of Plant Nutrition and Soil Science.

Bol R, Lucke A, Tappe W, Kummer S, Krause M, Weigand S, Putz T, Vereecken H (2015) Spatio-Temporal Variations of Dissolved Organic Matter in a German Forested Mountainous Headwater Catchment. Vadose Zone Journal 14:12.

Brady NC, Weil RR (1996) The Nature and Properties of Soils. vol Ed. 11. Prentice-Hall Inc.

Buffle J, Leppard GG (1995) Characterization of Aquatic Colloids and Macromolecules. 2. Key Role of Physical Structures on Analytical Results. Environmental Science and Technology 29:2176-2184.

Cabaniss SE, Madey G, Leff L, Maurice PA, Wetzel R (2005) A Stochastic Model for the Synthesis and Degradation of Natural Organic Matter. Part I. Data Structures and Reaction Kinetics. Biogeochemistry 76:319-347.

Celi L, Barberis E, Turner B, Frossard E, Baldwin D (2005) Abiotic Stabilization of Organic Phosphorus in the Environment. In: Turner BL, Frossard E, Baldwin DS (ed) Organic Phosphorus in the Environment:113-132.

Crini G, Badot PM (2010) Sorption Processes and Pollution: Conventional and Non-Conventional Sorbents for Pollutant Removal from Wastewaters. Presses universitaires de Franche-Comté.

Dahlqvist R, Benedetti MF, Andersson K, Turner D, Larsson T, Stolpe B, Ingri J (2004) Association of Calcium with Colloidal Particles and Speciation of Calcium in the Kalix and Amazon Rivers. Geochimica et Cosmochimica Acta 68:4059-4075.

Darch T, Blackwell MSA, Hawkins JMB, Haygarth PM, Chadwick D (2014) A Meta-Analysis of Organic and Inorganic Phosphorus in Organic Fertilizers, Soils, and Water: Implications for Water Quality. Critical Reviews in Environmental Science and Technology 44:2172-2202.

de Jonge LW, Kjærgaard C, Moldrup P (2004) Colloids and Colloid-Facilitated Transport of Contaminants in Soils. Vadose Zone Journal 3:321-325.

Decker J (2010) Feinkartierung eines Fichtenforstes als Basis für ein Langzeitmonitoring. Landesamt Für Natur, Umwelt und Verbraucherschutz Nordrhein-Westfalen, 4th edn.

Deletic A (1998) The First Flush Load of Urban Surface Runoff. Water Research 32:2462-2470.

Dietz M, Strock J (2016) Phosphorus Cycle. Southwest Research and Outreach Center, University of Minnesota. http://swroc.cfans.umn.edu/agricultural-programs/soil-science/phosphorus-cycle. Acessed 03/22/2016

Duncker PS, Barreiro SM, Hengeveld GM, Lind T, Mason WL, Ambrozy S, Spiecker H (2012) Classification of Forest Management Approaches: A New Conceptual Framework and Its Applicability to European Forestry. Ecology and Society 17:51.

Dynesius M, Nilsson C (1994) Fragmentation and Flow Regulation of River Systems in the Northern 3rd of the World. Science 266:753-762.

Egli M, Alioth L, Mirabella A, Raimondi S, Nater M, Verel R (2007) Effect of Climate and Vegetation on Soil Organic Carbon, Humus Fractions, Allophanes, Imogolite, Kaolinite, and Oxyhydroxides in Volcanic Soils of Etna (Sicily). Soil Science 172:673-691.

Egli M, Filip D, Mavris C, Fischer B, Götze J, Raimondi S, Seibert J (2012) Rapid Transformation of Inorganic to Organic and Plant-Available Phosphorous in Soils of a Glacier Forefield. Geoderma 189:215-226.

El-Farhan YH, DeNovio NM, Herman JS, Hornberger GM (2000) Mobilization and Transport of Soil Particles During Infiltration Experiments in an Agricultural Field, Shenandoah Valley, Virginia. Environmental Science and Technology 34:3555-3559.

Elser JJ, Fagan WF, Denno RF, Dobberfuhl DR, Folarin A, Huberty A, Interlandi S, Kilham SS, McCauley E, Schulz KL, Siemann EH, Sterner RW (2000) Nutritional Constraints in Terrestrial and Freshwater Food Webs. Nature 408:578-580.

Erickson HP (2009) Size and Shape of Protein Molecules at the Nanometer Level Determined by Sedimentation, Gel Filtration, and Electron Microscopy. Biological Procedures Online 11:32-51.

Etmann M (2009) Dendrologische Aufnahmen im Wassereinzugsgebiet Oberer Wüstebach anhand Verschiedener Mess- und Schätzverfahren. Universität Münster

European Virtual Institute for Speciation Analysis EVISA (2015) LC-ICP-MS: The Most Often Used Hyphenated System for Speciation Analysis. http://www.speciation.net/Public/Document/2007/06/21/2914.html. Accessed 04/07/2016

Fent K (2007a) 1.2.2 Phosphor und Stickstoff: Vom Nährstoff Zum Schadstoff. In: Fent K (ed) Ökotoxikologie, vol 3. Georg Thieme Verlag, Stuttgart, pp 7-11.

Fent K (2007b) 4.3 Bioverfügbarkeit in Umweltsystemen. In: Fent K (ed) Ökotoxikologie, vol 3. Georg Thieme Verlag, Stuttgart, pp 100-103.

Fernández-Martínez M, Vicca S, Janssens IA, Sardans J, Luyssaert S, Campioli M, Chapin III FS, Ciais P, Malhi Y, Obersteiner M, Papale D, Piao SL, Reichstein M, Roda F, Penuelas J (2014) Nutrient Availability as the Key Regulator of Global Forest Carbon Balance. Nature Climate Change 4:471-476.

Filella M, Deville C, Chanudet V, Vignati D (2006) Variability of the Colloidal Molybdate Reactive Phosphorous Concentrations in Freshwaters. Water Research 40:3185-3192.

Flint KR, Davis AP (2007) Pollutant Mass Flushing Characterization of Highway Stormwater Runoff from an Ultra-Urban Area. Journal of Environmental Engineering 133:616-626.

Francko DA, Heath RT (1982) UV-Sensitive Complex Phosphorus - Association with Dissolved Humic Material and Iron in a Bog Lake. Limnology and Oceanography 27:564-569.

Franco A, Fu WJ, Trapp S (2009) Influence of Soil Ph on the Sorption of Ionizable Chemicals: Modelling Advances. Environmental Toxicology Chemistry 28:458-464.

Gerke J (1992) Orthophosphate and Organic Phosphate in the Soil Solution of Four Sandy Soils in Relation to pH-Evidence for Humic-Fe-(Al-)Phosphate Complexes. Communications in Soil Science and Plant Analysis 23:601-612.

Gerke J (2015) The Acquisition of Phosphate by Higher Plants: Effect of Carboxylate Release by the Roots. A Critical Review. Journal of Plant Nutrition and Soil Science 178:351-364.

Gerke J, Hermann R (1992) Adsorption of Orthophosphate to Humic-Fe-Complexes and to Amorphous Fe-Oxide. Zeitschrift für Pflanzenernahrung und Bodenkunde 155:233-236.

Giddings J, Yang F, Myers M (1976) Flow-Field-Flow Fractionation: A Versatile New Separation Method. Science 193:1244-1245.

Gimbert LJ, Andrew KN, Haygarth PM, Worsfold PJ (2003) Environmental Applications of Flow Field-Flow Fractionation (FlFFF). TrAC-Trends in Analytical Chemistry 22:615-633.

Gordley LL, Marshall BT, Allen Chu D (1994) Linepak: Algorithms for Modeling Spectral Transmittance and Radiance. Journal of Quantitative Spectroscopy and Radiative Transfer 52:563-580.

Gottselig N, Bol R, Nischwitz V, Vereecken H, Amelung W, Klumpp E (2014) Distribution of Phosphorus-Containing Fine Colloids and Nanoparticles in Stream Water of a Forest Catchment. Vadose Zone Journal 13:1-11.

Gottselig N, Nischwitz V, Meyn T, Amelung W, Bol R, Halle C, Vereecken H, Siemens J, Klumpp E (submitted) Phosphorus Binding to Nanoparticles and Colloids in Forest Stream Waters. Biogeochemistry.

Grace JB (2006) Structural Equation Modeling and Natural Systems. Cambridge University Press, Cambridge.

Grace JB, Pugesek BH (1998) On the Use of Path Analysis and Related Procedures for the Investigation of Ecological Problems. American Naturalist 152: 151-159.

Grim R, Kodama H (2014) Clay Mineral. Encyclopedia Britannica. http://www.britannica.com/EBchecked/topic/120723/clay-mineral. Acessed 07/22/2015

Grindlay G, Mora J, de Loos-Vollebregt M, Vanhaecke F (2013) A Systematic Study on the Influence of Carbon on the Behavior of Hard-to-Ionize Elements in Inductively Coupled Plasma–Mass Spectrometry. Spectrochimica Acta Part B: Atomic Spectroscopy 86:42-49.

Hagedorn F, Schleppi P, Waldner P, Fluhler H (2000) Export of Dissolved Organic Carbon and Nitrogen from Gleysol Dominated Catchments - the Significance of Water Flow Paths. Biogeochemistry 50:137-161.

Hagendorfer H, Kaegi R, Traber J, Mertens SFL, Scherrers R, Ludwig C, Ulrich A (2011) Application of an Asymmetric Flow Field Flow Fractionation Multi-Detector Approach for Metallic Engineered Nanoparticle Characterization - Prospects and Limitations Demonstrated on Au Nanoparticles. Analytica Chimica Acta 706:367-378.

Hart BT, Douglas GB, Beckett R, Vanput A, Vangrieken RE (1993) Characterization of Colloidal and Particulate Matter Transported by the Magella Creek System, Northern Australia. Hydrological Processes 7:105-118.

Hartland A, Lead JR, Slaveykova V, O'Carroll D, Valsami-Jones E (2013) The Environmental Significance of Natural Nanoparticles. Nature Education Knowledge 4:7.

Hasselloev M, Lyven B, Haraldsson C, Sirinawin W (1999) Determination of Continuous Size and Trace Element Distribution of Colloidal Material in Natural Water by on-Line Coupling of Flow Field-Flow Fractionation with ICPMS. Analytical Chemistry 71:3497-3502.

Hasselloev M, von der Kammer F (2008) Iron Oxides as Geochemical Nanovectors for Metal Transport in Soil-River Systems. Elements 4:401-406.

Hathaway J, Tucker R, Spooner J, Hunt W (2012) A Traditional Analysis of the First Flush Effect for Nutrients in Stormwater Runoff from Two Small Urban Catchments. Water, Air and Soil Pollution 223:5903-5915.

Heathwaite AL, Dils RM (2000) Characterising Phosphorus Loss in Surface and Subsurface Hydrological Pathways. Science of the Total Environment 251:523-538.

Hecky RE, Campbell P, Hendzel LL (1993) The Stoichiometry of Carbon, Nitrogen, and Phosphorus in Particulate Matter of Lakes and Oceans. Limnology and Oceanography 38:709-724.

Henderson R, Kabengi N, Mantripragada N, Cabrera M, Hassan S, Thompson A (2012) Anoxia-Induced Release of Colloid- and Nanoparticle-Bound Phosphorus in Grassland Soils. Environmental Science and Technology 46:11727-11734.

Hill DM, Aplin AC (2001) Role of Colloids and Fine Particles in the Transport of Metals in Rivers Draining Carbonate and Silicate Terrains. Limnology and Oceanography 46:331-344.

Huber SA (2015a) How LC-OCD Works - Basics. DOC Labor Dr. Huber, Karlsruher, Germany. http://doc-labor.de/Basics.html. Accessed 01/23/2015

Huber SA (2015b) LC-OCD Operation Manual. DOC Labor Dr. Huber, Karlsruhe, Germany.

Huber SA, Balz A, Abert M, Pronk W (2011) Characterisation of Aquatic Humic and Non-Humic Matter with Size-Exclusion Chromatography - Organic Carbon Detection - Organic Nitrogen Detection (LC-OCD-OND). Water Research 45:879-885.

Huber SA, Frimmel FH (1991) Flow Injection Analysis of Organic and Inorganic Carbon in the Low-ppb Range. Analytical Chemistry 63:2122-2130.

Hudak PF, Banks KE (2006) Compositions of First Flush and Composite Storm Water Runoff in Small Urban and Rural Watersheds, North-Central Texas. Urban Water Journal 3:43-49.

Jarvie HP, Neal C, Rowland AP, Neal M, Morris PN, Lead JR, Lawlor AJ, Woods C, Vincent C, Guyatt H, Hockenhull K (2012) Role of Riverine Colloids in Macronutrient and Metal Partitioning and Transport, Along an Upland-Lowland Land-Use Continuum, under Low-Flow Conditions. Science of the Total Environment 434:171-185.

Jeanneau L, Denis M, Pierson-Wickmann A-C, Gruau G, Lambert T, Petitjean P (2015) Sources and Transfer Mechanisms of Dissolved Organic Matter During Storm and Inter-Storm Conditions in a Lowland Headwater Catchment: Constraints from High-Frequency Molecular Data. Biogeosciences Discussions 12.

Jiang X, Bol R, Nischwitz V, Siebers N, Willbold S, Vereecken H, Amelung W, Klumpp E (2015) Phosphorus Containing Water Dispersible Nanoparticles in Arable Soil. Journal of Environmental Quality 44:1772-1781.

Jirsa F, Neubauer E, Kittinger R, Hofmann T, Krachler R, von der Kammer F, Keppler BK (2013) Natural Organic Matter and Iron Export from the Tanner Moor, Austria. Limnologica 43:239-244.

Kalbitz K, Solinger S, Park JH, Michalzik B, Matzner E (2000) Controls on the Dynamics of Dissolved Organic Matter in Soils: A Review. Soil Science 165:277-304.

Keiluweit M, Nico P, Harmon ME, Mao J, Pett-Ridge J, Kleber M (2015) Long-Term Litter Decomposition Controlled by Manganese Redox Cycling. Proceedings of the National Academy of Sciences of the United States of America 112:E5253-E5260.

Khresat SE, Al-Bakri J, Al-Tahhan R (2008) Impacts of Land Use/Cover Change on Soil Properties in the Mediterranean Region of Northwestern Jordan. Land Degradation and Development 19:397-407.

Kirschbaum MUF (1995) The Temperature-Dependence of Soil Organic-Matter Decomposition, and the Effect of Global Warming on Soil Organic-C Storage. Soil Biology and Biochemistry 27:753-760.

Kirschbaum MUF (2006) The Temperature Dependence of Organic-Matter Decomposition - Still a Topic of Debate. Soil Biology and Biochemistry 38:2510-2518.

Kjaergaard C, Moldrup P, De Jonge LW, Jacobsen OH (2004a) Colloid Mobilization and Transport in Undisturbed Soil Columns. II. The Role of Colloid Dispersibility and Preferential Flow. Vadose Zone Journal 3:424-433.

Kjaergaard C, Poulsen TG, Moldrup P, De Jonge LW (2004b) Colloid Mobilization and Transport in Undisturbed Soil Columns. I. Pore Structure Characterization and Tritium Transport. Vadose Zone Journal 3:413-423.

Klitzke S, Lang F (2007) Hydrophobicity of Soil Colloids and Heavy Metal Mobilization: Effects of Drying. Journal of Environmental Quality 36:1187-1193.

Kronvang B, Vagstad N, Behrendt H, Bogestrand J, Larsen SE (2007) Phosphorus Losses at the Catchment Scale within Europe: An Overview. Soil Use and Management 23:104-116.

Lampert W, Sommer U (1999a) 3.1.6 Wasser Als Lösungsmittel. In: Limnoökologie. Georg Thieme Verlag, Stuttgart, pp 30-35.

Lampert W, Sommer U (1999b) 4.2.3 pH-Wert. In: Limnoökologie. Georg Thieme Verlag, Stuttgart, pp 75-78.

Lampert W, Sommer U (1999c) 4.3.7 Mineralische Nährstoffe. In: Limnoökologie. Georg Thieme Verlag, Stuttgart, pp 125-128.

Langley S (1883) XXII. The Selective Absorption of Solar Energy. The London, Edinburgh, and Dublin Philosophical Magazine and Journal of Science 15:153-183.

Lee JH, Bang KW, Ketchum Jr LH, Choe JS, Yu MJ (2002) First Flush Analysis of Urban Storm Runoff. Science of the Total Environment 293:163-175.

Leppard GG, Buffle J, Devitre RR, Perret D (1988) The Ultrastructure and Physical Characteristics of a Distinctive Colloidal Iron Particulate Isolated from a Small Eutrophic Lake. Archiv für Hydrobiologie 113:405-424.

Libecki B, Dziejowski J (2008) Optimization of Humic Acids Coagulation with Aluminum and Iron(III) Salts. Polish Journal of Environmental Studies 17:397-403.

Lindo Z, Visser S (2003) Microbial Biomass, Nitrogen and Phosphorus Mineralization, and Mesofauna in Boreal Conifer and Deciduous Forest Floors Following Partial and Clear-Cut Harvesting. Canadian Journal of Forest Research-Revue Canadienne De Recherche Forestiere 33:1610-1620.

Liski J, Perruchoud D, Karjalainen T (2002) Increasing Carbon Stocks in the Forest Soils of Western Europe. Forest Ecology and Management 169:159-175.

Liu J, Liang X, Yang J, Ye Y, Su M, Nie Z, Chen Y (2011) Size Distribution and Composition of Phosphorus in the East Tiao River, China: The Significant Role of Colloids. Journal of Environmental Monitoring 13:2844-2850.

Loeschner K, Navratilova J, Legros S, Wagner S, Grombe R, Snell J, von der Kammer F, Larsen EH (2013) Optimization and Evaluation of Asymmetric Flow Field-Flow Fractionation of Silver Nanoparticles. Journal of Chromatography A 1272:116-125.

Lofts S, Tipping E, Hamilton-Taylor J (2008) The Chemical Speciation of Fe(III) in Freshwaters. Aquatic Geochemistry 14:337-358.

Lopez Molinero A, Castillo JR, Chamorro P, Muniozguren JM (1997) Multivariate Statistical Characterization of the Tolerance of Argon Inductively Coupled Plasmas to Organic Solvents. Spectrochimica Acta Part B: Atomic Spectroscopy 52:103-112.

Luong ET, Houk RS (2003) Determination of Carbon Isotope Ratios in Amino Acids, Proteins, and Oligosaccharides by Inductively Coupled Plasma-Mass Spectrometry. Journal of the American Society for Mass Spectrometry 14:295-301.

Lyven B, Hassellov M, Turner DR, Haraldsson C, Andersson K (2003) Competition between Iron- and Carbon-Based Colloidal Carriers for Trace Metals in a Freshwater Assessed Using Flow Field-Flow Fractionation Coupled to ICPMS. Geochimica et Cosmochimica Acta 67:3791-3802.

Marschner B, Kalbitz K (2003) Controls of Bioavailability and Biodegradability of Dissolved Organic Matter in Soils. Geoderma 113:211-235.

Marti E, Sabater F (1996) High Variability in Temporal and Spatial Nutrient Retention in Mediterranean Streams. Ecology 77:854-869.

Martin JM, Dai MH, Cauwet G (1995) Significance of Colloids in the Biogeochemical Cycling of Organic Carbon and Trace Metals in the Venice Lagoon (Italy). Limnology and Oceanography 40:119-131.

Mayer TD, Jarrell WM (1995) Assessing Colloidal Forms of Phosphorus and Iron in the Tualatin-River Basin. Journal of Environmental Quality 24:1117-1124.

Michel FM, Ehm L, Antao SM, Lee PL, Chupas PJ, Liu G, Strongin DR, Schoonen MAA, Phillips BL, Parise JB (2007) The Structure of Ferrihydrite, a Nanocrystalline Material. Science 316:1726-1729.

Missong A, Bol R, Willbold S, Siemens J, Klumpp E (2016) Phosphorus Forms in Forest Soil Colloids as Revealed by Liquid-State ^{31}P-NMR. Journal of Plant Nutrition and Soil Science 179:159-167.

Montalvo D, Degryse F, McLaughlin MJ (2015) Natural Colloidal P and its Contribution to Plant P Uptake. Environmental Science and Technology 49:3427-3434.

Montaser A, McLean JA, Huiying L, Mermet J-M (1998) An Introduction to ICP Spectrometries for Elemental Analysis. Inductively Coupled Plasma Mass Spectrometry. Wiley, Weinheim.

Natural Resources Conservation Service Soil Science Division (1993) Soil Survey Manual, Chapter 3. Selected Chemical Properties. United States Department of Agriculture.

Neill C, Deegan LA, Thomas SM, Cerri CC (2001) Deforestation for Pasture Alters Nitrogen and Phosphorus in Small Amazonian Streams. Ecological Applications 11:1817-1828.

Neubauer E, v. d. Kammer F, Hofmann T (2013) Using FlowFFF and HPSEC to Determine Trace Metal Colloid Associations in Wetland Runoff. Water Research 47:2757-2769.

Neubauer E, v.d. Kammer F, Hofmann T (2011) Influence of Carrier Solution Ionic Strength and Injected Sample Load on Retention and Recovery of Natural Nanoparticles Using Flow Field-Flow Fractionation. Journal of Chromatography A 1218:6763-6773.

Nischwitz V, Goenaga-Infante H (2012) Improved Sample Preparation and Quality Control for the Characterisation of Titanium Dioxide Nanoparticles in Sunscreens Using Flow Field Flow Fractionation on-Line with Inductively Coupled Plasma Mass Spectrometry. Journal of Analytical Atomic Spectrometry 27:1084-1092.

Nischwitz V, Gottselig N, Missong A, Meyn T, Klumpp E (under review) Field Flow Fractionation Online with ICP-MS as Novel Approach for the Quantification of Particle-Bound Carbon in Stream Water Samples and Soil Extracts. Journal of Analytical Atomic Spectrometry Special Issue on Speciation Analysis.

Ognalaga M, Frossard E, Thomas F (1994) Glucose-1-Phosphate and Myoinositol Hexaphosphate Adsorption Mechanisms on Goethite. Soil Science Society of America Journal 58:332-337.

Owens LB, Shipitalo MJ (2006) Surface and Subsurface Phosphorus Losses from Fertilized Pasture Systems in Ohio. Journal of Environmental Quality 35:1101-1109.

Peel MC, Finlayson BL, McMahon TA (2007) Updated World Map of the Koppen-Geiger Climate Classification. Hydrology and Earth System Sciences 11:1633-1644.

Perry DA, Oren R, Hart SC (2008) Forest Ecosystems. JHU Press, Baltimore.

Peterson BJ, Wollheim WM, Mulholland PJ, Webster JR, Meyer JL, Tank JL, Martí E, Bowden WB, Valett HM, Hershey AE, McDowell WH, Dodds WK, Hamilton SK, Gregory S, Morrall DD (2001) Control of Nitrogen Export from Watersheds by Headwater Streams. Science 292:86-90.

Plathe KL, von der Kammer F, Hassellov M, Moore JN, Murayama M, Hofmann T, Hochella MF, Jr. (2013) The Role of Nanominerals and Mineral Nanoparticles in the Transport of Toxic Trace Metals: Field-Flow Fractionation and Analytical Tem Analyses after Nanoparticle Isolation and Density Separation. Geochimica et Cosmochimica Acta 102:213-225.

Post WM, Emanuel WR, Zinke PJ, Stangenberger AG (1982) Soil Carbon Pools and World Life Zones. Nature 298:156-159.

Postnova Analytics G (2015) AF2000 MF Supplies and Consumables Brochure. Landsberg, Germany.

Qafoku NP (2010) Terrestrial Nanoparticles and Their Controls on Soil-/Geo-Processes and Reactions. In: Sparks DL (ed) Advances in Agronomy, vol 107. pp 33-91.

Ran Y, Fu JM, Sheng GY, Beckett R, Hart BT (2000) Fractionation and Composition of Colloidal and Suspended Particulate Materials in Rivers. Chemosphere 41:33-43.

Ranville JF, Macalady DL (1997) Natural Organic Matter in Catchments. Geochemical Processes, Weathering and Groundwater Recharge in Catchments:263-303.

Redfield AC (1934) On the Proportions of Organic Derivatives in Sea Water and Their Relation to the Composition of Plankton. James Johnstone Memorial Volume 1934.

Regelink IC, Koopmans GF, van der Salm C, Weng L, van Riemsdijk WH (2013) Characterization of Colloidal Phosphorus Species in Drainage Waters from a Clay Soil Using Asymmetric Flow Field-Flow Fractionation. Journal of Environmental Quality 42:464-473.

Regelink IC, Voegelin A, Weng LP, Koopmans GF, Comans RNJ (2014) Characterization of Colloidal Fe from Soils Using Field-Flow Fractionation and Fe K-Edge X-Ray Absorption Spectroscopy. Environmental Science and Technology 48:4307-4316.

Regelink IC, Weng L, van Riemsdijk WH (2011) The Contribution of Organic and Mineral Colloidal Nanoparticles to Element Transport in a Podzol Soil. Applied Geochemistry 26:S241-S244.

Reszat TN, Hendry MJ (2005) Characterizing Dissolved Organic Carbon Using Asymmetrical Flow Field-Flow Fractionation with on-Line UV and DOC Detection. Analytical Chemistry 77:4194-4200.

Richardson CJ (1985) Mechanisms Controlling Phosphorus Retention Capacity in Fresh-Water Wetlands. Science 228:1424-1427.

Rohde RA (2007) "Radiation Transmitted by the Atmosphere" Based on Data from Gordley, L., Marshall, B., Allen, C. (1994) Linepak: Algorithms for Modeling Spectral Transmittance and Radiance. https://commons.wikimedia.org/wiki/File:Atmospheric_Transmission.png. Accessed 03/22/2016

Rosenbaum U, Bogena HR, Herbst M, Huisman JA, Peterson TJ, Weuthen A, Western AW, Vereecken H (2012) Seasonal and Event Dynamics of Spatial Soil Moisture Patterns at the Small Catchment Scale. Water Resources Research 48.

Rubens H, Aschkinass E (1898) Observations on the Absorption and Emission of Aqueous Vapor and Carbon Dioxide in the Infra-Red Spectrum. The Astrophysical Journal 8:176.

Santamaria-Fernandez R (2010) Precise and Traceable Carbon Isotope Ratio Measurements by Multicollector ICP-MS: What Next?. Analytical and Bioanalytical Chemistry 397:973-978.

Schelde K, de Jonge LW, Kjaergaard C, Laegdsmand M, Rubæk GH (2006) Effects of Manure Application and Plowing on Transport of Colloids and Phosphorus to Tile Drains. Vadose Zone Journal 5:445-458.

Schimpf M, Caldwell KD, Giddings JC (2000) Field-Flow Fractionation Handbook. Wiley, New York.

Schindler DW (1977) Evolution of Phosphorus Limitation in Lakes. Science 195:260-262.

Schmitt D, Taylor HE, Aiken GR, Roth DA, Frimmel FH (2002) Influence of Natural Organic Matter on the Adsorption of Metal Ions onto Clay Minerals. Environmental Science and Technology 36:2932-2938.

Shafer MM, Overdier JT, Hurley JP, Armstrong D, Webb D (1997) The Influence of Dissolved Organic Carbon, Suspended Particulates, and Hydrology on the Concentration, Partitioning and Variability of Trace Metals in Two Contrasting Wisconsin Watersheds (USA). Chemical Geology 136:71-97.

Siemens J, Ilg K, Pagel H, Kaupenjohann M (2008) Is Colloid-Facilitated Phosphorus Leaching Triggered by Phosphorus Accumulation in Sandy Soils? Journal of Environmental Quality 37:2100-2107.

Simon KS, Townsend CR, Biggs BJF, Bowden WB (2005) Temporal Variation of N and P Uptake in 2 New Zealand Streams. Journal of the North American Benthological Society 24:1-18.

Six J, Elliott ET, Paustian K (1999) Aggregate and Soil Organic Matter Dynamics under Conventional and No-Tillage Systems. Soil Science Society of America Journal 63:1350-1358.

Smith C, Jensen BP, Wilson ID, Abou-Shakra F, Crowther D (2004) High-Performance Liquid Chromatography/Inductively Coupled Plasma Mass Spectrometry and Tandem Mass Spectrometry for the Detection of Carbon-Containing Compounds. Rapid Communications in Mass Spectrometry 18:1487-1492.

Sohmen R, Stark U, Moldenhauer E, Klein T, Grieshaber R (2012) Detection of Nanoscale Bioparticles Generated from E. Coli Bacteriophage Phix174 and Bovine Serum Albumin (Bsa) by Asymmetric Flow Field-Flow Fractionation. Gefahrstoffe Reinhaltung der Luft 72:494-497.

Soller J, Stephenson J, Olivieri K, Downing J, Olivieri AW (2005) Evaluation of Seasonal Scale First Flush Pollutant Loading and Implications for Urban Runoff Management. Journal of Environmental Management 76:309-318.

Spivakov BY, Maryutina TA, Muntau H (2009) Phosphorus Speciation in Water and Sediments. Pure and Applied Chemistry 71:2161-2176.

Stockinger MP, Bogena HR, Luecke A, Diekkrueger B, Weiler M, Vereecken H (2014) Seasonal Soil Moisture Patterns: Controlling Transit Time Distributions in a Forested Headwater Catchment. Water Resources Research 50:5270-5289.

Stolpe B, Guo L, Shiller AM, Hassellov M (2010) Size and Composition of Colloidal Organic Matter and Trace Elements in the Mississippi River, Pearl River and the Northern Gulf of Mexico, as Characterized by Flow Field-Flow Fractionation. Marine Chemistry 118:119-128.

Stolpe B, Hassellov M, Andersson K, Turner DR (2005) High Resolution ICPMS as an on-Line Detector for Flow Field-Flow Fractionation; Multi-Element Determination of Colloidal Size Distributions in a Natural Water Sample. Analytica Chimica Acta 535:109-121.

Stumm W, Morgan JJ (1981) Aquatic Chemistry: An Introduction Emphasizing Chemical Equilibria in Natural Waters. Wiley, Weinheim.

Stutter M, Langan S, Cooper R (2008) Spatial Contributions of Diffuse Inputs and within-Channel Processes to the Form of Stream Water Phosphorus over Storm Events. Journal of Hydrology 350:203-214.

Stutter MI, Shand CA, George TS, Blackwell MSA, Bol R, MacKay RL, Richardson AE, Condron LM, Turner BL, Haygarth PM (2012) Recovering Phosphorus from Soil: A Root Solution? Environmental Science and Technology 46:1977-1978.

Suhr D (2008) Step Your Way through Path Analysis. Western Users of SAS Software Conference Proceedings.

Taebi A, Droste RL (2004) First Flush Pollution Load of Urban Stormwater Runoff. Journal of Environmental Engineering and Science 3:301-309.

Tipping E, Hurley M (1992) A Unifying Model of Cation Binding by Humic Substances. Geochimica et Cosmochimica Acta 56:3627-3641.

Turner B, Frossard E, Baldwin D (2005) Organic Phosphorus Transfer from Terrestrial to Aquatic Environments. In: Turner BL, Frossard E, Baldwin DS (ed) Organic Phosphorus in the Environment:269-294.

Turner BL (2008) Resource Partitioning for Soil Phosphorus: A Hypothesis. Journal of Ecology 96:698-702.

Turner BL, Condron LM, Richardson SJ, Peltzer DA, Allison VJ (2007) Soil Organic Phosphorus Transformations During Pedogenesis. Ecosystems 10:1166-1181.

Turrion MB, Glaser B, Solomon D, Ni A, Zech W (2000) Effects of Deforestation on Phosphorus Pools in Mountain Soils of the Alay Range, Khyrgyzia. Biology and Fertility of Soils 31:134-142.

van Ranst E, De Coninck F, Van Rompaey K (2004) Synthesis of HNO3 from Organic Matter and Its Influence on Nutrient Replenishment in Forest Soils. Environmental Monitoring and Assessment 98:409-420.

Vanhaecke F (2012) Single-Collector Inductively Coupled Plasma Mass Spectrometry. Isotopic Analysis: Fundamentals and Applications Using ICP-MS. Wiley, Weinheim.

Velde B, Meunier A (2008) Clay Minerals Present in Soils as a Response to Climate. In: The Origin of Clay Minerals in Soils and Weathered Rocks. Springer Verlag, Stuttgart.

Vitousek P (1982) Nutrient Cycling and Nutrient Use Efficiency. American Naturalist 119:553-572.

Vitousek PM, Porder S, Houlton BZ, Chadwick OA (2010) Terrestrial Phosphorus Limitation: Mechanisms, Implications, and Nitrogen-Phosphorus Interactions. Ecological Applications 20:5-15.

Vogl J, Heumann KG (1998) Development of an ICP−IDMS Method for Dissolved Organic Carbon Determinations and Its Application to Chromatographic Fractions of Heavy Metal Complexes with Humic Substances. Analytical Chemistry 70:2038-2043.

von der Kammer F, Legros S, Hofmann T, Larsen EH, Loeschner K (2011) Separation and Characterization of Nanoparticles in Complex Food and Environmental Samples by Field-Flow Fractionation. TrAC Trends in Analytical Chemistry 30:425-436.

Walker TW, Syers JK (1976) Fate of Phosphorus During Pedogenesis. Geoderma 15:1-19.

Wasserwirtschaftsamt Ansbach B (2015) 1. Platz Für Mensch Und Natur. Wasserwirtschaftlicher Lehrpfad an der Haslach in Burghaslach.
http://www.wwa-an.bayern.de/wasser_erleben/lehrpfade/burghaslach/stationen/index.htm.
Accessed 03/22/2016

Wells ML, Goldberg ED (1991) Occurrence of Small Colloids in Sea Water. Nature 353:342-344.

Wen LS, Santschi P, Gill G, Paternostro C (1999) Estuarine Trace Metal Distributions in Galveston Bay: Importance of Colloidal Forms in the Speciation of the Dissolved Phase. Marine Chemistry 63:185-212.

Wigginton NS, Haus KL, Hochella Jr MF (2007) Aquatic Environmental Nanoparticles. Journal of Environmental Monitoring 9:1306-1316.

Wild A (1988) Plant Nutrients in Soil: Phosphate. Russell's Soil Conditions and Plant Growth, 11th edn:695-742.

Wilkinson KJ, Joz-Roland A, Buffle J (1997) Different Roles of Pedogenic Fulvic Acids and Aquagenic Biopolymers on Colloid Aggregation and Stability in Freshwaters. Limnology and Oceanography 42:1714-1724.

Williams J, Walker T (1969) Fractionation of Phosphate in a Maturity Sequence of New Zealand Basaltic Soil Profiles: 2. Soil Science 107:213-219.

Yaghi N, Hartikainen H (2013) Enhancement of Phosphorus Sorption onto Light Expanded Clay Aggregates by Means of Aluminum and Iron Oxide Coatings. Chemosphere 93:1879-1886.

Zacharias S, Bogena H, Samaniego L, Mauder M, Fuss R, Puetz T, Frenzel M, Schwank M, Baessler C, Butterbach-Bahl K, Bens O, Borg E, Brauer A, Dietrich P, Hajnsek I, Helle G, Kiese R, Kunstmann H, Klotz S, Munch JC, Papen H, Priesack E, Schmid HP, Steinbrecher R, Rosenbaum U, Teutsch G, Vereecken H (2011) A Network of Terrestrial Environmental Observatories in Germany. Vadose Zone Journal 10:955-973.

Zhang AD, Oldham C (2001) The Use of an Ultrafiltration Technique for Measurement of Orthophosphate in Shallow Wetlands. Science of the Total Environment 266:159-167.

Zirkler D, Lang F, Kaupenjohann M (2012) "Lost in Filtration"-the Separation of Soil Colloids from Larger Particles. Colloids and Surfaces A-Physicochemical and Engineering Aspects 399:35-40.

List of Figures

List of Tables

List of Abbreviations

A	Sampling site Aneboda
AF^4	Asymmetric Flow Field Flow Fractionation
AG	Sampling site Agia
Al	Aluminum
AM	Sampling site Allt a'Mharcaidh
Ar	Argon
B	Sampling site Bode
BPC	Sampling site Barranco de Porta Coeli
C	Sampling site Costiglione
Ca	Calcium
CON	Sampling site Conventwald
CW	Sampling site Cotley Wood
(k)Da	(kilo)Dalton
DC	Direct current
DLS	Dynamic light scattering
DOM/DOC	Dissolved organic matter/carbon
E	Sampling site Erlenbach
F	Sampling site Franchesiello
Fe	Iron
FFF	Field Flow Fractionation
G	Sampling site Gårdsjön
He	Helium
HPLC	High performance liquid chromatography
ICP-MS	Inductively coupled plasma mass spectrometer
K	Sampling site Krycklan
KED	Kinetic energy discrimination
L	Sampling site Lettosuo
LÄ	Sampling site Lägeren
LEI	Sampling site Leirelva
LOD	Limit of detection
LP	Sampling site La Peyne
LÜ	Sampling site Lümpenenbach
LZ	Sampling site Lourizela
µm	Micrometers
MIT	Sampling site Mitterfels
Mn	Manganese
MP	Sampling site Muntanyes de Prades

MWCO	Molecular weight cut-off
N	Sampling site Norunda
nm	Nanometers
NNP	Natural nanoparticle
NOM	Natural organic matter
NTU	Nephelometric Turbidity Unit
OCD	Organic carbon detector
org C	Organic carbon
P	Phosphorus
P	Sampling site Pallas
PEEK	Polyether ether ketone
PR	Sampling site Piano Rabelli
PSS	Polystyrene sulfonic acid
PUL	Pullulan
RF	Radio frequency
RS	Sampling site Ribera Salada
S	Sampling site Soroe
SB	Sampling site Strengbach
SC	Sampling site Sierra de Cima
Si	Silicon
TERENO	Terrestrial Environmental Observatories
TOC	Total organic carbon
UV	Ultra violet
V	Sampling site Vogelbach
VES	Sampling site Vessertal
W	Sampling site Wüstebach

List of Symbols

α	Degree of ionization or ionization efficiency
D	Particle diffusion coefficient [m^2/s]
d_H	Hydrodynamic particle diameter [m]
η	Dynamic viscosity [Pa*s]
f	Radio frequency current [Hz]
h	Planck's constant [eV*s]
IE	Ionization potential [eV]
k	Boltzmann's constant [J/K]
λ	Wavelength [m]
λ_r	Retention parameter
l	Thickness of equilibrium cloud [m]
m/z	Mass to charge ratio
n_a	Density of atoms (number of particles per unit volume)
n_e	Density of electrons (number of particles per unit volume)
n_i	Density of ions (number of particles per unit volume)
P	Potential of each pair of quadrupole rods [V]
R	Retention ratio
r	Radius [m]
T	Absolute temperature [K]
T_{ion}	Ionization temperature in the ICP [K]
t_r	Retention time [s]
U_V	Induced velocity [m/s]
U	DC potential [V]
V	Maximum amplitude [m]
V^0	Void volume [L]
V_c	Volumetric cross flow rate [m^3/s]
V_d	Volumetric detector flow rate [m^3/s]
V^r	Retention volume [L]
ν_c	Cross flow [L/s]
ν_d	Detector flow [L/s]
ν_f	Focus flow [L/s]
ν_i	Injection flow [L/s]
w	Channel thickness [m]
Z_a	Partition functions for atomic state
Z_i	Partition functions for ionic state

Scientific contributions

Journal articles

Gottselig N, Bol R, Nischwitz V, Vereecken H, Amelung W, Klumpp E (2014) Distribution of Phosphorus-Containing Fine Colloids and Nanoparticles in Stream Water of a Forest Catchment. Vadose Zone Journal 13:1-11.

Bogena HR, Bol R, Borchard N, Brüggemann N, Diekkrüger B, Drüe C, Groh J, **Gottselig N**, Huisman JA, Lücke A, Missong A, Neuwirth B, Pütz T, Schmidt M, Stockinger M, Tappe W, Weihermüller L, Wiekenkamp I, Vereecken H (2014) A Terrestrial Observatory Approach to the Integrated Investigation of the Effects of Deforestation on Water, Energy, and Matter Fluxes. Science China Earth Science 58:61-75.

Liu S, Herbst M, Bol R, **Gottselig N**, Pütz T, Weymann D, Wiekenkamp I, Vereecken H, Brüggemann N (2016) The Contribution of Hydroxylamine Content to Spatial Variability of N2O Formation in Soil of a Norway Spruce Forest. Geochimica et cosmochimica acta 178:76-86.

Gottselig N, Nischwitz V, Meyn T, Amelung W, Bol R, Halle C, Vereecken H, Siemens J, Klumpp E. Phosphorus Binding to Nanoparticles and Colloids in Forest Stream Waters. Biogeochemistry, submitted.

Bol R, Julich D, Brödlin D, Siemens J, Dippold MA, Spielvogel S, Zilla T, Mewes D, von Blanckenburg F, Puhlmann H, Holzmann S, Kaiser K, Weiler M, Amelung W, Lang F, Kuzyakov Y, Feger KH, **Gottselig N**, Klumpp E, Missong A, Winkelmann C, Uhlig D, Sohrt J, von Wilpert K, Wu B, Hagedorn F. Transport of Dissolved and Colloidal Phosphorus in Temperate Forests – An Almost Blind Spot in Ecosystem Research. Journal of Plant Nutrition and Soil Science, under review.

Nischwitz V, **Gottselig N**, Missong A, Meyn T, Klumpp E. Field Flow Fractionation Online with ICP-MS as Novel Approach for the Quantification of Particle-Bound Carbon in Stream Water Samples and Soil Extracts. Journal of Analytical Atomic Spectrometry Special Issue on Speciation Analysis, under review.

Gottselig N, Amelung W, Kirchner J, Avila Castells A, Båth A, Batalla R, Bol R, Blomkvist P, Estany D, Eugster W, Falgin C, Granger S, Hernandez Crespo C, Herrmann F, Jackson-Blake L, Keizer JJ, Knöller K, Laudon H, Laurila T, Lehner I, Lindroth A, Löfgren S, Ottosson Löfvenius M, Lohila A, MacLeod K, Martín Monerris M, Mölder M, Müller C, Nasta P, Nischwitz V, Paul-Limoges E, Pierret MC, Pilegaard K, Romano N, Stähli M, Sebatià MT, Taberman I, Voltz M, Wendland F, Vereecken H, Siemens J, Klumpp E. Natural Nanoparticles and Colloids in European Forest Stream Waters and their Role for Phosphorus Transport. Global Biogeochemical Cycles, ready for submission.

Articles in preparation

Gottselig N and Wiekenkamp I (mutual first authorship), Amelung W, Bogena HR, Bol R, Brüggemann N, Huisman JA, Klumpp E, Pütz T, Vereecken H. Soil Biogeochemistry in a Forested Headwater Catchment – A Three Dimensional View. Journal of Environmental Quality, in preparation.

Meyn T, **Gottselig N**, Missong A, Klumpp E. Oxidation Efficiency of Online Carbon Detection for Polymers and Nanoparticles, in preparation.

Berns AE, **Gottselig N**, Ockert C, Hezel D, Wombacher F, Bol R, Münker C, Vereecken H, Amelung W, Wu B. Iron isotopes in different reservoirs of a forested catchment, in preparation.

Conference contributions (oral)

Gottselig N, Nischwitz V, Bol R, Küppers S, Klumpp E (2014) Field Flow Fractionation in Environmental Research: Characterization of Natural Nanoparticles in a Forest Stream. GDCh Separation Science PhD seminar, Hohenroda, Germany.

Gottselig N, Nischwitz V, Bol R, Vereecken H, Klumpp E (2014) Fine Colloidal and Nanoparticulate P, Fe, Al and C Distribution in Stream Water of a German Mountainous Forest Catchment. International Workshop Nanoparticles in Soils and Waters: Fate, Transport and Effects, Landau, Germany.

Gottselig N, Bol R, Nischwitz V, Amelung W, Vereecken H, Klumpp E (2014) Fine Colloidal and Nanoparticulate P, Fe, Al and C Distribution in Stream Water of a German Mountainous Forest Catchment. BIOGEOMON 2014, 8th International Symposium on Ecosystem Behavior, Bayreuth, Germany.

Gottselig N, Nischwitz V, Meyn T, Halle C, Amelung W, Vereecken H, Bol R, Siemens J, Klumpp E (2014) Fine Colloidal and Nanoparticulate driven Ecosystem Nutrient Transport in Stream Water of Forest Catchments. Flux Cluster meeting in the framework of the SPP 1685 project "Ecosystem Nutrition: Forest Strategies for Limited Phosphorus Resources", Bonn, Germany.

Gottselig N, Nischwitz V, Meyn T, Halle C, Bol R, Vereecken H, Amelung W, Siemens J, Klumpp E (2015) Phosphorus in Forest Stream Waters – The Relevance of Nanoparticles and Colloids. SPP 1685 "Ecosystem Nutrition: Forest Strategies for Limited Phosphorus Resources" meeting, Dipperz/Fulda, Germany.

Gottselig N, Nischwitz V, Meyn T, Halle C, Bol R, Vereecken H, Amelung W, Siemens J, Klumpp E (2015) Phosphorus Nanoparticles and Colloids of Forest Stream Waters – Fractionation and Potential Role in Ecosystems. Soil interfaces for Sustainable Development (ISMOM), Montreal, Canada.

Conference contributions (poster)

Gottselig N, Bol R, Nischwitz V, Amelung W, Vereecken H, Klumpp E (2014) Distribution of Phosphorous-Containing Fine Colloids and Nanoparticles in Stream Water of a Forest Catchment. International Conference on Interfaces against Pollution, Interfaces in Water and Environmental Science, Leeuwarden, Netherlands.

Gottselig N, Meyn T, Nischwitz V, Bol R, Sohrt J, Puhlmann H, Halle C, Vereecken H, Siemens J, Klumpp E (2014) Phosphorus Containing Natural Nanoparticles and Fine Colloids – Forest Stream Fingerprinting. SPP 1685 "Ecosystem Nutrition: Forest Strategies for Limited Phosphorus Resources" meeting, Freising, Germany.

Wolff J, **Gottselig N,** Brödlin D, von Sperber C, Siemens J, Klumpp E (2015) Potential Bioavailability of Nanoparticulate and Colloidal bound P. SPP 1685 "Ecosystem Nutrition: Forest Strategies for Limited Phosphorus Resources" meeting, Dipperz/Fulda, Germany.

Gottselig N, Meyn T, Nischwitz V, Halle C, Vereecken H, Amelung W, Bol R, Siemens J, Klumpp E (2015) Forested Headwater Catchment Analysis on Nanoparticulate and Fine Colloidal Bound Phosphorus. Deutsche Bodenkundliche Gesellschaft (DBG) annual conference, Munich, Germany.

Funding

Jan. 2014 - Dec. 2015: Project funding acquired from the German Academic Exchange Program (DAAD), Forschungsmobilität - Program des Projektbezogenen Personenaustauschs (PPP) with Dr. Thomas Meyn of the Department of Hydraulic and Environmental Engineering, Norwegian University of Science and Technology, Trondheim, Norway.

Award

1st place, Scientific Poster: Gottselig N, Bol R, Nischwitz V, Amelung W, Vereecken H, Klumpp E (2014) Distribution of Phosphorous-Containing Fine Colloids and Nanoparticles in Stream Water of a Forest Catchment. International Conference on Interfaces against Pollution, Interfaces in Water and Environmental Science, Leeuwarden, Netherlands.

Curriculum Vitae

Name	Nina Gottselig
Address	Antwerpener Str. 14 D-50672 Cologne
Telephone	+49 (0) 177 / 3387037
Email	n.gottselig@fz-juelich.de
Nationality	German
Date of Birth	June 23rd, 1988

Education und qualifications

2007	Allgemeine Hochschulreife (Abitur)
2007 - 2010	Rheinisch Westfälische Technische Hochschule Aachen, Bachelor of Science in Biology
	Bachelor thesis topic: Mutagenic activity in sediments and fish samples of the quarry pond Karlskopf of River Rhine: linking effects from the laboratory to the field
2010 - 2012	University of Cologne, International Master of Environmental Sciences
	Master thesis topic: On the use of bacterivorous flagellates and ciliates to reduce harmful bacteria in wastewater
Jan. 2013 - present	Ph.D. student at the Institute for Bio- and Geosciences, Agrosphere (IBG-3), Forschungszentrum Jülich and at Institute of Environmental Research (Biology 5), RWTH Aachen

Work experience

2009 - 2010	Student assistant, Chair for Ecosystem Analyses at the Institute of Environmental Research (Biology 5), RWTH Aachen, Germany
Sept. - Oct. 2010	UROP Abroad Internship, Prof. Dr. Karen Kidd, University of New Brunswick, New Brunswick, Canada
Jul. - Sept. 2011	Research assistant, Institute for General Ecology, University of Cologne, Germany
Nov. - Dec. 2011	Preparation BIMUN/SINUB Conference 2011, Bonn, Germany
Mar. 2012	Wildlife and Protected Area Management, Institute of Environment Education and Research, Pune, India
Oct. - Dec. 2015	International research exchange with Prof. Dr. Kirchner, Department of Environmental Systems Science, ETH Zurich, Switzerland

Further Work and Qualifications

2009 - 2010	Intensive work in an ecotoxicological laboratory with major focus on the Ames Fluctuation Assay at the Chair for Ecosystem Analyses, Institute of Environmental Research (Biology 5), RWTH Aachen, Germany

2011 - 2012	Experience with Protista molecular ecology in the context of wastewater treatment at the Institute for General Ecology, University of Cologne, Germany
2013 - 2015	Practical work at long term monitoring field sites and organization of a complex sampling campaign to assess the soil characteristics pre- and post-deforestation in the context of the TERENO project
2013 - present	Extensive practical experience with field flow based separation of environmental nanoparticles and colloids (FFF) and detection with numerous non-destructive (UV, Fluorescence, MALS, DLS) and destructive (ICP-MS, OCD) detectors as well as manifold data analysis techniques at the Institute for Bio- and Geosciences, Agrosphere (IBG-3), Forschungszentrum Jülich, Germany
2013	Transmission electron microscopy at the Ernst-Ruska-Center, Forschungszentrum Jülich GmbH, Germany
2014 - 2015	Liquid ^{31}P-NMR at the Central Institute for Engineering, Electronics and Analytics, Analytics (ZEA-3), Forschungszentrum Jülich GmbH, Germany
Jan. 2014 - Dec. 2015	Project funding acquired from the German Academic Exchange Program (DAAD), Forschungsmobilität - Program des Projektbezogenen Personenaustauschs (PPP) with Dr. Thomas Meyn of the Department of Hydraulic and Environmental Engineering, Norwegian University of Science and Technology, Trondheim, Norway
May 2014	1st place, Scientific Poster: Gottselig N, Bol R, Nischwitz V, Amelung W, Vereecken H, Klumpp E (2014) Distribution of Phosphorous-Containing Fine Colloids and Nanoparticles in Stream Water of a Forest Catchment. International Conference on Interfaces against Pollution, Interfaces in Water and Environmental Science, Leeuwarden, Netherlands
2014 - present	Establishment of a European network for stream water sampling in forested headwater catchment encompassing 26 sites across two transects in Europe
2014 - 2015	Supervision of a M.Sc. student at Forschungszentrum Jülich, Germany, topic: Bioavailability of nanoparticulate and colloidal bound P
2015 - present	Preparative techniques for iron isotope extraction from environmental samples, practical experience in the measurement of the isotopic signatures with Multicollector ICP-MS (MC ICP-MS) and data analysis approaches at the Steinmann-Institute for Geology, Mineralogy und Paleontology, University Bonn and at the Institute for Geology and Mineraology, University of Cologne

Skills

Languages	German (fluent), English (fluent), Spanish (basics), French (basics)
PC	Microsoft Office, Statistica, JMP, R, GraphPad

Personal Interests

Travelling the world, exotic cultures, music, artistic work with wood and stone, sustainable building techniques

Acknowledgements

This work would not have been possible without the support from the following people:

First of all I would like to thank my doctoral supervisor Prof. Dr. Erwin Klumpp. Through his terrific support, the fruitful discussions and the strong belief he has in his PhD students, a great atmosphere with many possibilities is present in his working group. Thank you so much!

I would also like to thank Prof. Dr. Andreas Schäffer for his inspirations during my Bachelor's degree and now his interest in my PhD work, which gives me the opportunity to graduate at the Chair of Environmental Biology and Chemodynamics, RWTH Aachen.

Special thanks goes to Prof. Dr. Wulf Amelung for his interest in my PhD topic, his immense support over the years and the detailed discussions on new concepts. Thank you very much!

Special thanks also to Prof. Dr. Harry Vereecken for the financial support and the opportunity to write my thesis at IBG-3. All of the presentations and reports were a good preparation for conferences, papers, and, ultimately, this thesis.

My gratitude also goes to Prof. Dr. Henner Hollert for the opportunity to work as a student assistant in his group through which I realized that I truly love the laboratory work.

Further, I would like to thank Dr. Roland Bol for his ideas, which always included thoughts about what would be best for me and my work. Thank you!

Dr. Stephan Küppers at the ZEA-3, Research Center Jülich, for supporting my PhD work through the provisioning of logistical support which enabled important measurements online with FFF.

Thank you very much also to Dr. Volker Nischwitz, ZEA-3, Research Center Jülich, for sharing his knowledge on ICP-MS and greatly supporting online measurements. Thank you very much!

I am very grateful for the opportunity to visit Prof. Dr. James Kirchner, ETH Zurich. Thank you for your support.

A very big thank you to the working group 'Biogeochemical Interfaces and Colloids' for the support. Somebody always had an idea to solve a problem, an open ear, could lend me a hand with a problem or opened up the possibility for me to join an interesting project. In this context I specifically want to thank Herbert Philipp. It was a joy to be able to work with you, your calm character and the knowledge on how things work at the Research Center helped me many times!

Further, I want to especially thank Anna Missong and Joanna Makselon. I had the pleasure to work with Anna from almost the beginning of my PhD and I will always cherish our team work, the great laughs we had and the friendship that grew out of it. Joanna, I am also very glad that you came to Jülich and to have become friends with you through this, your laughs and energy will always amaze me!

Thank you also to Dr. Anne Berns and Dr. Bei Wu for your ideas, time and the great project work together on Fe isotopes, which gave me the idea for my PostDoc project.

Thank you Dr. Wolfgang Tappe for your thoughts, ideas and advice!

Further, thanks to Wolfgang, Sirgit, Thomas, Christian, Nils, Werner, Jannis, Normen, Bernd and Michael for the enjoyable lunch breaks, wonderful trips to the field sites, great discussions, ideas and the many laughs together.

Thank you to all of my colleagues at IBG-3, you are a very interesting bunch of people!

Finally, I would like to thank my friends and family, especially my parents for their continuous support, their inspiring ideas and for teaching me so much. I am very grateful to be your daughter! Another special thank you goes to Johannes for his unconditional patience, support and care-taking. I am very grateful to have you in my life!

Annex

Methods of sample digestion, Fe isotope extraction and measurements[10]

Soil samples were obtained from the Wüstebach catchment through drilling of soil cores up to 1.5 m depth in a Cambisol and a Gleysol soil of the catchment in August 2013. Of the soil cores, each identified soil horizon was separately sampled. Beech leaves and spruce needles were collected directly from living trees in the source area in November 2013. Stream water samples were dried down and the dry residues were digested in 2 mL of aqua regia (1:3 (v:v), 3 M HNO_3 / 6 M HCl (supra pure quality, Merck Millipore, Darmstadt, Germany) at 110 °C overnight in closed Savillex beakers to remove remaining organic matter and subsequently dried down in open beakers. Soil samples were dried at room temperature and sieved to 2 mm. Of each sample an aliquot of 50-100 mg was suspended in 2 mL 3 M HNO_3 (supra pure, Merck Millipore, Darmstadt, Germany) and subsequently dried down at 110°C in open beakers. The residues were then resuspended in 4 mL of a mixture of conc. HNO_3 and conc. HF (1:1, vol/vol) and heated to 180°C in high-pressure Parr bombs for 24 h. The cooled mixtures were dried down at 120°C in open beakers. The residues were resuspended in 3 mL of 3 M HNO_3 and dried down. If necessary this step was repeated a second time to remove remaining fluorides or organic matter. Vegetation samples were dried at 50°C and either ground manually in an agate mortar or milled in a centrifugal mill (0.5 mm sieve, Retsch, Germany). Digestion of the plant samples was done similarly to the soil samples. After treatment in 3 M HNO_3, the dried residues were digested in aqua regia at room temperature overnight and subsequently dried down. The samples were then bombed in a HNO_3:HF mixture as described above to dissolve the samples completely and dried down. For all samples certified reference materials, if possible of matching matrix, were treated in parallel. For soil samples TILL-1 (geochemical soil and till reference material, CCRMP, Canada) and NIST SRM 2709a (San Joaqium soil, NIST, USA) were used. For vegetation samples NIST SRM 1515 (apple leaves, NIST, USA) and NIST SRM 1575a (pine needles, NIST, USA) were used.

The separation of Fe ions from further cations present in the matrix was done by ion chromatography. Poly-Prep® chromatography columns (Bio-Rad Laboratories GmbH, Germany), with 2 mL bed volume and 10 mL reservoir, were filled with 1 mL of analytical grade anion exchange resin AG® 1-X4 (200-400 dry mesh size, chloride form, Bio-Rad Laboratories GmbH, Germany). Before separation the columns were cleaned by passing subsequently 1 reservoir of double distilled water, 1 reservoir of 6 M HCl and 1 reservoir of 0.05 M HCl through them. The columns were then conditioned with 1 reservoir of 6 M HCl. The dried samples (see above) were dissolved in 0.5 mL (water samples)

[10] Contains excerpts from: Berns AE, **Gottselig N**, Ockert C, Hezel D, Wombacher F, Bol R, Münker C, Vereecken H, Amelung W, Wu B. Iron isotopes in different reservoirs of a forested catchment, in preparation.

or 1.5 mL (soil and vegetation samples) of 6 M HCl and aliquots of 500 µL (water samples) or 200 µL (soil and vegetation samples) were loaded onto the conditioned columns. For each set of ion chromatography samples 1 column was loaded with 0.5 mL of 6 M HCl as blank. First matrix ions were washed out with several washings (2 x 0.5 mL, 1 x 1 mL, 2 x 2 mL) of 6 M HCl (= 6 mL matrix cut). The Fe ions were then eluted with several washings (2 x 0.5 mL, 1 x 1 mL, 1 x 2 mL) of 0.05 M HCl (= 4 mL iron cut). The columns were subsequently cleaned by passing 1 reservoir of 6 M HCl, 1 reservoir of 0.05 M HCl and 1 reservoir of Milli-Q water through them and were then stored in 6 M HCl until further use. The matrix and iron cuts were collected in cleaned Savillex beakers and dried down (90°C overnight). The residues were picked up in 1 mL of 0.5 M HNO_3 and transferred to Eppendorf tubes for storage.

Element analysis of the matrix and iron cuts was done on an ICP-OES (Spectro Arcos, SPECTRO Analytical Instruments, Germany). Before measurement samples were diluted to match the calibration range, blanks were diluted only to allow for a large enough sample volume. Calibration was done with a set of five multi-element ICP standard solutions (NIST certified ICP-MS standards) plus a blank solution giving a range of 0, 10, 50, 100, 500 and 1000 ppb for matrix elements and 0, 40, 200, 400, 2000 and 4000 ppb for iron. The iron separation was considered successful when no iron was detected in the matrix cut and none of the matrix elements in the iron cut.

Iron isotope ratios were determined on a MultiCollector-ICP-MS (Neptune, Thermo Fisher Scientific, USA) (MC-ICP-MS). According to the concentrations determined in the ICP-OES, samples were prepared to contain 1 ppm of iron. The samples were spiked with a Cu-solution (NIST-976) with a final concentration of 1 ppm of copper. Measurement was done in medium resolution mode and mass bias was corrected via the internal Cu-standard. Each sample was bracketed by standard analysis of a 1 ppb solution of NIST IRMM-014.

The values are given in δ^{56}Fe notation:

$$\delta^{56}Fe = \left(\frac{\left(\frac{^{56}Fe}{^{54}Fe}\right)_{sample}}{\left(\frac{^{56}Fe}{^{54}Fe}\right)_{standard}} - 1 \right) * 10^3$$

Tables

Table S1: *Organic C, Al, Si, Mn, Fe results of the national scale study: Total sample concentrations and percentage of elemental binding in the nanoparticulate and fine colloidal fractions over all sampling points per site. n = 29.*

		Organic C		Al		Si		Mn		Fe	
	samples	*Total [mg/L]*	*[%]*	*Total [µg/L]*	*[%]*	*Total [µg/L]*	*[%]*	*Total [µg/L]*	*[%]*	*Total [µg/L]*	*[%]*
Conventwald	1	1.3	22.7	240	6.7	5500	6.4	4.9	100.0	146	71.8
	2	1.5	18.1	7	3.3	4900	0.1	0.1	69.9	3	55.3
	3	0.9	11.1	6	1.0	5100	0.0	1.4	1.5	1	42.5
	4	0.8	14.3	6	1.6	5200	0.1	0.1	52.2	1	58.5
	5	0.6	17.5	4	7.7	5500	0.1	0.2	71.4	1	100.4
Mitterfels	6	35.5	17.0	140	4.0	5000	0.2	0.9	49.7	113	53.6
	7	11.5	42.8	106	5.0	5000	0.2	0.9	44.0	102	53.8
	8	12.7	95.9	330	4.5	4900	0.8	2.2	90.3	380	67.6
	9	14.6	27.0	200	3.7	5400	1.0	1.3	48.7	143	47.4
	10	11.2	48.0	240	4.2	5600	0.9	1.9	44.0	200	46.7
	11	25.3	16.7	270	3.8	5900	0.4	4.2	27.4	210	44.9
	12	11.6	35.3	210	4.2	5200	0.7	1.9	23.1	140	51.1
	13	2.2	100.0	139	4.6	5500	0.4	1.3	63.8	85	75.9
Vessertal	14	0.7	9.8	8	0.3	5900	0.0	0.3	2.1	1	12.6
	15	0.7	7.6	5	0.3	6700	0.0	0.1	7.1	1	4.0
	16	0.7	6.0	6	0.8	6800	0.0	0.4	3.6	1	25.3
	17	1.4	4.6	12	0.9	6500	0.0	0.1	45.6	3	22.7
	18	1.2	5.4	10	1.6	5900	0.0	0.1	72.0	3	68.7
Wüstebach	19	13.2	18.4	460	0.4	1380	0.4	350.0	0.1	960	17.7
	20	22.9	30.5	590	1.1	830	1.8	240.0	0.2	2100	28.6
	21	5.7	47.0	68	4.1	2200	0.5	49.0	1.0	490	52.8
	22	9.6	21.9	200	2.1	2200	0.5	190.0	0.5	480	43.7
	23	14.0	45.2	117	6.9	1700	1.4	2.8	100.0	630	62.8
	24	1.5	7.8	200	0.1	2800	0.0	92.0	0.0	21	7.8
	25	5.6	25.3	200	1.7	2600	0.8	120.0	0.7	250	39.3
Leirelva	26	6.0	19.0	21	0.4	700	0.1	0.2	100.0	13	36.7
	27	8.3	20.0	24	0.4	1640	0.3	0.4	57.8	61	16.3
	28	5.8	18.3	21	0.4	900	0.0	0.1	99.2	15	42.3
	29	5.3	17.6	16	0.4	1010	0.1	0.1	100.0	10	59.2

Table S2: *Pearson r values for clustering of all analyzed elements with each other per size fraction across all geographic regions (Figure 4.4.3) of the continental scale study. Red values are Pearson r≥0.5, bold red values mark upper 5% of Pearson r values. n=96.*

1st fraction

	org C	Al	Si	P	Ca	Mn	Fe
org C		**0.84**	0.32	0.23	**0.86**	0.42	**0.84**
Al	**0.84**		0.37	0.20	0.59	0.25	0.67
Si	0.32	0.37		0.01	0.32	0.02	0.30
P	0.23	0.20	0.01		0.11	-0.05	0.30
Ca	**0.86**	0.59	0.32	0.11		0.36	0.62
Mn	0.42	0.25	0.02	-0.05	0.36		0.44
Fe	**0.84**	0.67	0.30	0.30	0.62	0.44	

2nd fraction

	org C	Al	Si	P	Ca	Mn	Fe
org C		0.69	0.47	0.07	0.52	0.21	**0.76**
Al	0.69		0.42	0.00	**0.79**	0.29	0.71
Si	0.47	0.42		0.03	0.45	0.35	0.54
P	0.07	0.00	0.03		0.00	-0.19	0.03
Ca	0.52	**0.79**	0.45	0.00		0.28	0.69
Mn	0.21	0.29	0.35	-0.19	0.28		0.46
Fe	**0.76**	0.71	0.54	0.03	0.69	0.46	

3rd fraction

	org C	Al	Si	P	Ca	Mn	Fe
org C		0.19	0.15	0.42	0.36	0.06	0.54
Al	0.19		**0.98**	0.23	0.09	0.14	0.59
Si	0.15	**0.98**		0.19	0.09	0.10	0.50
P	0.42	0.23	0.19		0.36	-0.08	0.48
Ca	0.36	0.09	0.09	0.36		-0.13	0.42
Mn	0.06	0.14	0.10	-0.08	-0.13		0.29
Fe	0.54	0.59	0.50	0.48	0.42	0.29	

Table S3: *Background data and information on the European sites. Abbr. = abbreviation, site abbreviations see Chapter 3.1.3. The degree of forest management was determined according to Duncker et al. (2012).*

abbr.	catchment size [km^2]	average elevation [m]	maximum elevation [m]	minimum elevation [m]	average slope	forest cover	forest management degree	mean annual runoff [mm]
A	0.19	225	240	210	0.13	0.73	0.25	280
AG	0.75	916	1489	272	0.28		0.75	
AM	9.79	716	1111	320		0.02	0.00	
B	1.27	515	569	461	0.07	1.00	0.00	
BPC	3.2	523	754	292	0.21	0.5		
C	10.95	563	750	427	0.32	1.00	0.50	225
CW	0.5	146	191	102	0.08	1.00	0.25	
E	0.73	1330	1510	1150	0.24	0.39	0.25	1778
F	10.95	563	750	427	0.32	1.00	0.50	225
G	0.07	127	140	114	0.22	0.65	0.25	520
K	679	260	405	114		0.87	0.25	311
L	1.25	111			0.01	1.00	1.00	413
LÄ		680	866	440	0.35	1.00	0.00	
MP								
LP	110	305	420	190	0.25	1.00	0.00	
LÜ	0.88	1260	1360	1160	0.15	0.19	0.25	2001
LZ	0.65	365	455	200	0.37	1.00	0.00	775
N	6084	45	78	30		1.00	0.00	250
P	5.15	308	347	269	0.08	0.6	0.25	220
PR	10.95	563	750	427	0.32	1.00	0.50	225
RS		1483	2385	580		1.00		
S		37	38	36	0.07	1.00	0.50	
SB	0.8	1015	1146	883	0.15	1.00	0.50	814
SC	0.52	432	485	275	0.16	1.00	0.00	775
V	1.58	1285	1450	1120	0.23	0.63	0.25	1601
W	3.85	612	628	595	0.04	1.00	0.00	

Figures

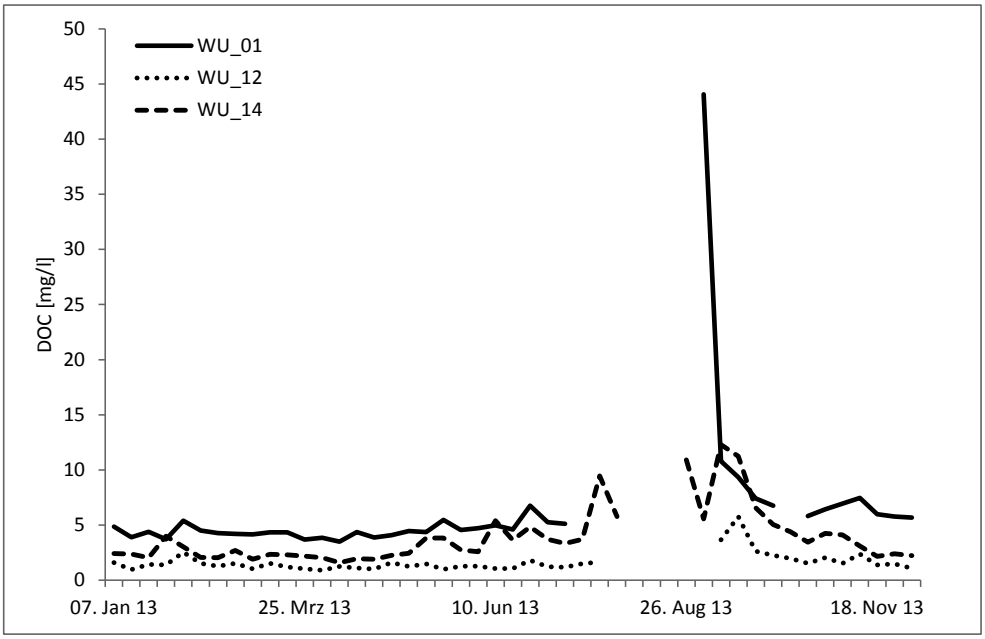

Figure S1: *Variation of the DOC content in the year 2013 measured in context of the TERENO monitoring. Missing data relates to the time of deforestation, where no sampling could take place. Not all sampling sites of this study are covered within the TERENO Project. Site SP1 = WU_01, T2 = WU_12, SP3 = WU_14.*

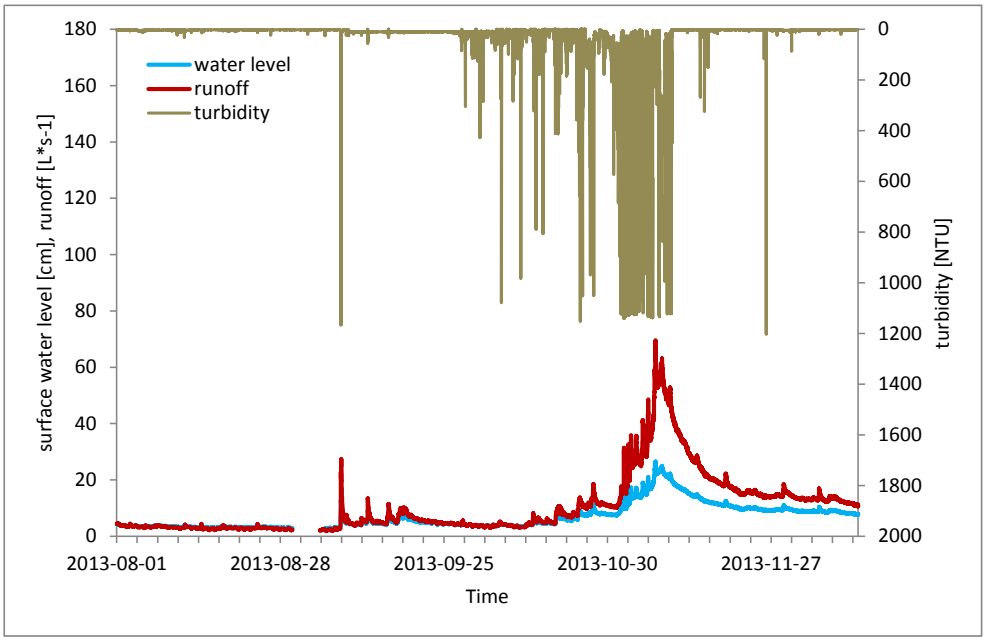

Figure S2: *Hydrological characteristics of sampling point SP3 of the Wüstebach stream in the year 2013 for the respective sampling period. Water level (blue line), runoff (red line) and turbidity (brown bars) are shown. Sampling prior to deforestation was done at the beginning of August, post deforestation at the beginning of December.*

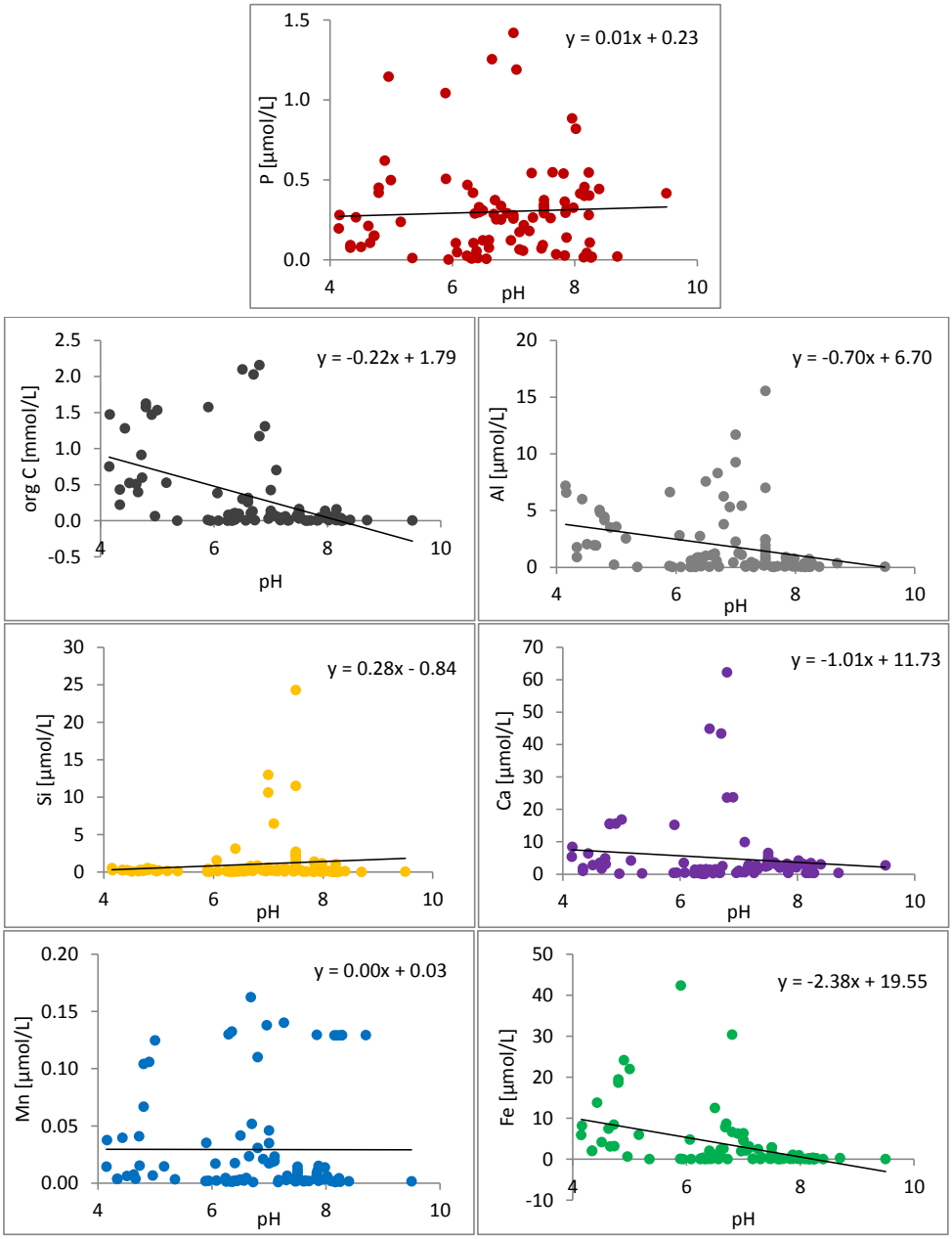

Figure S3: *All particulate concentration as function of forest stream water pH at sampling of the continental scale study. n=96.*

Band / Volume 317
Thermoschockverhalten und temperaturabhängige Eigenschaften kohlenstoffarmer und -freier Feuerfestwerkstoffe
A. Böhm (2016), VI, 153 pp
ISBN: 978-3-95806-139-2

Band / Volume 318
Theoretical and experimental studies of runaway electrons in the TEXTOR tokamak
S.S. Abdullaev, K.H. Finken, K. Wongrach, O. Willi (2016), X, 109 pp
ISBN: 978-3-95806-140-8

Band / Volume 319
Modelling Thermodynamic Properties of Intercalation Compounds for Lithium Ion Batteries
S. O. Dang (2016), x, 133 pp
ISBN: 978-3-95806-141-5

Band / Volume 320
Atmospheric Mixing in a Lagrangian Framework
M. Tao (2016), 146 pp
ISBN: 978-3-95806-142-2

Band / Volume 321
Statistical analysis and combination of active and passive microwave remote sensing methods for soil moisture retrieval
K. Rötzer (2016), XIV, 112 pp
ISBN: 978-3-95806-143-9

Band / Volume 322
Langzeitstabilität der Polymerelektrolyt-Wasserelektrolyse bei reduziertem Iridiumgehalt
C. G. Rakousky (2016), VII, 199 pp
ISBN: 978-3-95806-147-7

Band / Volume 323
Light induced water splitting using multijunction thin film silicon solar cells
F. Urbain (2016), xi, 173, XLVI pp
ISBN: 978-3-95806-148-4

Band / Volume 324
Properties of convective gravity waves derived by combining global modeling and satellite observations
Q. T. Trinh (2016), 140 pp
ISBN: 978-3-95806-150-7

Band / Volume 325
Feasible and Reliable Ab initio Atomistic Modeling for Nuclear Waste Management
G. Beridze (2016), xix, 128 pp
ISBN: 978-3-95806-151-4

Band / Volume 326
Sauerstoffspeicher für die oxidkeramische Batterie: Herstellung, Charakterisierung und Betriebsverhalten
C. M. Berger (2016), XV, 128 pp
ISBN: 978-3-95806-154-5

Band / Volume 327
Institute of Energy and Climate Research IEK-6: Nuclear Waste Management Report 2013 / 2014
Material Science for Nuclear Waste Management
S. Neumeier, M. Klinkenberg, D. Bosbach (Eds.)
(2016), 219 pp
ISBN: 978-3-95806-155-2

Band / Volume 328
Conductivity and Structure of Sputtered ZnO:Al on Flat and Textured Substrates for Thin-Film Solar Cells
N. Sommer (2016), vii, 195, XIV pp
ISBN: 978-3-95806-156-9

Band / Volume 329
Glaslotfügen von Festoxid-Brennstoffzellen durch Laseraufschmelzung
M. Willberg (2016), 99 pp
ISBN: 978-3-95806-157-6

Band / Volume 330
The Role of Natural Nanoparticles and Colloids for Phosphorus Binding in Forested Headwater Catchments
N. Gottselig (2016), VIII, 116 pp
ISBN: 978-3-95806-160-6

Energie & Umwelt /
Energy & Environment
Band / Volume 330
ISBN 978-3-95806-160-6